



DIRECT-STRENGTH METHOD DESIGN OF SPHERICALLY-HINGED COLD-  
FORMED STEEL EQUAL-LEG ANGLE COLUMNS

Kathleen Guimarães Santana

Dissertação de Mestrado apresentada ao Programa de Pós-graduação em Engenharia Civil, COPPE, da Universidade Federal do Rio de Janeiro, como parte dos requisitos necessários à obtenção do título de Mestre em Engenharia Civil.

Orientador: Alexandre Landesmann

Rio de Janeiro

Junho de 2018

DIRECT-STRENGTH METHOD DESIGN OF SPHERICALLY-HINGED COLD-  
FORMED STEEL EQUAL-LEG ANGLE COLUMNS

Kathleen Guimarães Santana

DISSERTAÇÃO SUBMETIDA AO CORPO DOCENTE DO INSTITUTO ALBERTO  
LUIZ COIMBRA DE PÓS-GRADUAÇÃO E PESQUISA DE ENGENHARIA  
(COPPE) DA UNIVERSIDADE FEDERAL DO RIO DE JANEIRO COMO PARTE  
DOS REQUISITOS NECESSÁRIOS PARA A OBTENÇÃO DO GRAU DE MESTRE  
EM CIÊNCIAS EM ENGENHARIA CIVIL.

Examinada por:

---

Prof. Alexandre Landesmann, D.Sc.

---

Prof. Eduardo de Miranda Batista, D.Sc.

---

Prof. Juarez Moara Santos Franco, D.Sc.

RIO DE JANEIRO, RJ - BRASIL

JUNHO DE 2018

Santana, Kathleen Guimarães

Direct-strength method design of spherically-hinged cold-formed steel equal-leg angle columns / Kathleen Guimarães Santana. - Rio de Janeiro: UFRJ/COPPE, 2018.

XI, 87 p.: il.; 29,7cm.

Orientador: Alexandre Landesmann

Dissertação (mestrado) – UFRJ/COPPE/ Programa de Engenharia Civil, 2018.

Referências Bibliográficas: p. 74 – 78.

1. Cold-formed steel equal-leg angles. 2. Short-to-intermediate spherically-hinged columns. 3. Experimental investigation. 4. FEM numerical analysis. I. Alexandre Landesmann *et al.* II. Universidade Federal do Rio de Janeiro, COPPE, Programa de Engenharia Civil. III. Título

Dedico este trabalho  
à minha mãe.

## **AGRADECIMENTOS**

Aos meus pais e ao meu irmão, pelo amor e suporte a mim dedicados.

Ao Carlos Alberto e à Renata, por todo o carinho e incentivo.

Ao João Pedro, pelo companheirismo e pela amizade.

Aos amigos, novos e antigos.

Ao orientador Alexandre Landesmann, pelos valiosos aprendizados.

Aos colegas e funcionários do LABEST, NUMATS, LTS e LAMEC, em especial: Anderson, André, Anysio, Arnaldo, Cláudio, Henrique, Renato, Santiago, Sarkis e Warley, por toda a atenção, colaboração e ensinamentos práticos.

Aos professores do Programa de Engenharia Civil da UFRJ e do curso de Engenharia Civil do IFMA, por todos os ensinamentos.

À CAPES (Coordenação de Aperfeiçoamento de Pessoal de Nível Superior) pela concessão da bolsa durante todo o período de realização deste mestrado.

À COPPE, agradeço o apoio, a estrutura e os incentivos prestados.

Por fim, agradeço ao povo brasileiro.

Resumo da Dissertação apresentada à COPPE/UFRJ como parte dos requisitos necessários para a obtenção do grau de Mestre em Ciências (M.Sc.)

DIMENSIONAMENTO PELO MRD DE COLUNAS EM PERFIL CANTONEIRA DE  
ABAS IGUAIS DE AÇO FORMADO A FRIO COM APOIOS ESFÉRICOS

Kathleen Guimarães Santana

Junho/2018

Orientador: Alexandre Landesmann

Programa: Engenharia Civil

Devido ao seu comportamento estrutural singular, colunas esbeltas em perfil cantoneira de aço de abas iguais formadas a frio não são atualmente pré-qualificadas para o dimensionamento pelo Método da Resistência Direta (MRD) na Especificação Norte Americana para Perfis Formados a Frio. Estes perfis também são excluídos da aplicação do fator de resistência  $\phi=0.85$ . Desta feita, existe um esforço para incorporar as características estruturais acima mencionadas a um novo método de dimensionamento baseado no MRD, o qual mostrou eficácia na previsão de resistência última para apoios fixos e pinados. Recentemente, este procedimento foi ampliado para apoios esféricos. Entretanto, ainda não há resultados para perfis cantoneira com apoios esféricos. Este trabalho consiste em uma busca para preencher esta lacuna por um estudo experimental conduzido na Universidade Federal do Rio de Janeiro sobre o comportamento e colapso destas colunas. Inicialmente, há o detalhamento da seleção das colunas a serem testadas, seguido pela descrição da instrumentação e dos procedimentos experimentais. Os resultados experimentais consistem em: (i) medição das imperfeições iniciais, (ii) trajetórias de equilíbrio referentes ao carregamento aplicado e aos deslocamentos principais da coluna, (iii) configurações deformadas e (iv) resistências últimas. Estes resultados são utilizados para validar um modelo de elementos finitos de casca desenvolvido previamente pelos autores, com uma aquisição de dados numéricos de falha adicionais por meio do mesmo modelo. Finalmente, há uma avaliação do mérito do procedimento de dimensionamento pela comparação dos resultados numéricos com os experimentais.

Abstract of Dissertation presented to COPPE/UFRJ as a partial fulfillment of the requirements for the degree of Master of Science (M.Sc.)

DIRECT-STRENGTH METHOD DESIGN OF SPHERICALLY-HINGED COLD-FORMED STEEL EQUAL-LEG ANGLE COLUMNS

Kathleen Guimarães Santana

June/2018

Advisor: Alexandre Landesmann

Department: Civil Engineering

Due to its complex structural behavior, short-to-intermediate equal-leg angle columns are currently not pre-qualified for the Direct-Strength Method (DSM) design in the North American Specification for Cold-Formed Steel Structures. These members are also excluded from the application of the LFRD resistance factor  $\phi=0.85$ . In light of this issue, there is an effort to incorporate the aforementioned behavioural features into a novel DSM-based design approach, which was shown to predict failure loads for fixed and pin-ended columns with accuracy. Recently, this approach was extended to the spherically hinged support condition. However, there are still no available experimental investigations on cold-formed spherically hinged angle columns. This work consists on an attempt to fill this gap by an experimental study carried out at the Federal University of Rio de Janeiro on the behaviour and collapse of short-to-intermediate spherically hinged cold-formed steel columns. First, the selection of the columns to be tested is detailed, followed by a description of the experimental test set-up and procedure. The experimental results consist on: (i) initial imperfection measurements, (ii) equilibrium paths concerning the applied load to key column displacements, (iii) deformed configurations and (iv) failure loads. Those results are used to validate a shell finite element model previously developed by the authors, with an additional numerical failure data acquisition. Finally, there is a merit assessment of the proposed design approach by comparing experimental to numerical results.

# INDEX

|   |           |
|---|-----------|
| <b>SYMBOLS.....</b>   | <b>ix</b> |
| <b>1 Introduction.....</b>  | <b>1</b>  |
| 1.1 Motivation.....   | 3         |
| 1.2 Objective.....  | 3         |
| 1.3 Outline .....   | 4         |
| <b>2 Literature Review .....</b>  | <b>5</b>  |
| 2.1 Buckling.....   | 5         |
| 2.1.1 Local Buckling.....   | 5         |
| 2.1.2 Global Buckling .....   | 6         |
| 2.2 Direct Strength Method (DSM) .....  | 8         |
| 2.3 DSM-based Design Procedures for Angle Columns .....                       | 11        |
| <b>3 Experimental Investigation.....</b>                                      | <b>33</b> |
| 3.1 Column Selection.....   | 33        |
| 3.2 Column Specimens .....  | 37        |
| 3.3 Mechanical Properties of the Mild Steel.....                              | 39        |
| 3.4 Test Set-Up .....   | 40        |
| 3.5 Displacement Measurements .....   | 42        |
| 3.6 Test Procedure .....  | 43        |
| 3.7 Test Results.....   | 46        |
| <b>4 Numerical Simulations .....</b>  | <b>57</b> |
| 4.1 ANSYS Shell Finite Element Model .....                                    | 57        |
| 4.2 Validation Study .....  | 60        |
| 4.3 Parametric Study – Numerical Failure Loads.....                           | 64        |
| <b>5 Assessment of the Proposed DSM Approach.....</b>                         | <b>68</b> |
| 5.1 Load and Resistance Factor Design (LRFD).....                             | 70        |
| <b>6 Concluding Remarks.....</b>  | <b>72</b> |
| 6.1 Suggestions for Future Work.....  | 73        |
| <b>7 References.....</b>  | <b>74</b> |
| <b>ANNEX A: Spherically-hinged Column Experimental Failure Load Data.....</b> | <b>79</b> |
| <b>ANNEX B: Spherically-hinged Column Numerical Failure Load Data .....</b>   | <b>80</b> |

## SYMBOLS

### Roman upper-case letters

|                |   |
|----------------|---|
| $A$            | cross-section area  |
| $C_\phi$       | calibration coefficient, equal to 1.52 for LRFD   |
| $C_p$          | correction factor that depends on the numbers of tests ( $n$ ) and degrees of freedom ( $m=n-1$ ) |
| $C_w$          | warping constant  |
| $E$            | Young's modulus for steel   |
| $F_m$          | fabrication factor of the material (1.0 for LRFD)   |
| $G$            | shear modulus   |
| $I$            | moment of area  |
| $I_t$          | moment of area related to the section's uniform torsion   |
| $KL$           | effective length of the column  |
| $K_tL$         | effective length related to torsional global buckling   |
| $L$            | nominal length  |
| $M_m$          | mean values of the material (1.10 for LRFD)   |
| $M_n$          | bending capacity  |
| $P$            | axial compression load  |
| $P_{bt}$       | torsional buckling load   |
| $P_{cr}$       | critical buckling load (or bifurcation load)  |
| $P_{cr,D}$     | critical buckling distortional load   |
| $P_{cr,ft}$    | flexural-torsional buckling loads   |
| $P_{crG}$      | critical global buckling load   |
| $P_{crL}$      | critical buckling load  |
| $P_e$          | Euler's flexural buckling load  |
| $P_{ex}$       | critical flexural buckling load   |
| $P_{exz}$      | critical global flexural-torsional buckling load  |
| $P_{ez}$       | critical global torsional buckling load   |
| $P_m$          | average of the $f_u/f_{nftc}$ ratios  |
| $P_n$          | axial predicted failure load  |
| $P_{nG}$       | global failure load   |
| $P_{n,\gamma}$ | design strength   |
| $P_{u,Exp}$    | experimental failure load   |
| $P_{u,Num}$    | numerical failure load  |
| $P_u$          | ultimate strength   |
| $P_y$          | squash load ( $P_y = Af_y$ )  |
| $V_F$          | coefficient of variation of the material factor (0.05)  |
| $V_M$          | fabrication factor (0.10)   |
| $V_P$          | standard deviation of the $f_u/f_{nftc}$ ratios   |
| $V_Q$          | load effect (0.21)  |

### **Roman lower-case letters**

|              |  |
|--------------|--|
| $b$          | wall width   |
| $b_e$        | effective part of the wall width $b$                                 |
| $b_f$        | leg width  |
| $d_H$        | “horizontal” DT measurement  |
| $d_M$        | translation due to major-axis flexure                                |
| $d_m$        | translation due to minor-axis flexure                                |
| $d_V$        | “vertical” DT measurement  |
| $e_0$        | shift of the effective centroid                                      |
| $f_{bf}$     | major-axis flexural buckling stress                                  |
| $f_{bt}$     | torsional buckling stresses  |
| $f_{cre}$    | minor-axis flexural buckling stress                                  |
| $f_{crft}$   | major-axis flexural-torsional buckling stresses                      |
| $f_{crl}$    | critical local buckling stress                                       |
| $f_e$        | elastic buckling stress  |
| $f_{max}$    | maximum longitudinal normal stress                                   |
| $f_n$        | axial buckling stress  |
| $f_{ne}$     | nominal strength against minor-axis flexural failure                 |
| $f_{nle}$    | local/global interactive strength                                    |
| $f_{nfte}$   | nominal strength against interactive failure                         |
| $f_{nfte}^F$ | $f_{nfte}$ for fixed support conditions                              |
| $f_{nfte}^P$ | $f_{nfte}$ for pinned support conditions                             |
| $f_u$        | ultimate stress  |
| $f_y$        | yield stress   |
| $k$          | local buckling coefficient   |
| $r_i$        | internal bending radius  |
| $r_0$        | polar radius of gyration of the cross-section about the shear center |
| $t$          | wall thickness   |

### **Greek letters**

|                 |   |
|-----------------|---|
| $\beta$         | reduction factor                                    |
| $\beta_0$       | target reliability index, equal to 2.5 in LRFD      |
| $\phi$          | LRFD resistance factor                              |
| $\delta_a$      | column axial shortening                             |
| $\lambda_c$     | minor-axis flexural (global) slenderness            |
| $\lambda_D$     | distortional slenderness                            |
| $\lambda_{fte}$ | flexural-torsional slenderness (based on $f_{ne}$ ) |
| $\lambda_G$     | global slenderness                                  |
| $\lambda_L$     | local slenderness                                   |

|                |  |
|----------------|--|
| $\lambda_{le}$ | column slenderness (related to $f_{nle}$ )       |
| $\lambda_{py}$ | plate slenderness calculated at the yield stress |
| $\rho$         | slenderness reduction factor                     |
| $\psi$         | numerical value of the stress ratio              |
| $\sigma_{cr}$  | critical stress                                  |
| $\nu$          | Poisson's ratio                                  |

### **Abbreviations**

|        |   |
|--------|---|
| ABNT   | Brazilian Association of Technical Standards                                    |
| AISI   | American Iron and Steel Institute   |
| ASTM   | American Society for Testing and Materials                                      |
| CFS    | Cold-formed Steel   |
| COPPE  | Alberto Luiz Coimbra Institute for Graduate Studies and Research in Engineering |
| DSM    | Direct Strength Method  |
| DT     | Displacement Transducer   |
| EWM    | Effective Width Method  |
| FEM    | Finite Element Method   |
| GBT    | Generalized Beam Theory   |
| LABEST | Structures Laboratory (at COPPE)  |
| LRFD   | Load and Resistance Factor Design   |
| NAS    | North American Standard   |
| SFE    | Shell Finite Element  |
| SFEA   | Shell Finite Element Analysis   |
| SSRC   | Structural Reliability Research Council   |
| UFRJ   | Federal University of Rio de Janeiro  |
| UTM    | Universal Testing Machine   |

# 1 Introduction

---

For their higher inertia/weight ratio when compared to hot-rolled profiles, cold formed steel (CFS) profiles are widely applicable in civil construction and, therefore, are gaining acceptance in the market due to its many advantages: higher availability for small to large quantities and higher optimization of the profiles in terms of the project. On the other hand, such profiles also present a higher width/thickness ratio, which requires the calculations to consider local, global and, in some cases, even distortional instability modes. Those instability modes must be analysed not only as they singly happen, but also with the possibility of occurring simultaneously.

WINTER [1] and CHILVER [2] were amongst the first researchers to work on experimental and analytical analysis concerning CFS profiles. CHILVER [2] made a compilation of the main discoveries, starting the study of these members at that time.

DUBINA & UNGUREANU [3] elicited that CFS profiles presented a singular behaviour in what concerns to initial geometric imperfections and the interaction phenomena between the instability modes. Combined to the fact that those kinds of steel profiles are markedly slender, this leads to an instability behaviour that differs from the one observed in hot-rolled and welded profiles. Therefore, specific strength curves for CFS profiles were needed, since Eurocode and SSRC (Structural Stability Research Council) procedures would not be fit for this purpose – the curves proposed in those standards were thought for the use in hot-rolled and welded profiles design, but were also applied on the design of CFS profiles.

The high slenderness presented in CFS structures was, according to SCHAFER [4] the cause of the frequent occurrence of buckling stresses far inferior to the yield strength.

CHODRAUI [5] points up some of the peculiar characteristics of CFS profiles, namely:

- (i) It is possible to obtain structures that are more economic for short spans (higher inertia/weight ratio).
- (ii) Non-usual cross-section configurations can be achieved due to the easy folding process of the plates.

- (iii) High width/thickness ration, which requires local and distortional buckling considerations, besides post-buckling strength analysis.
- (iv) High possibility of interaction between instability modes.
- (v) Residual stresses distribution caused by the cold forming process differs from the ones caused by the cooling of the hot-rolled profiles.
- (vi) Connections need to be carefully analysed due to the small thickness of the walls.

Other aspects in which cold formed steel profiles differ from hot-rolled and welded profiles are noted by YU [6]:

- (i) Cold-formed steel profiles normally present low stiffness to torsion, for it is related to  $t^3$ , considering that the centroid does not generally coincide with the shear centre, as the profiles are often mono-symmetric.
- (ii) The effective length method for the local instability analysis in cold-formed profiles leads to recalculations of geometrical properties of the cross-section, with centroid translations, which is not predicted in the design of hot-rolled and welded profiles.
- (iii) Web-crippling takes place due to not using stiffeners in cold-formed profiles' webs.
- (iv) Plastic analysis is not usual in cold-formed profiles due to the high width/thickness ratio, which conducts to a local instability mode prior to the plasticisation of the cross-section.

Specifically in what concerns to angle sections, the elastic stability analysis points to a coincidence of the local mode with the torsional global mode, which can be better classified as the global flexural-torsional instability mode. This fact raised doubts related to the consideration of the interactions between those instability modes in the design procedures, as it is possible to note in [7].

In this work, analyses were carried in order to best assess this theme, aiming to validate a novel approach based on the Direct Strength Method to comprise angles with spherical supports.

## 1.1 Motivation

Due to its structural particularities, the behaviour of cold-formed steel angles has been the focus of several recent numerical and experimental researches. Aiming to obtain the ultimate load capacity of those angles, a considerable number of authors performed tests that allowed assessing the quality and precision of the standards' predictions.

In chronological order, the experimental tests were performed and published by PRABHU [8], WILHOITE *et al.* [9], POPOVIC *et al.* [10], YOUNG [11], CHODRAUI *et al.* [5], MAIA *et al.* [12], MESACASA JR. [13] and LANDESMANN *et al.* [14]. Since the first experimental results, it was clear that the ultimate loads differed from the standard procedures, which would apply the Effective Width Method (EWM). Consequently, authors started elaborating procedures to predict the ultimate load, aiming a design approach that was precise and would closely reflect the results obtained experimentally.

In light of these happenings, the Direct Strength Method (DSM) was developed and gained attention, being currently adopted by ABNT NBR 14762:2010 [15], as an alternate procedure to determine the ultimate loads of cold-formed profiles. Nevertheless, angles were not included in the DSM calibration, due to the fact that their experimental results would still differ from this design procedure.

Therefore, studies sought to adapt the DSM in order to include angles or adapt the application of the EWM for that end. The works of RASMUSSEN [7], YOUNG [11], SILVESTRE *et al.* [16], DINIS & CAMOTIM [17], [18] document those efforts.

The procedures developed by DINIS & CAMOTIM ([17] and [18]) are especially important, for they include flexural-torsional design curves in order to replace the local resistance curves for determining the profile's ultimate load. Nonetheless, additional numerical and an experimental validation are still needed before the design approach proposed in their study reaches the codification stage results in order to validate the procedure for a spherically-hinged support condition [18].

## 1.2 Objective

Considering all that was exposed above, there is still an expressive amount of research to be performed in what concerns CFS angles. Moreover, taking into account that there are slenderness ranges unexplored in this research area, it is of great importance that a wide series of numerical analyses are carried, in order to guarantee the reliability

of the design approaches recently proposed. The present work aims at thoroughly studying the subject, carrying experimental tests and performing additional numerical analyses of equal-leg cold-formed angle columns subjected to axial loading, with pinned supports that simulate spherical hinges, for short-to-intermediate lengths of columns, exhibiting a failure mode of flexural-torsional instability and presenting a wider slenderness range than the one previously reached by the predecessors of this work. This is done as to provide a better understanding of the buckling and post-buckling behaviour of angle columns, as well as to validate a new DSM design approach proposed in [18].

### **1.3 Outline**

Chapter 2 presents the literature review on the structural behaviour of cold-formed equal-leg angle columns subjected to axial loading and the design procedures developed until 2017. Next, Chapter 3 comprises the experimental campaign carried to reach the goals listed in the previous subsection, by demonstrating the (i) method chosen to select the columns tested, (ii) the design of the spherical supports, (iii) the initial geometrical imperfection acquisition procedure, (iv) the test set-up and (v) the procedure followed in order to carry the experimental tests.

Chapter 4 comprises a numerical analysis, which contains a parametric study involving the simulation using 16 different characteristic strengths ( $f_y$ ) and the validation of the experimental tests through a FEM analysis. Chapter 5 is an assessment of the DSM approach proposed in [18].

Finally, Chapter 6 is an assembly of the conclusions achieved in this study, with suggestions for further analyses on this area.

## 2 Literature Review

---

### 2.1 Buckling

Typically, CFS profiles exhibit three instability configurations: global (flexural, torsional and flexural-torsional), distortional and local. For equal-leg angle profiles, Figure 2.1 demonstrates the main deformation modes observed. According to the literature, there are three global and two local modes which present highest significance in the study of CFS profiles: (a) major-axis (global), (b) minor axis (global), (c) torsional (global), (d) symmetrical (local) and (e) asymmetrical (local).

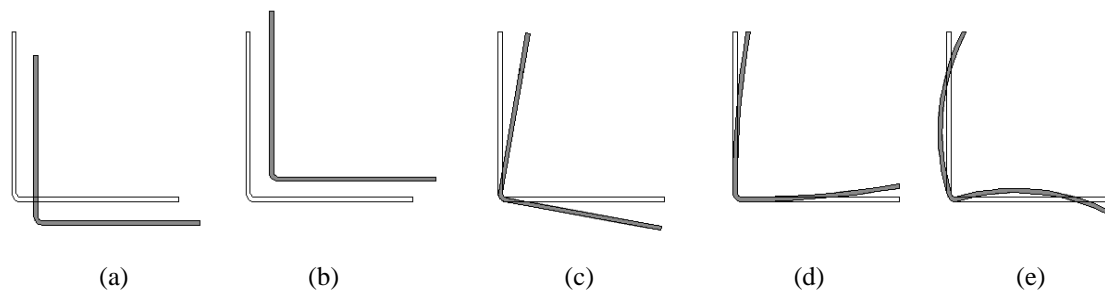


Figure 2.1: Cold-formed profiles buckling modes [20].

#### 2.1.1 Local Buckling

The local buckling mode alters the column section-wise, allowing only the legs of the profile to present a certain "waving", which will not alter the position of the external nodes. Thus, while the plates exhibit loss of stability, the profile's edges remain straight. This can be assumed to be a plate instability mode and Eq. 2.1 describes the critical stress observed here, where  $\sigma_{cr}$  is the critical stress,  $k$  is the local buckling coefficient,  $\nu$  is the poisson coefficient,  $b$  is the component elements width and  $t$  is the plate thickness.

$$\sigma_{cr} = \frac{k \cdot \pi^2 \cdot E}{12(1-\nu^2)} \cdot \left(\frac{t}{b}\right)^2 \quad (2.1)$$

## 2.1.2 Global Buckling

Cold formed steel profiles present global buckling in three different modes: minor-axis flexure, flexural-torsional and torsional buckling. Nevertheless, the torsional buckling does not occur in mono-symmetric profiles (such as angle columns) alone.

### *a) Global flexural buckling*

Global flexural buckling is caused by the column's lateral deflection around one of the main inertia axis, without shape loss of the cross-section. Eq. 2.2 shows the classic Euler's flexural buckling load, which is used to calculate the axial buckling load, where  $P_e$  is the Euler's flexural buckling load,  $EI$  is the cross-section stiffness ( $E$  is the Young's modulus for steel and  $I$  is the main moment of inertia) and  $kL$  is the effective length of the column.

$$P_e = \frac{\pi^2 EI}{(kL)^2} \quad (2.2)$$

### *b) Global torsional buckling*

This type of buckling is never purely observed in mono-symmetric sections, it may only occur in doubly symmetric profiles, with low torsional rigidity [20]. When global torsional buckling happens, the whole cross section presents a rotation around the shear centre. Eq. 2.3 presents the critical load for this kind of instability to occur, where  $r_o^2$  is the polar radius of gyration of the cross-section about the shear centre,  $C_w$  is the warping constant,  $G$  is the shear,  $I_t$  is the moment of area related to the section's uniform torsion and  $k_t L$  is the effective length related to torsional global buckling.

$$P_{ez} = \frac{1}{r_o^2} \left[ \frac{\pi^2 EC_w}{(k_t L)^2} + GI_t \right] \quad (2.3)$$

### c) Global flexural-torsional buckling

The flexural-torsional mode of global buckling is determined by the cross section's rotation around the shear centre and the lateral deflection around one of the main inertia axis. This kind of buckling occurs mainly in compressed columns presenting asymmetrical and mono-symmetrical cross sections, and in those presenting a high and torsion-free length.

The theory of elastic stability [21] established an equation to express the axial flexural-torsional buckling load, which is written in Eq. 2.4, where  $P_{exz}$  is the flexural-torsional buckling load,  $P_{ex}$  is the column's flexural buckling strength about the  $x$  axis and  $x_0$  is the distance between the shear centre and the main axes of the cross-section.

$$P_{exz} = \frac{P_{ex} + P_{ez}}{2 \left[ 1 - (x_0 / r_0)^2 \right]} \left[ 1 - \sqrt{1 - \frac{4P_{ex}P_{ez} \left[ 1 - (x_0 / r_0)^2 \right]}{(P_{ex} + P_{ez})^2}} \right] \quad (2.4)$$

Angle profiles submitted to compression exhibit two buckling modes: flexural-torsional, for small-to-intermediate lengths, and global minor-axis flexural buckling for longer lengths [12]. The following figure shows the curve  $P_{cr}/P_y$  obtained by CHODRAUI [5] in his work, where two different buckling modes can be observed.

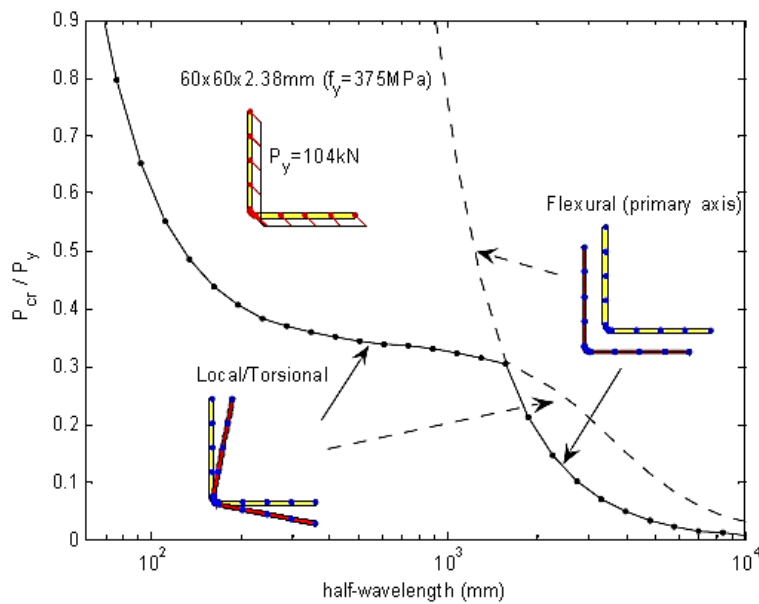


Figure 2.1:  $P_{cr}/P_y \times L$  curve of a cold-formed steel angle column [5].

The flexural-torsional mode is represented by the first curve, where a plateau can be observed, and it ends as the second curve begins. The second curve represents the global minor axis flexure buckling.

Due to the need of reaching a better understanding of the structural behaviour of angle profiles, DINIS *et al.* [22] studied CFS angles buckling and post-buckling states. They used the computational code GBTUL [23], based on the Generalized Beam Theory (GBT), to simulate two kinds of end-support: (i) pinned, in which the minor-axis flexure is free, although major-axis rotation is restricted (the so called P-columns) and (ii) fixed (so called F-columns). GBTUL allowed measuring the modal percentage in the critical buckling load, while the software ABAQUS was used to analyse the post-buckling state.

## 2.2 Direct Strength Method (DSM)

For their singularly slender thin-walled open cross-sections, cold-formed steel members are particularly vulnerable to instability phenomena, namely local, distortional and global (flexural or flexural-torsional) buckling. Thus, there was an urgent need to incorporate considerations regarding these phenomena in cold-formed steel specifications. As a result of this necessity, the Direct Strength Method (DSM) started to take form.

Previously, cold-formed steel members were designed through the “Effective Width Method”, which is still present in standards worldwide. Nonetheless, the emerging of new and more complex cross-sections, in addition to the discovery of the distortional buckling phenomena in lipped cross-sections led to progress towards the DSM development. Additionally, fruitless attempts to efficiently predict distortional failures by means of an effective-width method have shown the importance of a new and more rational approach.

In light of these happenings, the DSM was rapidly incorporated in design codes, for it provided a unified approach for cold-formed steel members design under compression and bending.

The procedure was first proposed by SCHAFER & PEKÖZ [24] in order to develop a new design approach for cold-formed steel beams. The result of that research is shown in Eq. 2.5, where  $b_e$  is the effective component elements width  $b$  and  $f_{crD}$  is the distortional stress.

$$\frac{b_e}{b} = \left( \frac{f_{crD}}{f_y} \right)^{0.4} \left[ 1 - 0.15 \left( \frac{f_{crD}}{f_y} \right)^{0.4} \right] \quad (2.5)$$

This equation is a modified version of the one previously proposed by HANCOCK *et al.* [24]. The DSM then proposed was shown to be accurate and reliable for predicting the ultimate strength of cold-formed steel beams failing in distortional modes. In consequence of the later on research activity conducted by SCHAFER [26]-[29], similar applications of the DSM followed, namely (i) cold-formed steel columns with local, distortional and global failure modes and (ii) cold-formed steel beams with local and global failure modes.

However, as much as the Direct Strength Method was proven to be reliable for most cold-formed steel members, it did not comprise angle sections, due to its singular structural behaviour. This fact led a number of researchers to investigate this specific geometry, aiming to adequate the DSM in a way that it is able to predict angle sections as well. Until the last few years, the most fruitful attempts to design equal-leg angle columns through a DSM approach were the ones reported by YOUNG [11], for fixed-ended columns, (ii) RASMUSSEN [7], for pin-ended columns and SILVESTRE *et al.* [16], for both pinned and fixed-ended. Those efforts comprised the use of the codified DSM curve or a slight variation of it. More recently, DINIS *et al.* [22] and MESACASA *et al.* [30] provided evidence that the failure of angle columns is due to interactions between two global modes (major-axis flexural torsional and minor-axis flexural). This unique behaviour was found to have extremely little to do with local deformations, in contrast to what was once believed.

The Effective Width Method proposed by VON KARMAN *et al.* [31] and calibrated by WINTER [32], is present in the current revisions of nearly all codes worldwide for the design of cold-formed steel members. It was not only until the cross-sections became more complex and distortional buckling was discovered that the Direct Strength Method gained popularity. The DSM was first codified in North America [33], in 2004, and was then included in the Australian/New Zealand Standard [34]. The Brazilian Standard [15] also included the DSM a few years later.

First, NAS [33] allowed using the DSM to determine the nominal axial and flexural strengths of any cold-formed steel columns and beams. Nevertheless, there is a

distinction made between “pre-qualified” and “non-pre-qualified” members, as different safety and resistance factors are employed. The pre-qualified cross-section shapes are lipped channels (plain and web-stiffened) and zed, hat and rack, hat (flange stiffened) and trapezoid (web-flange-stiffened) deck cross-sections.

For global failure estimates, the 1996 AISI Specification [35] was adopted, in which the expressions on Eq. 2.6 figure:

$$P_{nG} = \begin{cases} P_y 0.658^{\lambda_G^2} & \text{for } \lambda_G \leq 1.5 \\ P_y \frac{0.877}{\lambda_G^2} & \text{for } \lambda_G > 1.5 \end{cases} \quad (2.6)$$

Where  $\lambda_G = (P_y/P_{crG})^{0.5}$  is the global slenderness, and  $P_{crG}$  is the critical global (flexural, torsional or flexural-torsional) buckling load.

SCHAFFER [24] also proposed replacing  $P_y$  and  $\lambda_L = (P_y/P_{crL})^{0.5}$  by  $P_{nG}$  and  $\lambda_L = (P_y/P_{nG})^{0.5}$  to account for the possible occurrence of local-global interactive failures, resulting in the expression in Eq. 2.7.

$$P_{nL} = \begin{cases} P_{nG} & \text{for } \lambda_L \leq 0.776 \\ P_{nG} \left( \frac{P_{crL}}{P_{nG}} \right)^{0.4} \left[ 1 - 0.15 \left( \frac{P_{crL}}{P_{nG}} \right)^{0.4} \right] & \text{for } \lambda_L > 0.776 \end{cases} \quad (2.7)$$

SCHAFFER [24] demonstrated that this DSM approach for columns was reliable, provided quite good estimates for the specimens tested in laboratory. Figure 2.2 shows strength curves proposed by SCHAFFER [24] in comparison to experimental tests. It is possible to observe that the curves represent the tests quite fairly, with the exception of the predictions obtained by WINTER [32], which were found to be too conservative.

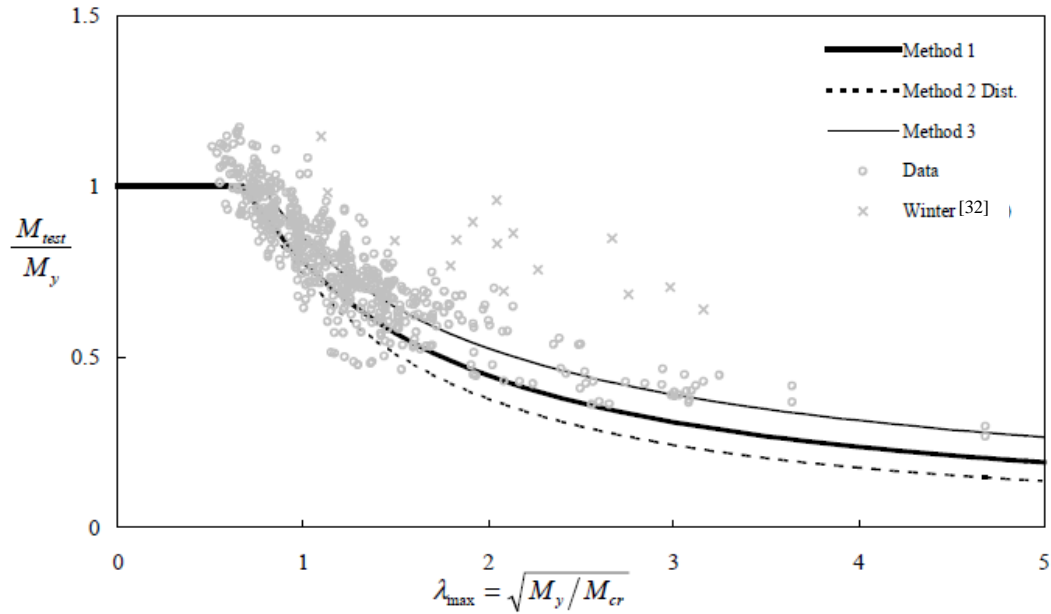


Figure 2.2: Strength curves obtained in [24] and experimental data. [24]

## 2.3 DSM-based Design Procedures for Angle Columns

### 2.3.1 Popovic *et al.* (1999)

In 1999, POPOVIC *et al.* [10] performed compression tests on 12 fixed-ended and 18 pin-ended cold-formed steel angle columns. Their aim was to provide enough test data to propose design rules for cold-formed angles that could be used in a DSM-based design procedure for those members. In order to achieve this goal, they intended to compare test results to existing standard procedures.

The failure mode of all stub column specimens tested in their work was inelastic local buckling of the legs. It was noted that the more slender sections would buckle earlier than the less slender ones. The most compact section tested was the only one to present a yield plateau.

The long column tests were performed by means of a test rig especially designed and built for this end. A servo-controlled hydraulic actuator was employed as to axially load the column specimens in the compression tests. The pin-ended support bearings were set to allow rotations about the minor axis and to restrain rotations about the major axis,

torsion and warping. The fixed-ended support bearings were set to keep both major and minor-axis rotations, as well as torsion and warping restrained. The specimens with both pinned and fixed-ended supports failed in flexural, flexural-torsional and coupled flexural-torsional modes. Figure 2.3 exhibits the on-set collapse of a column failing in coupled flexural/flexural-torsional mode.

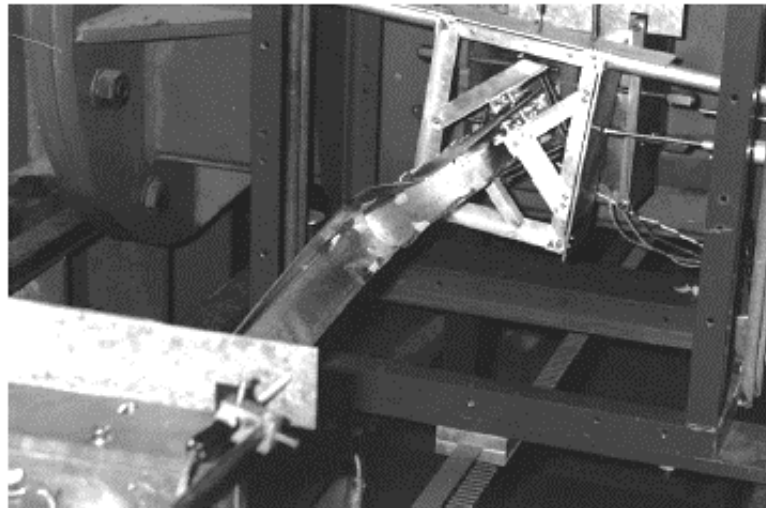


Figure 2.3: Coupled Flexural/Flexural-Torsional failure mode [10].

By comparing the test results and the design rules [35], POPOVIC *et al.* [10] reached the following conclusions:

- (i) The stub column ultimate strengths obtained based on AISI [35] were found to be increasingly conservative, as the slenderness of the section raises.
- (ii) The additional moment equal to  $L/1000$  about the minor axis causing compression in the tips of the angle legs should only be employed in slender sections.
- (iii) For slender sections, the additional eccentricity between the centroids of the gross and effective sections was not necessary, as it appeared to be too conservative).

### 2.3.2 Young (1999)

YOUNG [11] performed tests on fixed-ended cold-formed steel angle columns considered slender. The previous test results obtained by POPOVIC *et al.* [10], as well as estimations obtained based on the American Specification (AISI 1996) [35] and Australian/New Zealand Standard (AS/NZ 1996) [34] for cold-formed steel structures were used for comparison with the ones obtained in [11]. As a result of this study, new design equations for concentrically loaded fixed-ended compression members of slender and non-slender angle sections were proposed in [11].

For the conduction of the experimental tests, two steel end plates were welded to the ends of the specimens. A servo-controlled hydraulic testing machine was employed in order to axially load the column in the compression tests. The different lengths of the specimens were assessed by adjusting a movable upper end support. A rigid flat bearing plate was attached to the upper end support, and the top end plate of the specimen was bolted to the rigid flat bearing plate, which was restrained against minor and major-axis rotations, torsion and warping. The set-up was equivalent to a fixed-ended support condition.

Three tests were retaken and the results for those repeated tests were very close to their final test values. This was important in order to demonstrate reliability on test results. The failure modes presented by the columns comprised local buckling, flexural buckling and flexural-torsional buckling. The failure modes were obtained by observing each deformed configuration of the specimens at the ultimate load phase. The majority of the columns failed in an interactive flexural and flexural-torsional buckling mode, with the exception of some of the stub columns, which failed by local buckling. Only one column failed by flexural-torsional buckling

Considering the conclusions in [37], according to which the method then recommended was too conservative, it was suggested in [11] that the design procedure should be completely reformulated for angles bent about a parallel leg. Also, considering that the column design strengths are generally not conservative for slender sections, but conservative for non-slender sections, DSM-based design expressions were proposed by YOUNG [11], as shown in Eq. 2.8.

$$f_n = \begin{cases} (0.5^{\lambda_c^2}) f_y & \text{for } \lambda_c \leq 1.4 \\ \left(\frac{0.5}{\lambda_c^2}\right) f_y & \text{for } \lambda_c > 1.4 \end{cases} \quad \text{in which} \quad \lambda_c = \sqrt{\frac{f_y}{f_e}} \quad (2.8)$$

The values of 0.658 and 0.877 previously stated in the main standards were adjusted to 0.5, while the non-dimensional slenderness ( $\lambda_c$ ) was set to 1.4, aiming at a smooth transition of the elastic and inelastic buckling stresses. The column design strengths proposed were calculated for all sections and the design strengths were calculated using the average cross-section dimensions and material properties measured. The calculations were also taken considering the base metal thickness.

The design equation proposed in [11] (see Eq. 2.8) required some small modifications of the critical inelastic and elastic buckling stress equations in the NAS Specification, AISI Specification [35] and AS/NZ Standard [34] by that time. The design strengths proposed were shown to be conservative for all column lengths considered in his work.

### 2.3.3 Rasmussen (2005)

In light of research's products until 2005 ([39] and [41]), RASMUSSEN [19] combined improved effective width equations previously proposed with a simple equation for the eccentricity ( $e_0$ ) induced by the shift of the effective centroid to propose another design approach for slender cold-formed angles

The provisions of the NAS Specification [35] and AS/NZS4600 [34] led to conservative estimates of the effective width. Consequently, the section modulus of the effective cross-section in bending and the bending strength predictions turned to be too conservative. The research of BAMBACH & RASMUSSEN ([39] and [41]) resulted in a new effective width approach for unstiffened members subjected to in-plane bending.

The effective width equation for the situation when bending causes a compressive stress at the unsupported edge ( $f_1$ ) in angles, the effective width can be assessed by using a slenderness reduction factor  $\rho = b/w$ , given by Eq. 2.9.

$$\rho = \begin{cases} 1 & \text{for } \lambda_p \leq 0.673(1+\psi) \\ \frac{(1+\psi) \left( 1 - \frac{0.22(1+\psi)}{\lambda_p} \right)}{\lambda_p} & \text{for } \lambda_p > 0.673(1+\psi) \end{cases} \quad (2.9)$$

where  $\psi = |f_2/f_1|$ ,  $k = 0.57 + 0.21\psi + 0.07\psi^2$  is determined for  $f = f_1$  and  $f_{cr} = \sigma_{cr}$  (see Eq. 2.1).  $\psi$  is the numerical value of the stress ratio and it is approximately equal to the unity for equal-leg angles in bending. Thus,  $k=0.85$ .

When bending causes a compression stress ( $f_1$ ) at the supported edge, it is possible to obtain the effective width by means of a slenderness reduction factor  $\rho$  given by Eq. 2.10 for  $\psi \geq 1$ .

$$\rho = \begin{cases} 1 & \text{for } \lambda_p \leq 0.673 \\ \frac{(1-\psi) \left( 1 - \frac{0.22}{\lambda_p} \right)}{\lambda_p} + \psi & \text{for } \lambda_p > 0.673 \end{cases} \quad (2.10)$$

Figure 2.10 illustrates the difference between compression at the supported and at the unsupported edges.

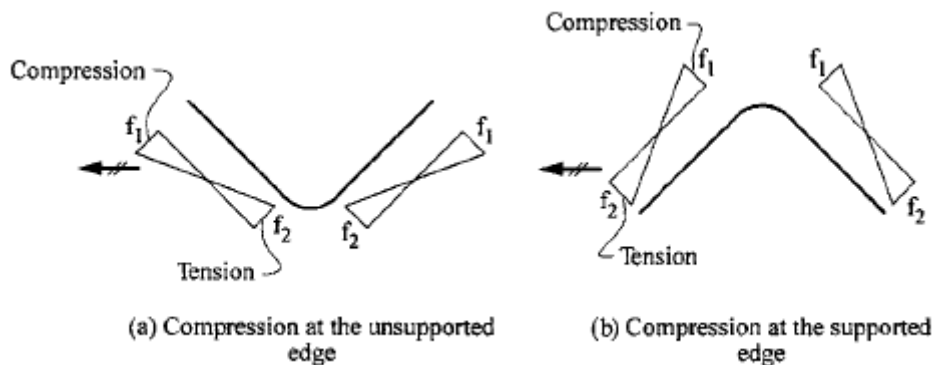


Figure 2.10: Definition of the design stresses  $f_1$  and  $f_2$  [19].

To account for the shift in the effective centroid, the NAS Specification [35] and AS/NZS4600 [34] determine the calculation of the eccentricity as the distance between the centroids of the gross and effective cross-sections. In the case of equal-leg angles in compression, the condition at the corner is exactly equivalent to the one of a simple support, and the stress distribution is found from Stowell's classical solution [42]. RASMUSSEN [19] presents an accurate estimate of the shift of the effective centroid of an equal-leg angle, given by Eq. 2.12.

$$e_0 = \begin{cases} 0 & \text{for } \lambda_{py} \leq 1.22 \\ \frac{5\lambda_{py} - 1.22}{16\sqrt{2}\lambda_{py} - 0.22} & \text{for } \lambda_{py} > 1.22 \end{cases} \quad (2.12)$$

where  $\lambda_{py} = \sqrt{f_y/f_{cr}}$  is the plate slenderness calculated at the yield stress,  $e_0$  is the shift of the effective centroid and  $f_{cr} = \sigma_{cr}$ , which is the critical buckling stress.

RASMUSSEN [19] used the experimental results of POPOVIC *et al.* [10] and WILHOITE *et al.* [9] as parameters of comparison to the NAS Specification [35] and AS/NZS4600 [34], in order to assess the design strength. The design strengths (NAS [35] and AS/NZS4600 [34]) were found to be unquestionably lower than the test strengths at short and intermediate lengths, partly because the torsional (local) buckling mode is considered when determining the axial capacity ( $P_n$ ) and the bending capacity ( $M_n$ ), as well as in the effective area's determination. RASMUSSEN [19] suggested a more efficient approach by ignoring the torsional mode in the  $P_n$  and  $M_n$  determination, and to use the effective area in  $P_n$  calculations. That means the elastic-buckling stress ( $f_e$ ) must be taken as the minor-axis flexural buckling stress and the bending capacity becomes the section capacity.

Although an accurate design model had been achieved, a more direct column design approach was proposed for the case when the load is applied at the centroid of the gross cross-section. In the limit where the column length  $L$  tends to 0, the interaction for a column loaded through the gross section centroid is defined by Eq. 2.13

$$\frac{P}{P_{n0}} + \frac{e_0 P}{M_n} = 1 \quad \text{in which} \quad P_{n0} = A_e \cdot f_y \quad (2.13)$$

Therefore, Eq. 2.14 is obtained.

$$P_{n0,\gamma} = \beta P_{n0} \quad (2.14)$$

where the reduction factor  $\beta$  is obtained by Eq. 2.15.

$$\beta = \frac{1}{1 + \frac{e_0 P_{n0}}{M_n}} \quad (2.15)$$

The reduction factor accounts for the effect of the shift of the effective centroid at short lengths ( $L \rightarrow 0$ ). It was also expressed in [7] and [19] in terms of  $\lambda_{py}$ , by means of a simplified expression given by Eq. 2.16.

$$\beta = \begin{cases} 1 & \text{for } \lambda_{py} \leq 1.22 \\ \frac{0.68}{(\lambda_{py} - 1)^{1/4}} & \text{for } \lambda_{py} > 1.22 \end{cases} \quad (2.16)$$

A simple column design procedure could be obtained in [11] by considering the application of the reduction factor to all lengths considered, by the use of Eq. 2.17.

$$P_{n,\gamma} = \beta P_n \quad (2.17)$$

Where  $P_n$  is obtained as  $f_n A_e$ . The design strength ( $P_{n,\gamma}$ ) was compared to WILHOITE *et al.* [9] (see Figure 2.11 (a)) and POPOVIC *et al.* [10] (see Figure 2.11 (b)) test results and it was found to be in close agreement with the beam-column design model proposed in [19].

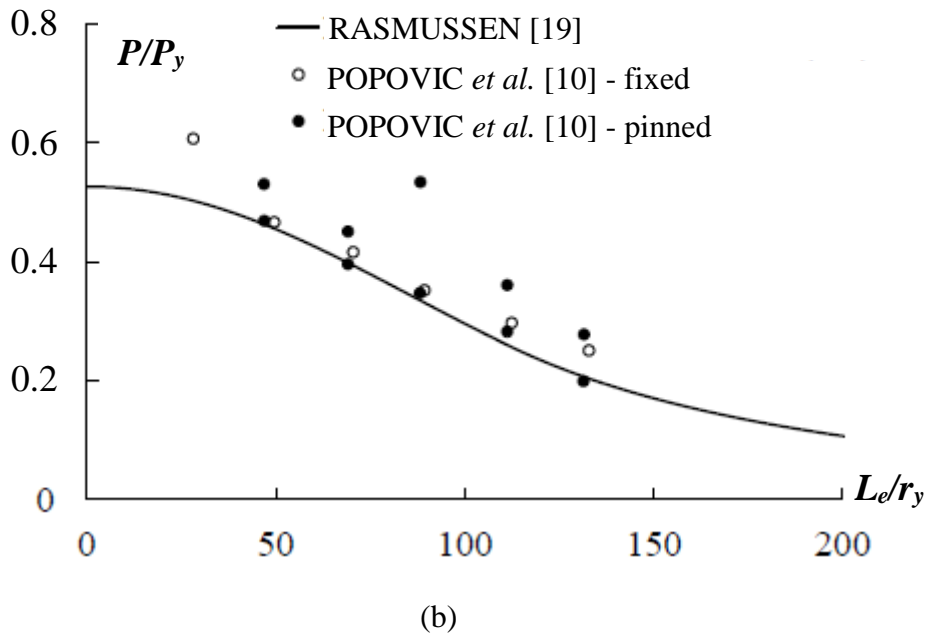
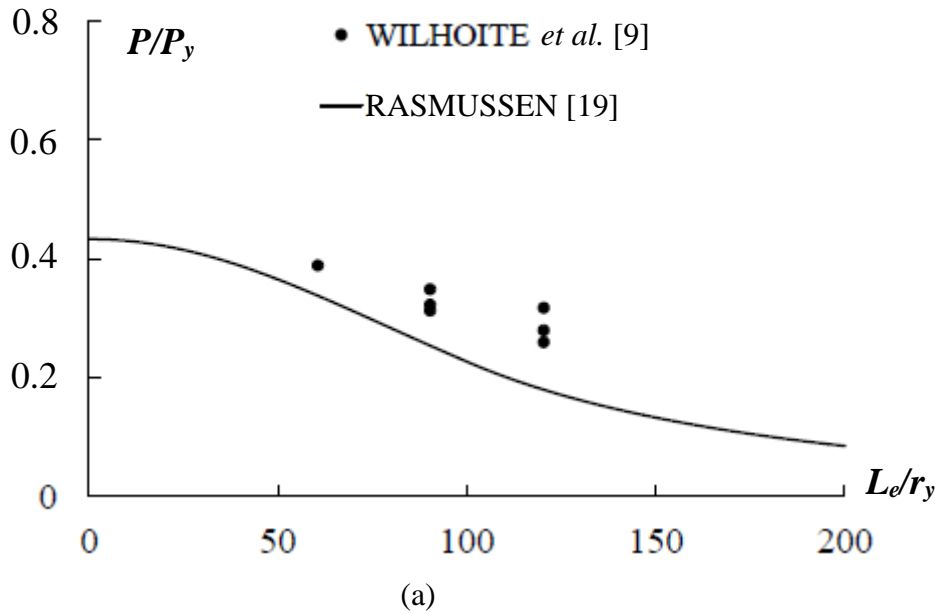


Figure 2.11: Comparison of column design strength ( $P_{n,\gamma} = \beta P_n$ ) with tests (a) in [9] (equal-leg angle sections) and (b) in [10] (fixed and pinned equal-leg angle sections).

In conclusion, RASMUSSEN [19] demonstrates that an accurate design model can be achieved by: (i) neglecting torsional buckling in determining the compression and bending member strengths, (ii) application of the recently developed effective width equations for unstiffened elements under stress gradient for the flexural section capacity calculation, and (iii) assessment of the shift of the effective centroid from a simple equation that is based on the post-buckling stress distribution.

### 2.3.4 Silvestre *et al.* (2013)

In view of the investigations, conducted by means of Generalized Beam Theory (GBT) and SFEA (shell finite element analysis), which presented another point of view on how to differentiate local and global buckling in equal-leg angle columns, SILVESTRE *et al.* [16] reported the numerical and experimental results of their work aiming to develop a rational DSM-based design approach for short-to-intermediate equal-leg angle columns. Their analysis considered fixed and pin-ended columns, but with end section secondary warping prevented.

SILVESTRE *et al.* [16] gathered the experimental results obtained by POPOVIC *et al.* [10], YOUNG [11], and MESACASA Jr. [13] for fixed-ended columns. For pin-ended, were assembled the tests by WILHOITE *et al.* [9], POPOVIC *et al.* [10], CHODRAUI *et al.* [5], and MAIA *et al.* [12].

For the numerical analysis, the software ABAQUS [43] was used, by adopting column discretization into fine 4-node element meshes and modelling the column supports by fully attaching the end sections to rigid end-plates, assuring prevented secondary warping and local displacement/rotation. The torsional rotations were restrained in both fixed and pin-ended supports by preventing (i) both the major and minor-axis flexural rotations (fixed condition), or (ii) preventing only the major-axis flexural rotations (pinned condition).

The rational DSM-based approach then proposed by SILVESTRE *et al.* [16] followed the criteria listed below:

- (i) Adoption of different procedure/design curves in order to predict the ultimate strength of fixed and pin-ended columns, labeled as DSM-*F* (fixed) and DSM-*P* (pinned).
- (ii) The procedure for DSM-*F* combines the global strength curve suggested in [11] with the current DSM design curve for local/global interactive failure.
- (iii) The procedure for DSM-*P* also combines the curve proposed by YOUNG [11] with proposed/new DSM curve for interactive local/global failure, defined by Eq. 2.18.

$$f_{nle} = \begin{cases} f_{ne} & \text{for } \lambda_{le} \leq 0.71 \\ f_{ne} \left( \frac{f_{crl}}{f_{ne}} \right) \left[ 1 - 0.25 \left( \frac{f_{crl}}{f_{ne}} \right) \right] & \text{for } \lambda_{le} > 0.71 \end{cases} \quad (2.18)$$

with  $\lambda_{le} = \sqrt{\frac{f_{ne}}{f_{crl}}}$

Where  $f_{nle}$  is the local/global interactive strength,  $f_{ne}$  is the global strength, obtained by Eq. 2.8, and  $f_{crl}$  is the critical local buckling stress.

From the work developed in [16], SILVESTRE *et al.* [16] reached the following conclusions:

- (i) The DSM-*F* approach led to quite accurate estimates of the fixed-ended column experimental ultimate strength values. The approach proposed by YOUNG [11] was significantly more conservative.
- (ii) The DSM-*F* procedure resulted in fairly precise estimations of the fixed-ended column numerical ultimate strengths.
- (iii) The DSM-*F* approach also led to generally accurate but largely scattered predictions of the pin-ended column experimental ultimate strengths. On the other hand, 16 out of 37 estimations presented errors that were greater than 20%: this happened due to the not accounting for the effective centroid shift effect. The DSM-*P* procedure, however, led to results significantly accurate and safe, although quite scattered, to predict pin-ended columns' experimental ultimate strengths. In comparison, RASMUSSEN [44] achieved more conservative, though marginally less scattered, results for the ultimate strength estimates applying his design approach.
- (iv) The DSM-*F* approach estimated the pin-ended column numerical ultimate strengths quite weakly: those are mostly largely overestimated. Conversely, the DSM-*P* procedure resulted on slightly conservative predictions, which presented considerably low scatter.
- (v) The ultimate-to-predicted stress ratios for both pin-ended and fixed-ended columns presented a fair scatter.
- (vi) The ultimate-to-predicted ratios for the fixed-ended columns were diffused on a quite extended local/global slenderness spectrum, for the pin-ended columns those values were mainly grouped in a restricted local/global

slenderness range ( $0.5 < \lambda_{le} < 1.5$ ); falling outside that space were only the numerical results. In order to assign the DSM-*P* procedure, additional experimental tests on pin-ended columns with a wider slenderness range were still needed. It was also highlighted that most of the numerical ultimate strengths associated with  $\lambda_{le}$  values were underestimated by the DSM-*P* procedure. Figure 2.12 shows the  $f_u/f_{nle}$  vs.  $\lambda_{le}$  plots for the DSM-*F* and DSM-*P* procedures.

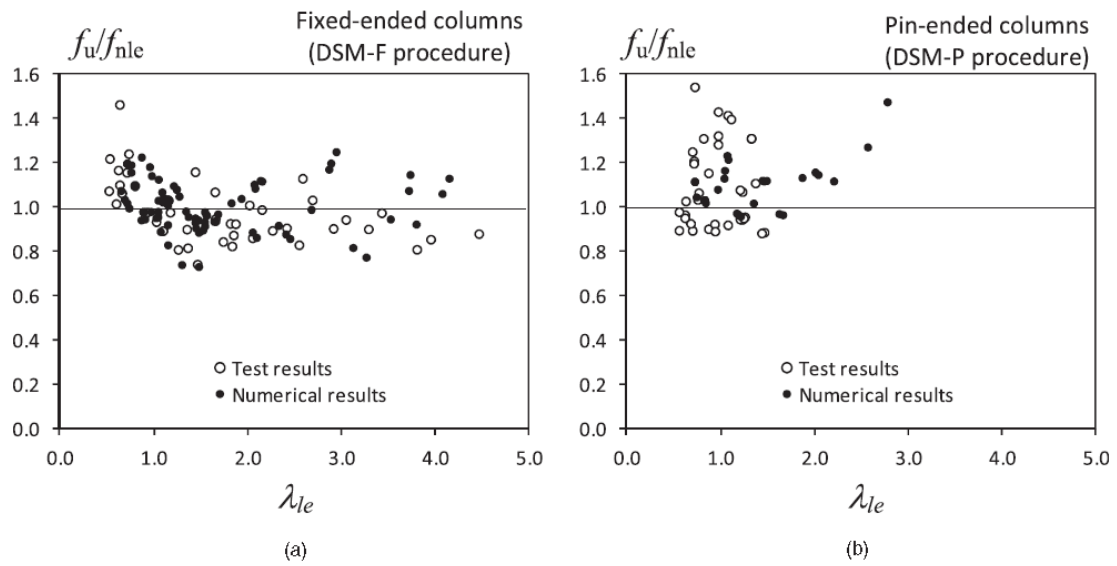


Figure 2.12: Variation of the  $f_{nle}/f_u$  with  $\lambda_{le}$  for the (a) DSM-F and (b) DSM-P procedures [16].

The design approach suggested in [16] provided considerably precise estimations for the ultimate strength of a fairly wide column slenderness range and presented a proposal which stood up to the level of the ones previously exposed on the literature for angle columns up to that year. Additionally, it was shown that the LRFD resistance factor adopted in [33] could be safely employed within the use of the proposed design approach.

### 2.3.5 Dinis & Camotim (2015)

DINIS & CAMOTIM [17] presented an approach development on fixed-ended and pin-ended short-to-intermediate equal-leg angle columns subjected to uniform compression as a continuity of an effort by a number of researchers (*e.g.* [16], [22]) to propose more rational design approaches based on the DSM which would include angles. They developed a set of flexural-torsional strength curves and proposed a DSM design approach for fixed-ended (*F*) angle columns. In what concerns to pin-ended (*P*) angle columns, the shift of the effective centroid effects had to be quantified before its design approach could be proposed.

In order to propose the flexural-torsional strength curves, the failure loads of 170 columns continuously restrained against minor-axis flexure and torsion were determined. All the columns analysed were fixed-ended and selected to ensure a wide coverage of flexural-torsional slenderness ( $\lambda_{fte}$ ) (see figure 2.13 (a)).

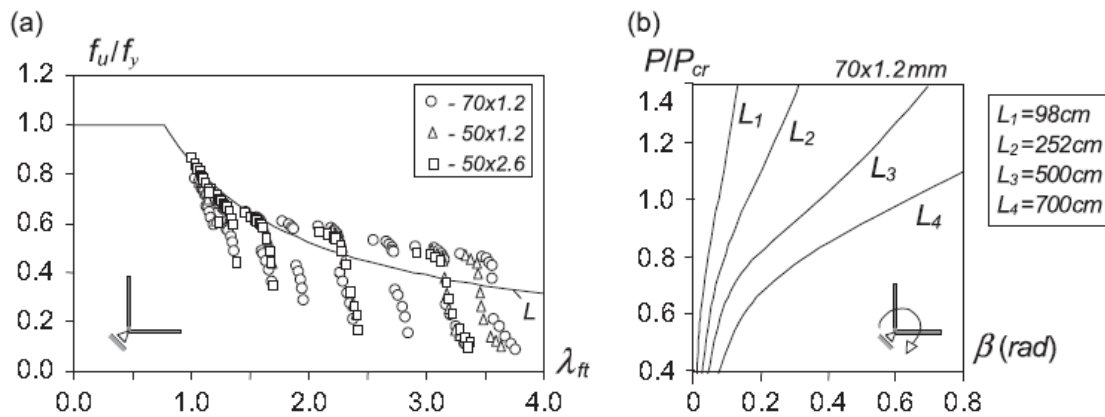


Figure 2.13: (a) Plot of the column flexural-torsional ultimate strength ratios  $f_u/f_y$  against  $\lambda_{ft}$  and (b) elastic equilibrium paths  $P/P_{cr}$  vs.  $\beta$  of the fixed-ended columns [17].

Figure 2.13 shows the  $f_u/f_y$  vs.  $\lambda_{ft}$  plots. The results obtained in [17] produced the following conclusions:

- (i) There is no noticeable difference between the  $f_u/f_y$  values for all the cross-sections considered in their work.
- (ii) The vertical dispersion observed in the  $f_u/f_y$  estimations led to the conclusion that there was no single winter-type curve that could safely and accurately describe all of these values. The results also clarify that a large number of

those values were under the current DSM local strength curve, which means that the curve is overestimated.

- (iii) The vertical dispersion was influenced by the column length.  $f_u/f_y$  values decreased as the column length increased (along the  $P_{cr}(L)$  plateau, see Figure 2.14). In addition, it was found that the restrained column post-buckling strength decreased consistently as the length increased.

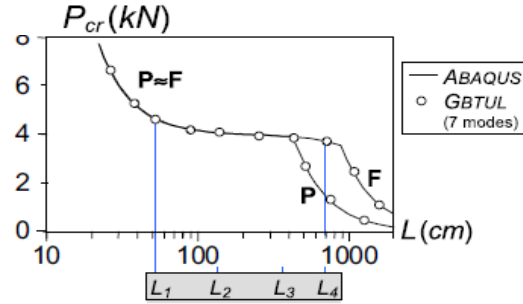


Figure 2.14:  $P_{cr}$  vs.  $L$  curves obtained by DINIS & CAMOTIM [17] for  $P$  and  $F$  columns.

Considering the observations listed and the fact that GBT modal distribution demonstrates that the participation of major-axis flexure in the column critical (flexural-torsional) buckling mode also increased with the length, DINIS & CAMOTIM [17] determined the following:

- (i) The columns would be arranged according to the ratio between the pure torsional ( $f_{bt}$ ) and the flexural-torsional ( $f_{cft}$ ) buckling stresses, calculated by Eqs. 2.19 and 2.20 respectively. The formulae analytically derived in [17] allows the calculation of the stresses specifically for fixed-ended equal-leg angle columns of width  $b$ , thickness  $t$  and length  $L$ .

$$f_{bt} = G \frac{t^2}{b^2} + \pi^2 \frac{E \cdot t^3}{12(L/2)^2} \quad (2.19)$$

$$f_{cft} = \frac{4}{5} \left( f_{bt} + f_{bf} - \sqrt{(f_{bt} + f_{bf})^2 - 2.5 f_{bt} f_{bf}} \right) \quad (2.20)$$

- (ii) A set of curves defined by “winter-type” expressions should be developed in order to predict the column flexural-torsional strengths ( $f_{nft}$ ) more precisely, as it is shown in Eq. 2.21.

$$f_{nft} = \begin{cases} f_y & \text{for } \lambda_{ft} \leq \left(0.5 + \sqrt{0.25 - b}\right)^{\frac{1}{2a}} \\ f_y \left(\frac{f_{crft}}{f_y}\right)^a \left[1 - b \left(\frac{f_{crft}}{f_y}\right)^a\right] & \text{for } \lambda_{ft} > \left(0.5 + \sqrt{0.25 - b}\right)^{\frac{1}{2a}} \end{cases} \quad (2.21)$$

$$\lambda_{ft} = \sqrt{\frac{f_y}{f_{crft}}}$$

The curves correspond, each one, to a combination of the parameters  $a$  and  $b$ , which allows to assess the column strength length dependence. Those parameters were expressed in terms of the weakening effect of major-axis flexure on the column post-critical strength, which is given according to Eq. 2.22:

$$\Delta_f = \frac{f_{bt} - f_{crft}}{f_{crft}} \times 100 \quad (2.22)$$

- (iii) Through a trial-and-error procedure, the expressions providing the parameters  $a$  and  $b$  were obtained, as shown in Eqs. 2.23 and 2.24.

$$a = \begin{cases} 0.001\Delta_f^3 + 0.032\Delta_f^2 + 0.250\Delta_f + 0.400 & \text{for } \Delta_f \leq 5.0 \\ 0.001\Delta_f + 0.970 & \text{for } \Delta_f > 5.0 \end{cases} \quad (2.23)$$

$$b = \begin{cases} 0.014\Delta_f + 0.150 & \text{for } \Delta_f \leq 7.0 \\ 0.248 & \text{for } \Delta_f > 7.0 \end{cases} \quad (2.24)$$

The DSM-based approach proposed by DINIS & CAMOTIM [17] to design fixed-ended equal-leg angle columns, which generally presented flexural-torsional/flexural interactive failure modes, were a combination of Eq. 2.21 with the existing DSM global

strength curve, with  $f_y$  being replaced by  $f_{ne}$  in Eq. 2.21, leading to the expression in Eq. 2.25:

$$f_{nfte}^F = \begin{cases} f_{ne} & \text{for } \lambda_{fte} \leq \left(0.5 + \sqrt{0.25 - b}\right)^{\frac{1}{2a}} \\ f_{ne} \left(\frac{f_{crft}}{f_{ne}}\right)^a \left[1 - b \left(\frac{f_{crft}}{f_{ne}}\right)^a\right] & \text{for } \lambda_{fte} > \left(0.5 + \sqrt{0.25 - b}\right)^{\frac{1}{2a}} \end{cases} \quad (2.25)$$

$$\lambda_{fte} = \sqrt{\frac{f_{ne}}{f_{crft}}}$$

As for pin-ended columns, they differed from the fixed-ended ones due to the effective centroid shift effects. The DSM-based approach for pin-ended equal-leg angle columns proposed by DINIS & CAMOTIM [17], as the proposal in [19], considered the effective centroid shift through a parameter  $\beta$  depending on the column slenderness. The column strength was obtained by Eq. 2.26.

$$f_{nfte}^P = \beta \times f_{nfte}^F \quad (2.26)$$

In which  $f_{nfte}^P$  is for pinned support conditions, whereas  $f_{nfte}^F$  is for the fixed condition.

Based on an ‘‘elastic reduction factor’’ concept that accounts for the variation of both the post-buckling strength and effective centroid shift effects with the column length (restricted to short-to-intermediate lengths), the procedure adopted to express the parameter  $\beta$  consisted of the following steps:

- (i) Elastic post-buckling analyses of  $F$  and  $P$  columns with the same geometry (sharing the same  $f_{bt}/f_{crft}$  ratio and critical-mode initial geometrical imperfections with amplitude  $L/1000$ ) and record the evolution with the increase of the applied load of the maximum longitudinal normal stresses ( $f_{max}$ ), given at the mid-span cross-section.
- (ii) Assumption that, for a given  $f_{max}$ , the difference between the  $F$  and  $P$  column applied loads is exclusively due to the effective centroid shift effects.

(iii)  $f_{max}$  and slenderness relation, by means of  $\lambda_{fte}=(f_{max}/f_{crft})^{0.5}$ , which led to the assumption that  $\beta$  is the strength reduction due to the effective centroid shift effects at the elastic limit state. That made it possible, then, to develop  $\beta(\lambda_{fte})$  curves.

(iv) Seeking for winter-type expressions connecting the parameter  $\beta$  with the slenderness  $\lambda_{fte}$  by another trial-and-error curve-fitting procedure, where the dependency of  $\beta$  to the length of the column is expressed through parameters  $c$  and  $d$  (which are also given in function of the ratio  $\Delta_f$ ). The expressions on Eqs. 2.27 – 2.29 account for the parameters  $\beta$ ,  $c$  and  $d$ .

$$\beta = \frac{0.68}{(\lambda_{fte} - c)^d} \leq 1 \quad (2.27)$$

$$c = \begin{cases} -300.0\Delta_f^3 + 110.0\Delta_f^2 - 12.8\Delta_f + 1.0 & \text{for } \Delta_f \leq 0.02 \\ -0.002\Delta_f^2 - 0.200\Delta_f + 0.480 & \text{for } 0.02 < \Delta_f < 5.0 \\ -0.01\Delta_f - 0.565 & \text{for } \Delta_f \geq 5.0 \end{cases} \quad (2.28)$$

$$d = \begin{cases} 380.0\Delta_f^3 - 140.0\Delta_f^2 + 15.2\Delta_f + 0.25 & \text{for } \Delta_f \leq 0.01 \\ -0.008\Delta_f^2 + 0.094\Delta_f + 0.712 & \text{for } 0.01 < \Delta_f \leq 0.15 \\ 0.001\Delta_f + 0.977 & \text{for } 0.15 < \Delta_f \leq 0.20 \end{cases} \quad (2.29)$$

Finally, the assessment of the performance of the two proposed DSM-based design procedures, which comprised gathering together  $f_{nfte}$  estimates with correspondent failure-to-predicted strength ratios,  $f_u/f_{nfte}$  against  $\lambda_{fte}$  plots (see Figure 2.15) for experimental and numerical  $F$  and  $P$  columns, led to the following considerations:

- (i) The procedure for fixed-ended columns (DSM- $F$ ) led to considerably precise estimates of the experimental and numerical ultimate strengths.
- (ii) The procedure for pin-ended columns (DSM- $P$ ) also resulted in considerably good predictions of the experimental and numerical ultimate strengths.
- (iii)  $f_u/f_{nfte}$  averages and standard deviations provide reliable evidence in what concerns to the fitting of the reasoning in which the development of the

flexural-torsional strength ( $F$  and  $P$  columns) and  $\beta$  vs.  $\lambda_{fte}$  ( $P$  columns) curves, and it still led to the conclusion that the outputs of these curves are a reliable reflex of the essential structural definitions.

- (iv) The results were also able to show that this approach's performance is equal or slightly better than the ones developed by YOUNG [11], RASMUSSEN [19] and SILVESTRE *et al.* [16]. Indeed, DINIS & CAMOTIM [17] showed that their approach was clearly more rational, since it reflected the angle column structural behaviour quite precisely and also comprised the current DSM global strength curve. In addition, it had a very straightforward appeal.
- (v) Lastly, it is mentioned that all available  $P$  column test results corresponded to a narrow slenderness range, which implied a need for more experimental data to cover a wider slenderness spectrum, in order to ensure proper validation of the design approaches.

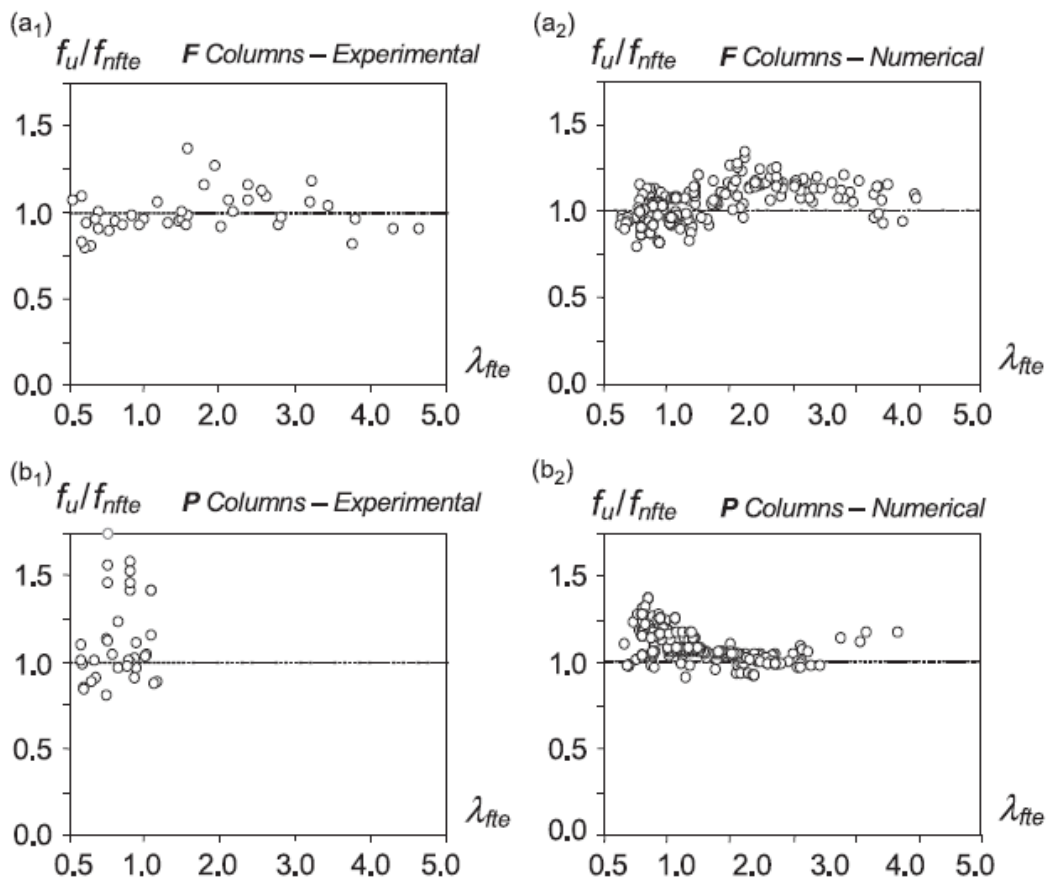


Figure 2.15: Plots of  $f_u/f_{nfte}$  against  $\lambda_{fte}$  for the (a)  $F$  and (b)  $P$  columns: (1) experimental and (2) numerical results [17].

### 2.3.6 Landesmann *et al.* (2017)

LANDESMANN *et al.* [14] carried an experimental study at the Federal University of Rio de Janeiro concerning short-to-intermediate slender pin-ended cold-formed steel equal-leg angle columns.

The column selection was conducted by a series of buckling analyses using GBTUL codes, based on the Generalised Beam Theory (GBT) and ANSYS (finite element analyses using shell elements). The criteria adopted in this stage were:

- (i) Cross-section dimensions commonly used in practice.
- (ii) Columns under buckling in flexural-torsional modes.
- (iii) Columns presenting intermediate-to-high slenderness values ( $1.5 \leq \lambda_{fte} \leq 3.5$ ).

The columns had nominal thickness  $t=1.55 \text{ mm}$  and were made of ZAR-345 mild steel [54]. Plus, the specimens exhibited nominal legs widths  $50\text{-}60\text{-}70\text{-}80\text{-}90 \text{ mm}$  and had lengths ranging from  $500 \text{ to } 1200 \text{ mm}$ . The columns had both ends welded to  $12 \text{ mm}$  thick steel plates to assure full contact between the specimens and the test machine bearings.

The specimens were tested in an AMSLER servo-controlled hydraulic UTM under displacement-control with a moveable end support that allowed various lengths of columns. The end supports prevented transverse displacements, major-axis flexural and torsional rotations, and secondary warping and local displacements/rotations. Thus, the support conditions were fixed in what concerns to major-axis flexure and torsion, and pinned in what concerns to minor-axis flexure. Figure 2.21 presents a representation of the pinned supports used.

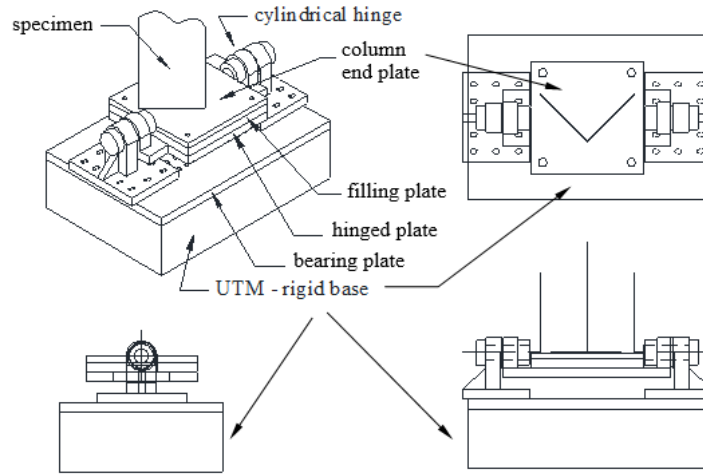


Figure 2.16: Specimens bottom end support: schematic representations [14]

LANDESMANN *et al.* [14] showed that the experimental and numerical failure loads obtained could be efficiently predicted by the design approach proposed by DINIS & CAMOTIM [17]. Besides, LANDESMANN *et al.* [14] covered a wider slenderness range in both experimental and numerical analyses, as depicted in Figure 2.17.

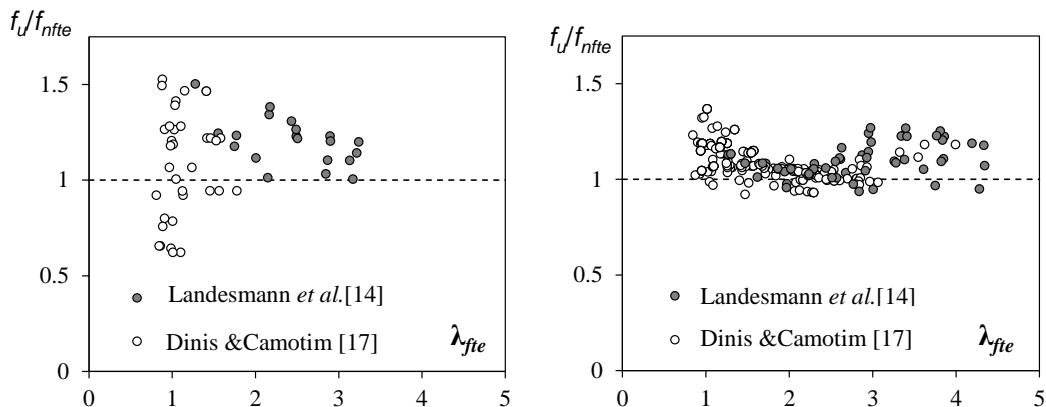


Figure 2.17: (a) Experimental and (b) numerical  $f_u/f_{ntte}$  vs.  $\lambda_{fte}$  plots concerning the values (i) obtained in [14] (ii) reported in [17].

### 2.3.7 Dinis & Camotim (2017)

DINIS & CAMOTIM [18] reported results of a numerical investigation on pin-ended short-to-intermediate equal-leg angle columns with end support conditions corresponding to rigid plates resting on spherical hinges. The spherically-hinged condition convey that such supports were: (i) pinned with respect to major and minor-axis flexure and (ii) fixed only with respect to torsion (“PS columns”).

By means of Generalized Beam Theory (GBT), this study concerned the buckling behaviour of *PS* columns with various leg slenderness values. In addition, the buckling behaviours of *F* (fixed-ended), *PC* and *PS* columns were compared, in a way that the difference between them is elicited. Then, the post-buckling (elastic and elastic-plastic) and failure behaviour of *PS* columns was addressed. Shell finite element analyses through the software *ABAQUS* were performed, comprising a parametric study, in order to gather a set of failure load data covering a wide slenderness amplitude. These numerical failure loads, along with the experimental results obtained from the works previously published, were used to evaluate the estimates provided by the DSM-based design approach previously suggested by DINIS & CAMOTIM [17]. It was observed that this design approach needed to be adjusted in order to be applicable to *PS* columns; this is due to a change in major-axis flexure support conditions, which noticeably influences the column flexural-torsional behaviour.

Figure 2.18 contains the  $f_{cr}$  vs.  $L$  found in [18] for fixed, pinned and spherically-hinged columns (*F*, *PC*, and *PS*), as well as GBT deformation modes (2-7) and 3 *PS* columns critical buckling mode.

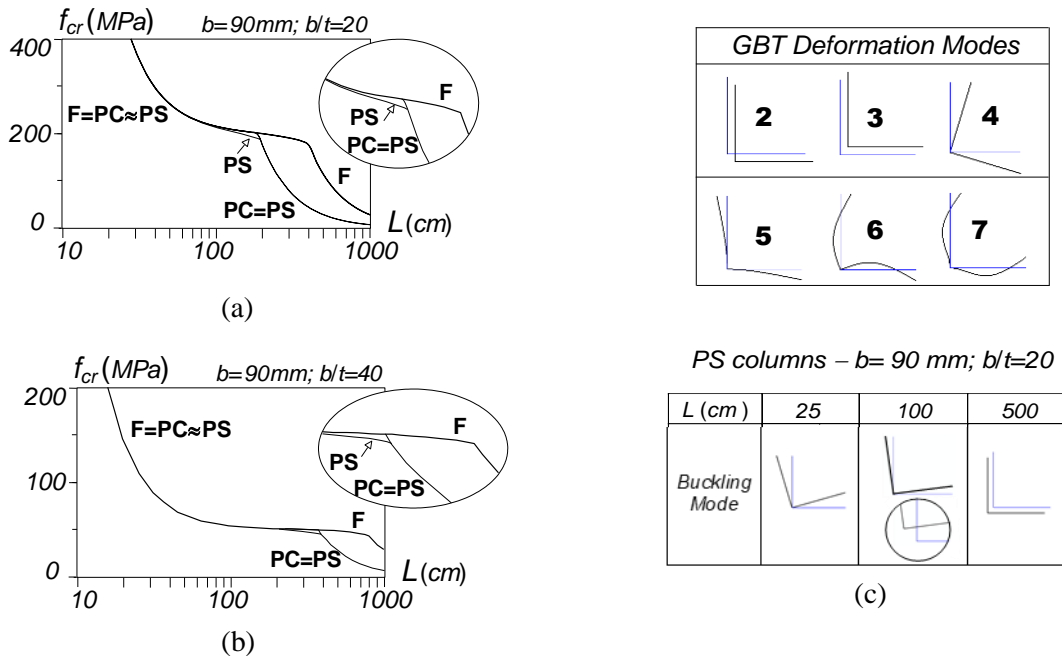


Figure 2.18: *F*, *PC* and *PS* columns ( $b=90\text{ mm}$ );  $f_{cr}$  vs.  $L$  curves for (a)  $b/t=20$  and (b)  $b/t=40$ , (c) in-plane shapes of GBT deformations 2-7 and 3 *PS* columns critical buckling mode [18].

The DSM approach for spherically-hinged equal-leg angle columns is based on the same concepts and procedures adopted for  $F$  and  $PC$  short-to-intermediate angle columns with slender legs [17]. The aim of the numerical approach adopted in [18] was to determine new length-dependent (i) flexural-torsional strength curves  $f_{nft}$  and (ii) curves providing the reduction coefficient  $\beta$ . The curves are similar to the ones obtained for  $F$  and  $PC$  columns: length-dependent “winter-type” via the  $\Delta_f$  parameter, as it is shown in Eqs. 2.30...

$$f_{bt} = G \frac{t^2}{b^2} + \pi^2 \frac{E \cdot t^3}{12(L/2)^2} \quad (2.30)$$

$$(2.31)$$

$$f_{cft} = \frac{4}{5} \left( f_{bt} + f_{bf} - \sqrt{(f_{bt} + f_{bf})^2 - 2.5 f_{bt} f_{bf}} \right)$$

$$f_{nfte} = \begin{cases} f_{ne} & \text{for } \lambda_{fte} \leq \left(0.5 + \sqrt{0.25 - b}\right)^{\frac{1}{2a}} \\ f_{ne} \left(\frac{f_{cft}}{f_{ne}}\right)^a \left[1 - b \left(\frac{f_{cft}}{f_{ne}}\right)^a\right] & \text{for } \lambda_{fte} > \left(0.5 + \sqrt{0.25 - b}\right)^{\frac{1}{2a}} \end{cases} \quad (2.32)$$

$$\lambda_{fte} = \sqrt{\frac{f_{ne}}{f_{cft}}}$$

$$\Delta_f = \frac{f_{bt} - f_{cft}}{f_{cft}} \times 100 \quad (2.33)$$

$$f_{nfte} = \beta \times f_{nfte}^F \quad (2.34)$$

The modifications in the proposal of DINIS & CAMOTIM [17] are restricted to new expressions for the functions  $a(\Delta_f)$ ,  $b(\Delta_f)$ ,  $c(\Delta_f)$  and  $d(\Delta_f)$ . Those changes are due to the fact that the new curves comprise columns (i) pinned with respect to major-axis flexure, (ii) fixed with respect to torsion and (iii) with prevented minor-axis flexural

displacements. Through a trial-and-error curve-fitting procedure based on the available numerical failure load data, new expressions for the functions  $a$ ,  $b$ ,  $c$  and  $d$  were obtained, as described in Eqs. 2.35 to 2.38.

$$a = \begin{cases} -0.001\Delta_f^3 + 0.014\Delta_f^2 + 0.007\Delta_f + 0.4 & \text{for } \Delta_f \leq 1 \\ 0.001\Delta_f^2 + 0.04\Delta_f + 0.365 & \text{for } 1 < \Delta_f < 10 \\ 0.865 & \text{for } \Delta_f \geq 10 \end{cases} \quad (2.35)$$

$$b = \begin{cases} -0.001\Delta_f^3 + 0.001\Delta_f^2 - 0.011\Delta_f + 0.15 & \text{for } \Delta_f \leq 1 \\ 0.005\Delta_f + 0.134 & \text{for } 1 < \Delta_f < 10 \\ 0.184 & \text{for } \Delta_f \geq 10 \end{cases} \quad (2.36)$$

$$c = \begin{cases} -300.0\Delta_f^3 + 110.0\Delta_f^2 - 12.8\Delta_f + 1.0 & \text{for } \Delta_f \leq 0.2 \\ -0.001\Delta_f^3 - 0.01\Delta_f^2 + 0.058\Delta_f + 0.451 & \text{for } 0.2 < \Delta_f < 8 \\ 0.115 & \text{for } \Delta_f \geq 8 \end{cases} \quad (2.37)$$

$$d = \begin{cases} 290\Delta_f^3 - 98\Delta_f^2 + 10.8\Delta_f + 0.25 & \text{for } \Delta_f \leq 0.2 \\ -0.001\Delta_f^2 + 0.03\Delta_f + 0.804 & \text{for } 0.2 < \Delta_f \leq 9.5 \\ 0.999 & \text{for } \Delta_f \geq 9.5 \end{cases} \quad (2.38)$$

The numerical analysis conducted in [18] resulted in the plot of  $f_u/f_{nfte}$  vs.  $\lambda_{fte}$  presented in Fig. 2.23.

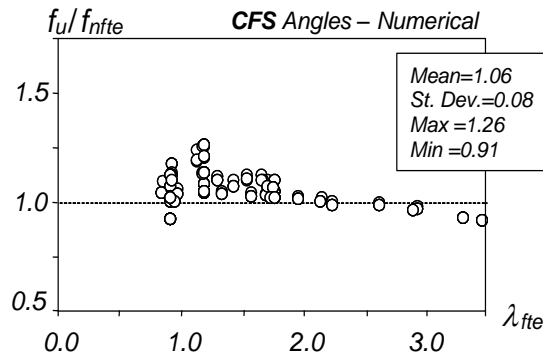


Figure 2.19: Plots of  $f_u/f_{nfte}$ , against  $\lambda_{fte}$ , for the CFS angles [18].

Although the curves obtained in [18] were shown to present reliable and safe yield failure load estimates, additional numerical and experimental validation was heavily advised before the design approach could figure in standards.

## 3 Experimental Investigation

---

This chapter concerns the experimental tests performed at the Structures Laboratory (LABEST) at COPPE – UFRJ (Federal University of Rio de Janeiro). Item 3.1 describes the column selection procedure, resuming the main characteristics of the specimens to be tested. Item 3.2 summarizes the geometrical properties of the columns. Item 3.3 describes the coupon strain tests performed and presents a summary of the data acquired in the tests, thus characterizing the material used to fabricate the column specimens tested in this study. Item 3.4 reports the test set-up, while item 3.5 details the displacement measures along the tests. Item 3.6 defines the test procedures adopted and, finally, item 3.7 reports the results obtained.

### 3.1 Column Selection

The first stage of this work consisted in carefully selecting the cross-section dimensions and lengths of the spherically-hinged angle columns to be tested experimentally and analysed numerically. At this point, recall that spherically-hinged columns (i) are pinned for minor and major-axis flexure, and (ii) have fully prevented torsional rotations and (secondary) warping. The selection procedure involved sequences of buckling analyses, performed using codes GBTUL (mostly), based on Generalised Beam Theory (GBT) [23], and ANSYS (shell finite element analyses) [45]. Concerning the columns to be tested experimentally (the main purpose of this work), the aim was to identify equal-leg angle columns (i) with cross-section dimensions commonly used in practice, (ii) buckling in flexural-torsional modes (*i.e.*, with short-to-intermediate lengths), (iii) exhibiting intermediate-to-high slenderness values ( $0.95 \leq \lambda_{fte} \leq 3.7$ ), (iv) satisfy the specimen fabrication restraints, namely: (iv<sub>1</sub>) Young's modulus  $E = 205 \text{ GPa}$ , (iv<sub>2</sub>) Poisson's ratio  $\nu = 0.3$ , (iv<sub>3</sub>) yield stress  $f_y = 366 \text{ MPa}$  and (iv<sub>4</sub>) nominal thicknesses  $t = 0.8 \text{ mm}$ ,  $t = 0.95 \text{ mm}$  and  $t = 1.25 \text{ mm}$ .

Fortunately, it was possible to fulfil the requirements listed in the previous paragraph and the selection procedure led to the various angle column geometries (leg widths and lengths – recall that  $t = 0.8 \text{ mm}$ ,  $t = 0.95 \text{ mm}$  and  $t = 1.25 \text{ mm}$ ) given in Table 3.1, which are divided in four sets, each of them sharing the same thickness  $t$  and leg

width  $b$  – the column designation indicates its thickness and length, both in  $mm$  (e.g., column 25t0.8L400 is  $0.8\text{ mm}$  thick,  $400\text{ mm}$  long and its leg width is of  $25\text{ mm}$ ). Table 3.1 also provides the column (i) areas  $A$ , (ii) squash loads  $P_y=A\cdot f_y$  (for  $f_y=366\text{ MPa}$ ), (iii) flexural-torsional (critical –  $P_{cft}$ ) and torsional ( $P_{bt}$ ) buckling loads, (iv)  $\Delta_f$  ratios (see Eq. (2.22)), (v) global failure load estimates  $f_{ne}$  and (vi) slenderness values  $\lambda_{fte}$  – note that one has  $0.95 \leq \lambda_{fte} \leq 3.7$ .

Table 3.1: Columns to be tested: geometry, squash load, buckling loads,  $\Delta_f$ ,  $f_{ne}$  and  $\lambda_{fte}$  ( $f_y=366\text{ MPa}$ ).

| Column designation | $b$<br>(mm) | $L$<br>(mm) | $A$<br>( $\text{cm}^2$ ) | $P_y$<br>(kN) | $P_{cft}$<br>(kN) | $P_{bt}$<br>(kN) | $\Delta_f$<br>(%) | $f_{ne}$<br>(MPa) | $\lambda_{fte}$ |
|--------------------|-------------|-------------|--------------------------|---------------|-------------------|------------------|-------------------|-------------------|-----------------|
| 25t0.8L400         | 25          | 400         | 0.4                      | 13.80         | 3.32              | 3.34             | 0.0060            | 222.53            | 1.64            |
| 25t0.8L600         |             | 600         |                          |               | 3.23              | 3.28             | 0.0134            | 128.36            | 1.26            |
| 25t0.8L800         |             | 800         |                          |               | 3.18              | 3.26             | 0.0241            | 72.20             | 0.95            |
| 50t0.8L400         | 50          | 400         | 0.8                      | 27.60         | 1.83              | 1.83             | 0.0004            | 309.18            | 3.68            |
| 50t0.8L600         |             | 600         |                          |               | 1.71              | 1.71             | 0.0009            | 269.59            | 3.55            |
| 50t0.8L800         |             | 800         |                          |               | 1.67              | 1.67             | 0.0015            | 222.53            | 3.27            |
| 50t0.95L400        | 50          | 400         | 0.95                     | 32.78         | 3.06              | 3.07             | 0.0006            | 309.18            | 3.10            |
| 50t0.95L600        |             | 600         |                          |               | 2.86              | 2.86             | 0.0012            | 269.59            | 2.99            |
| 50t0.95L800        |             | 800         |                          |               | 2.79              | 2.79             | 0.0021            | 222.53            | 2.75            |
| 50t0.95L1000       |             | 1000        |                          |               | 2.75              | 2.76             | 0.0033            | 173.89            | 2.45            |
| 50t1.25L400        | 50          | 400         | 1.25                     | 43.13         | 6.98              | 6.98             | 0.0010            | 309.18            | 2.35            |
| 50t1.25L600        |             | 600         |                          |               | 6.51              | 6.53             | 0.0021            | 269.59            | 2.27            |
| 50t1.25L800        |             | 800         |                          |               | 6.34              | 6.37             | 0.0036            | 222.53            | 2.09            |
| 50t1.25L1000       |             | 1000        |                          |               | 6.26              | 6.29             | 0.0056            | 173.89            | 1.86            |

For illustration purposes, Figs. 3.1(a)-(b) (i) show the  $P_{cr}$  vs.  $L$  ( $L$  in logarithmic scale) curves concerning the five cross-sections (i.e., leg widths) considered and, on each of them, indicates the lengths of the columns selected. The close observation of the values given in Table 3.1 and the buckling results displayed in Figs. 3.1(a)-(b) prompts the following remarks:

- (i) As already expected in [47], each  $P_{cr}$  vs.  $L$  curve consists of (i<sub>1</sub>) an initial more or less horizontal plateau, associated with major-axis flexural-torsional buckling, followed by (i<sub>2</sub>) a fast descending branch, associated with minor-axis buckling.

- (ii) The column length corresponding to the transition from flexural-torsional buckling to flexural buckling increases with the leg width – in fact, the correlation is with  $b/t$ .
- (iii) For each cross-section dimensions, the value  $\Delta_f$  grows steadily with the column length.
- (iv) As mentioned before, the  $\lambda_{fte}$  values are comprised between 0.95 and 3.7, thus covering a fairly wide range. It is worth noting that, in general, quite high  $\lambda_{fte}$  values correspond to rather short columns – conversely, the longest columns selected ( $L=1000\text{ mm}$ ) exhibit the lowest slenderness. In order to understand this apparently surprising feature, it is necessary to look at the definition of  $\lambda_{fte}$ , given in Eq. 2.1: it is the square root of the ratio between (iv<sub>1</sub>) the global strength  $f_{ne}$ , which decreases very fast with the column length, and (iv<sub>2</sub>) the flexural-torsional (critical) buckling stress  $f_{crft}$ , which exhibits a much less pronounced decrease with  $L$  (except for very short lengths). In order to illustrate the above assertion, Figs.3.2(a)-(b) show, for columns with  $t=0.95\text{ mm}$ , the variations with  $L$  of (iv<sub>1</sub>)  $f_{ne}$  and  $f_{crft}$ , and (iv<sub>2</sub>)  $\lambda_{fte}$  – the length range shown contains all the values selected. It is noted that the highest slenderness occurs for  $L\approx 230\text{ mm}$ , which stems from the fact that (iv<sub>1</sub>)  $f_{ne}$  decreases continuously with  $L$ , (iv<sub>2</sub>) the  $f_{crft}$  vs.  $L$  curve displays a maximum at  $L < 250\text{ mm}$ , followed by a drop until  $L\approx 325\text{ mm}$  (from  $50\text{ MPa}$  to about  $25\text{ MPa}$ ) and an almost horizontal plateau for longer columns. Thus, the highest  $f_{ne}/f_{crft}$  ratios occur for fairly short columns.
- (v) In order to assess the impact of the yield stress on  $\lambda_{fte}$ , Figs. 3(a)-(b) show, for the column series  $0.95L600$ , the variations with  $f_y$  of (v<sub>1</sub>)  $f_{ne}$  and  $f_{crft}$ , and (v<sub>2</sub>)  $\lambda_{fte}$ . It is noted that increasing the yield stress only leads to a visible slenderness rise up to a certain value (e.g., it is not possible to reach  $\lambda_{fte}=5$ ).

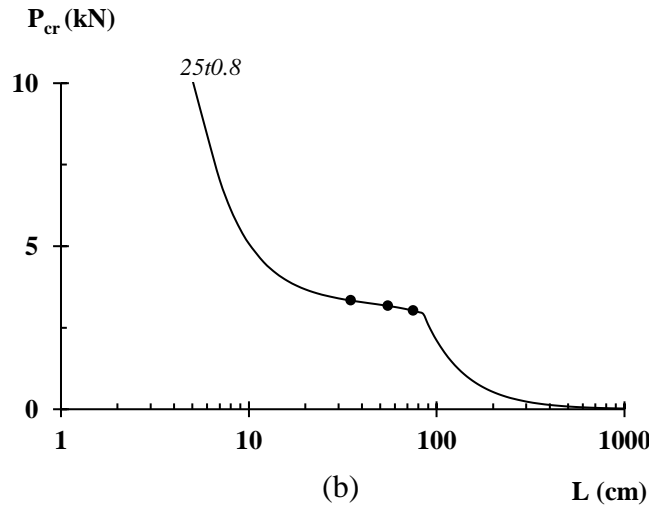
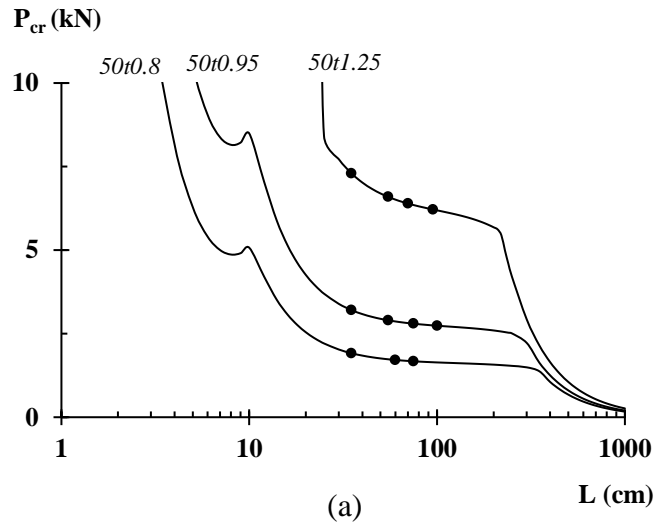


Figure 3.1: Curves  $P_{cr}$  vs.  $L$  indicating the selected column lengths for (a)  $b = 50 \text{ mm}$  and (b)  $b = 25 \text{ mm}$ .

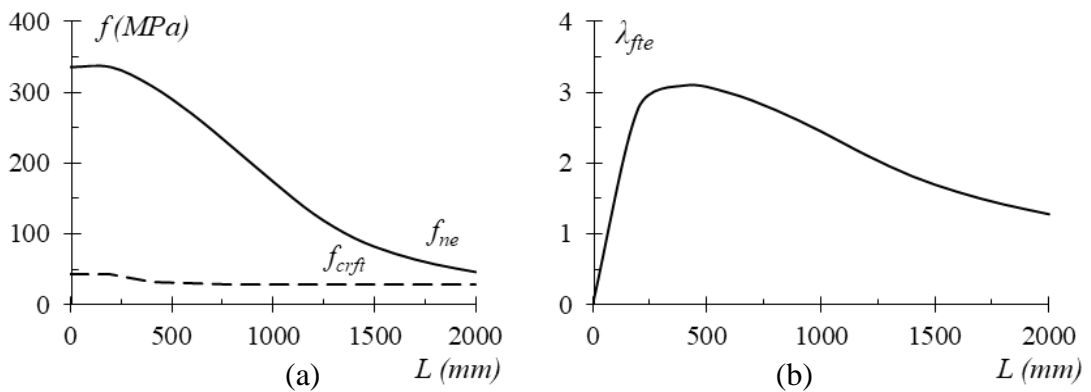


Figure 3.2: Variation with the length of (a)  $f_{ne}$  and  $f_{crft}$  and (b)  $\lambda_{fte}$  for columns with thickness  $t = 0.95 \text{ mm}$ .

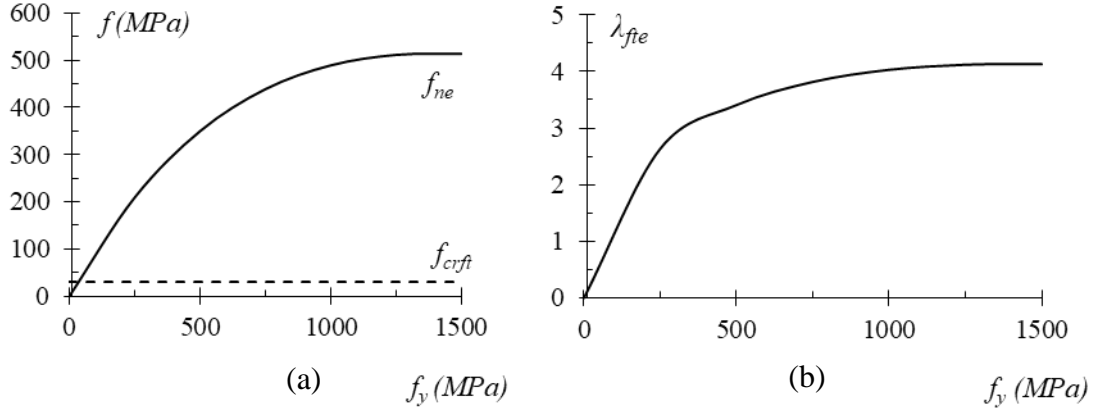
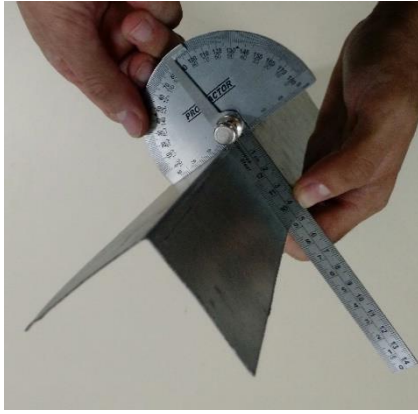


Figure 3.3: Variation with the yield stress of (a)  $f_{ne}$  and  $f_{crft}$  and (b)  $\lambda_{fte}$  for the 50t0.95L600 column.

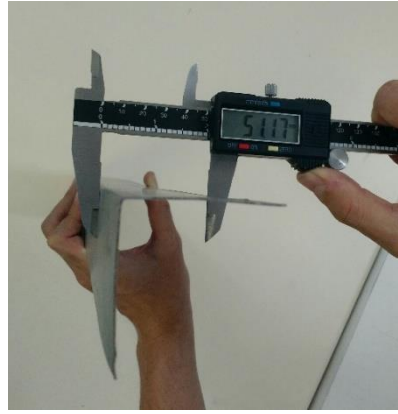
Concerning the columns to be analysed numerically (just to obtain some additional failure load data), it was decided to consider the 16 columns selected previously, whose characteristics are given in Table 3.1, and vary their yield stresses, in order to widen the slenderness range covered. The yield stresses chosen were  $f_y=150; 200; 250; 275; 300; 350; 375; 400; 450; 475; 500; 550; 575; 600; 650; 700$  MPa and Table 3.1 contains the columns'  $P_y, f_{ne}, \lambda_{fte}$  values – note that  $0.82 \leq \lambda_{fte} \leq 4.91$ .

### 3.2 Column Specimens

The column specimens were manufactured by press braking from zinc-coated structural sheets with nominal thicknesses  $t = 0.8-0.95-1.25$  mm and made of ZAR-345 mild steel [54]. Table 3.2 presents the columns nominal geometries and their corresponding measured geometries, besides, it contains the average values of the measured specimens leg width, thickness and length. Additionally, Table 3.2 details the cross-section with the representation of the centroid (G) and the principal axes (1-major and 2-minor). The labels for the columns are the same from Table 3.1, and the letter “R” identifies the specimens repeated (in order to assess the reliability of the experimental set-up and procedure). The cross-section dimensions and the angle formed by the two legs ( $\theta_b$ ) were measured at five equally spaced locations along the specimen length  $L_0$  (0.00-0.25-0.50-0.75-1.00  $L_0$ ). Figure 3.4 illustrates the measuring process. It is also important to highlight that the press braking manufacturing condition imposed internal bending radii ( $r_i$ ) approximately equal to the sheet thickness ( $t=0.80-0.95-1.25$ mm).



(a)

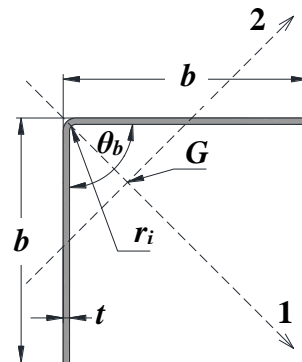


(b)

Figure 3.4: Geometrical imperfection measuring of the (a) leg angles and (b) leg lengths.

Table 3.2: Average values of the measured columns cross-section dimensions, leg angles, lengths and areas.

| Column        | $b$<br>(mm) | $t$<br>(mm) | $\theta_b$<br>(deg) | $L_0$<br>(mm) | $A$<br>(cm <sup>2</sup> ) |
|---------------|-------------|-------------|---------------------|---------------|---------------------------|
| 25t0.8L400    | 25.63       | 0.80        | 88                  | 401.3         | 0.41                      |
| 25t0.8L400-R  | 25.50       | 0.80        | 87                  | 400.5         | 0.41                      |
| 25t0.8L600    | 26.03       | 0.81        | 89                  | 601           | 0.42                      |
| 25t0.8L800    | 25.56       | 0.80        | 89                  | 800           | 0.41                      |
| 50t0.8L400    | 50.02       | 0.80        | 91                  | 401           | 0.80                      |
| 50t0.8L400-R  | 49.09       | 0.80        | 90                  | 400.5         | 0.79                      |
| 50t0.8L600    | 50.98       | 0.80        | 90                  | 600           | 0.82                      |
| 50t0.8L600-R  | 52.00<br>5  | 0.80        | 87                  | 600           | 0.83                      |
| 50t0.8L800    | 50.21       | 0.80        | 87                  | 800           | 0.80                      |
| 50t0.95L400   | 49.86       | 0.96        | 88                  | 400           | 0.96                      |
| 50t0.95L600   | 50.65       | 0.96        | 84                  | 599           | 0.97                      |
| 50t0.95L600-R | 50.65       | 0.96        | 86                  | 600           | 0.97                      |
| 50t0.95L800   | 49.86       | 0.96        | 88.5                | 800.8         | 0.96                      |
| 50t0.95L1000  | 49.85       | 0.96        | 89.5                | 1001          | 0.96                      |
| 50t1.25L400   | 50.10       | 1.23        | 87                  | 400           | 1.23                      |
| 50t1.25L600   | 50.97       | 1.22        | 86                  | 600           | 1.24                      |
| 50t1.25L600-R | 51.13       | 1.22        | 86                  | 600           | 1.25                      |
| 50t1.25L800   | 49.85       | 1.22        | 87                  | 800.3         | 1.22                      |
| 50t1.25L1000  | 50.01       | 1.23        | 88                  | 1001.<br>2    | 1.23                      |



### 3.3 Mechanical Properties of the Mild Steel

The mechanical properties of the structural ZAR-345 [54] steel sheet selected to manufacture the column specimens were obtained experimentally through nine standard tensile coupon tests. The coupons were longitudinally extracted from virgin steel sheets – the coupon dimensions and the test procedure conformed to ABNT NBR ISO 6892-1:2015 [48] and ASTM E8/E8M-16a [49] and were performed on a *Shimadzu Autograph®* AG-X 100kN press. Figure 3.5 (a) depicts the geometry of the coupons and Figure 3.5 (b) shows the coupon tensile test set-up.

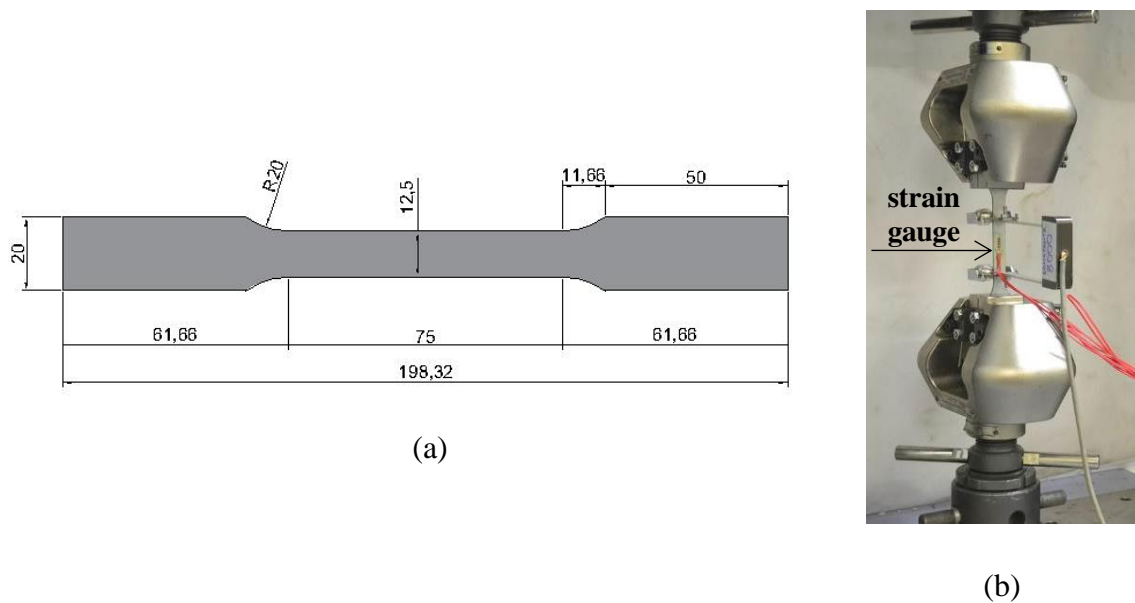
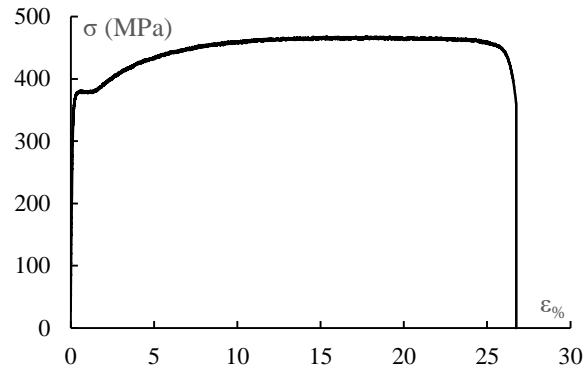


Figure 3.5: Coupon tensile test. (a) Specimens' dimensions and (b) general view of the test.

The average values obtained for the steel mechanical properties are  $f_y=366\text{ MPa}$  (yield stress),  $f_u=458\text{ MPa}$  (ultimate stress) and  $E\approx 205\text{ GPa}$  (Young's modulus). Moreover, a Poisson's ratio  $\nu=0.3$  was always assumed. Figures 3.6 (a)-(d) show the results measured for 3 of the nine total coupons, one of each thickness chosen, as well as their *stress x strain* plots.

| t<br>(mm) | E<br>(GPa) | $\sigma_y$<br>(MPa) | $\sigma_u$<br>(MPa) | $\epsilon$<br>(%) |
|-----------|------------|---------------------|---------------------|-------------------|
| 0.8       | 204742     | 369                 | 482                 | 21                |
| 0.95      | 215619     | 369                 | 444                 | 25                |
| 1.25      | 194060     | 361                 | 450                 | 18                |

(a)



(b)

Fig 3.6: (a) Average material properties of each thickness and (b) typical stress-strain curve.

### 3.4 Test Set-Up

The specimens were tested by means of a frame structure, composed of four screw columns and a load cell attached to a hydraulic actuator under displacement-control, which can supply loads up to  $500\text{ kN}$  – the loads imposed during a test were measured with  $50\text{ N}$  accuracy and recorded in a data acquisition system. Figures 3.7 (a) and (b) provide an overall view of the test set-up, showing a moveable upper part of the frame that allowed testing specimens with various lengths. Figure 3.7 (c) contains the data acquisition system employed during the tests.

As for Figs. 3.8(a)-(c), they provide a view of the strain-gauges used to monitor the strain during the test, a general view and schematic representations of the bottom (spherical) end support, formed by a pair of spherical hinges (i) built from machine-finished carbon steel and (ii) mounted on two  $15\text{ mm}$  thick epoxy-resin end plates – the top end support is similar. The end supports were designed to ensure null vertical distances between the specimen end cross-sections and the axes of rotation, thus eliminating the need to consider minor-axis flexural buckling length correction factors [10][30]. These end supports prevent (i) transverse displacements, (ii) torsional rotations, and (iii) secondary warping and local displacements/rotations – the corresponding support conditions are “fixed” with respect to torsion, and “pinned” with respect to major and minor-axis flexure.

The casting of the epoxy-resin bases was carefully performed on a “set-square” set-up (see Figure 3.9-(a)), in order to guarantee vertical alignment. In addition, millimetre paper was used to maintain a concentric loading procedure by placing the specimens in the centre of the support plate (see Figure 3.9-(b)). Since considerable attention was paid to meticulously aligning the plates and epoxy-resin bases providing correct load transfer to the specimens, it seems fair to argue that the tests are performed under virtually concentric loading conditions.

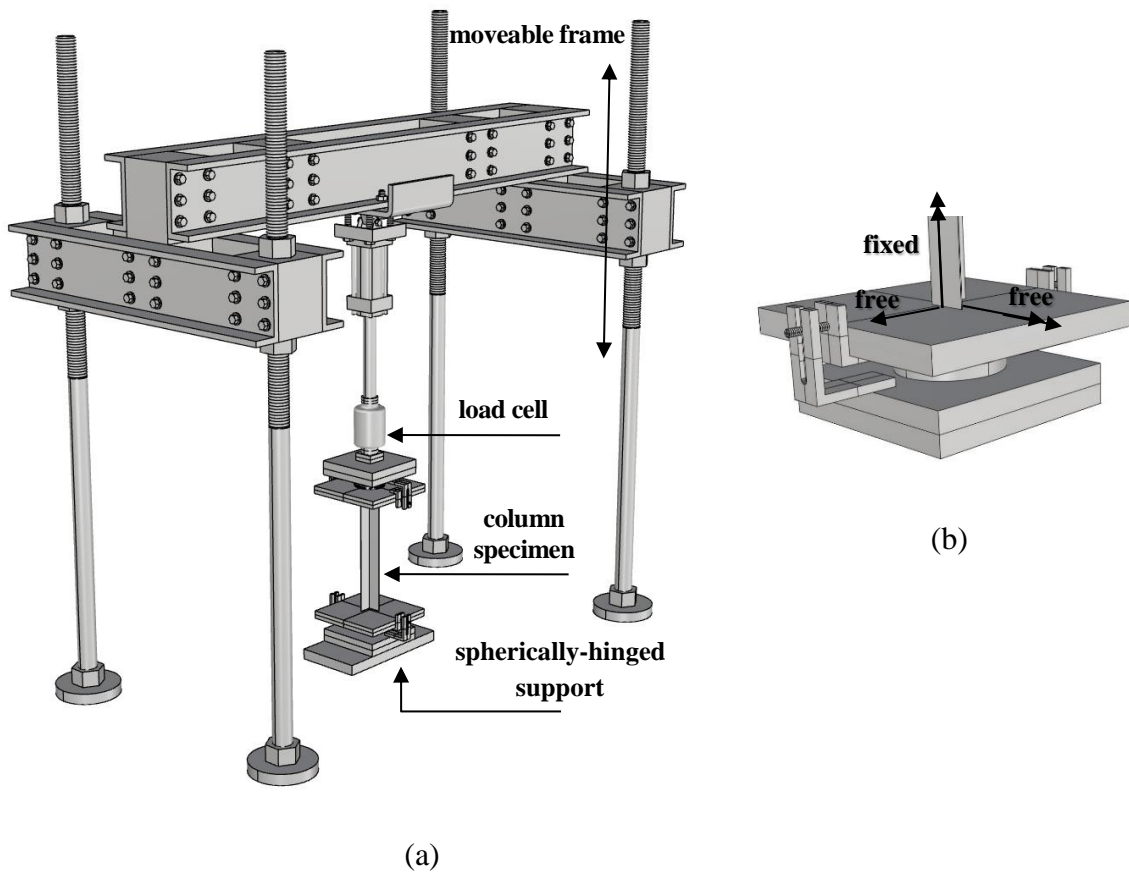


Figure 3.7: 3D view of (a) the test set-up and (b) the spherical support with its degrees of freedom.

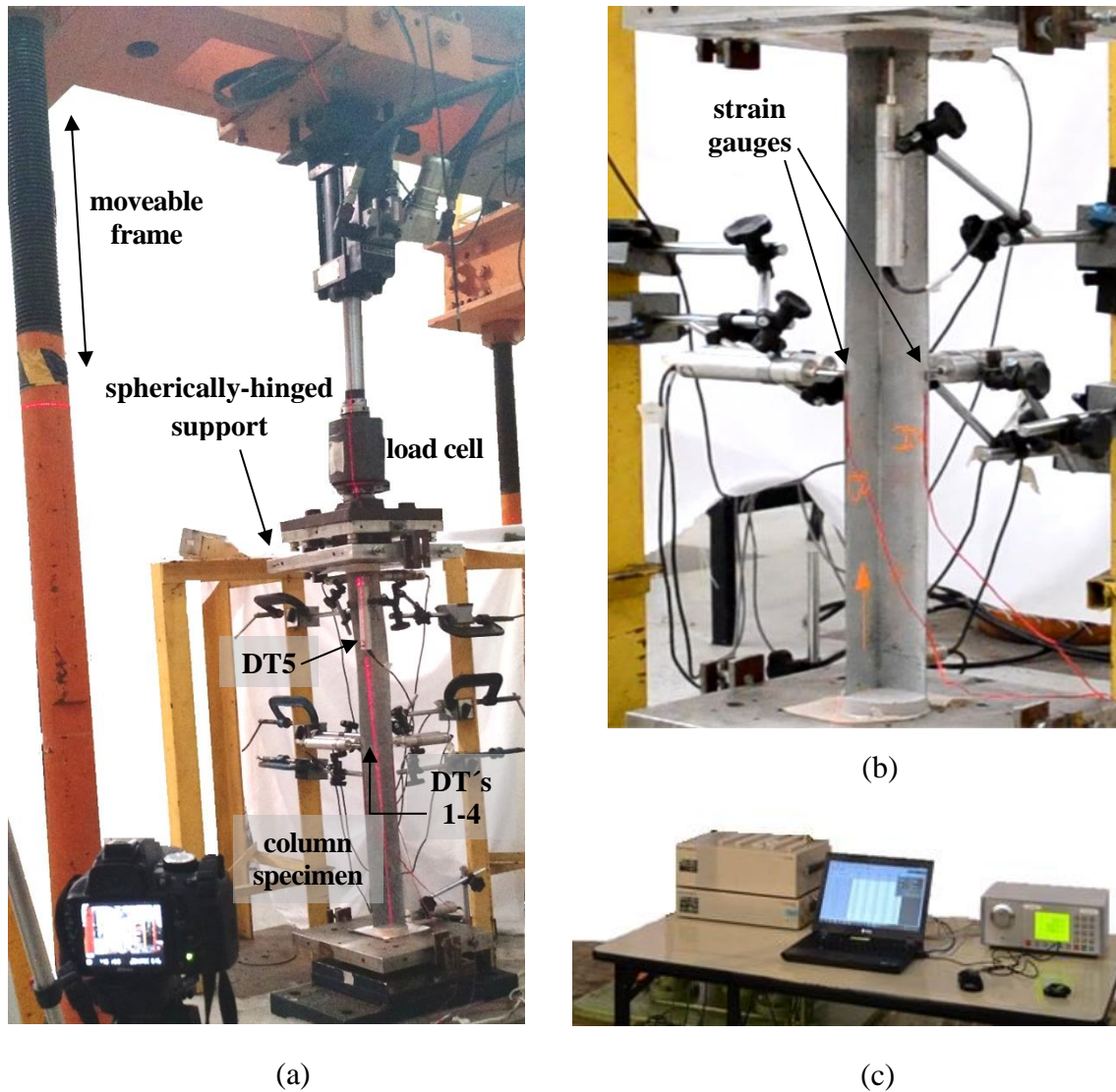


Figure 3.8: (a) overall view of the set-up, (b) location of the strain gauges and (c) data acquisition system.

### 3.5 Displacement Measurements

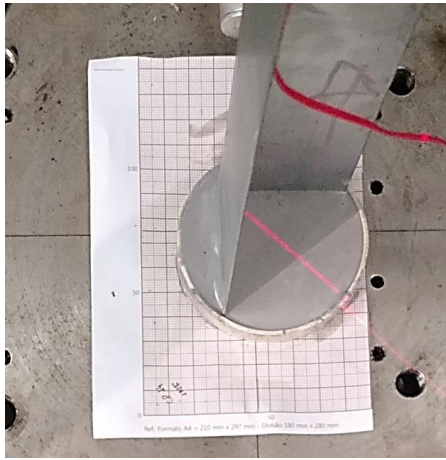
Two sets of five displacement transducer (DT) measurements were made for each specimen, with the DTs (i) able to move along the specimen outer surface, prior to the test, and (ii) placed at the specimen mid-height, during the test. The corresponding DT locations along the cross-section contour, selected to enable capturing the column major-axis flexural-torsional and minor-axis flexural displacements, are depicted in Figs. 3.10(a)-(c). The first arrangement involves four DTs (DT1-4) supported by a rigid device, mounted on a milling machine working table, able to move horizontally along the specimen and monitored by a fifth DT (DT5), as illustrated in Figure 3.10(a). The second

arrangement also involves four DTs (DT1-4) in order to acquire measurements (i) at the specimen's mid-height, (ii) at the top support, to assure torsion is absent, (iii) at the bottom support, only in the first 3 tests, since torsion was discovered to be totally absent during those tests and (iv) at the centre of the epoxy-resin plate, in order to acquire shortening measurements. Strain gauges were used as well, to ensure the columns' behaviour is well detected: they were disposed so that there were put two per specimen, at the columns' mid-height.

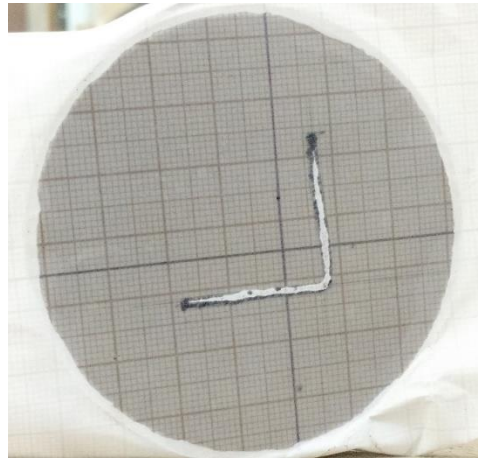
### 3.6 Test Procedure

Each column specimen test involved the sequential performance of the following tasks:

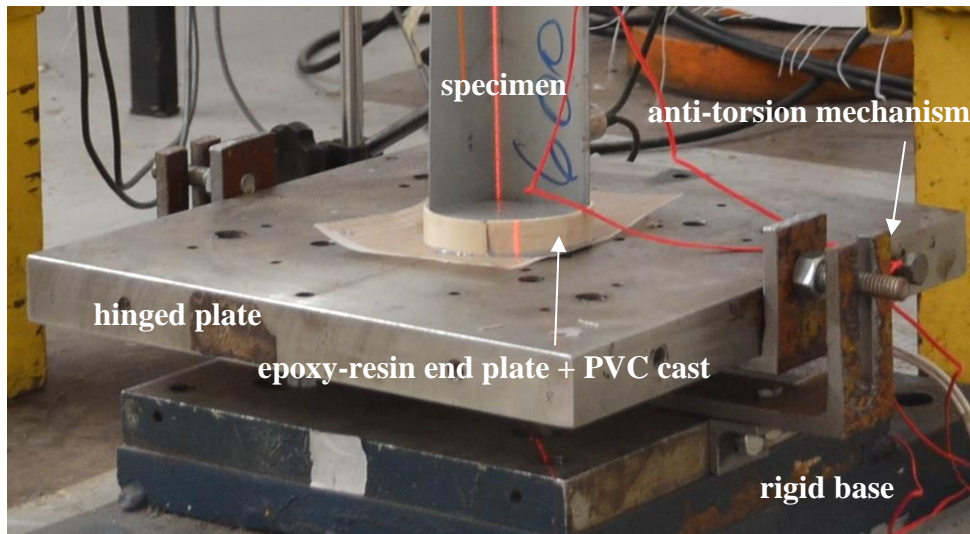
- (i) Manufacture of the *15mm* thick epoxy resin plates by means of a PVC (poly-vinyl chloride) cast.
- (ii) Attachment of two strain gauges per specimen, located at the column's mid-height.
- (iii) Positioning of the specimen on the spherical support using millimetre paper, thus ensuring negligible load eccentricity.
- (iv) Placing eight DT transducers, four of which at the column mid-height and one at the centre of the top epoxy-resin base.
- (v) Slow (*0.005mm/s*) loading and unloading of an initial small compressive load (*0.5 kN*) to eliminate gaps between the spherical supports and the specimen's end plates.
- (vi) Application of the displacement-controlled loading, by the servo-controlled hydraulic actuator and the load cell, at a sufficiently low rate to preclude relevant dynamic effects.
- (vii) Continuous recording by a *15Hz* data acquisition system of the DT outputs, the load cell readings and the strain gauges' readings.
- (viii) The specimens' deformed configurations are photographed during the test, as the load approaches the predicted ultimate strength, so that the evidence on the nature of the column failure mode is well documented.



(a)

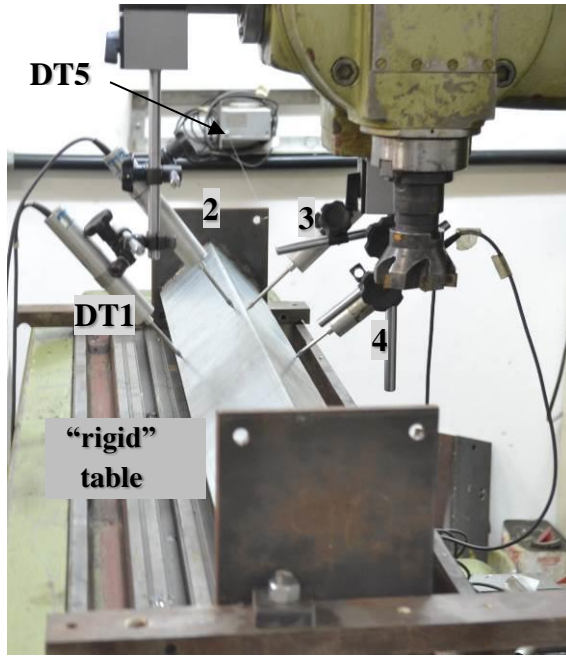


(b)

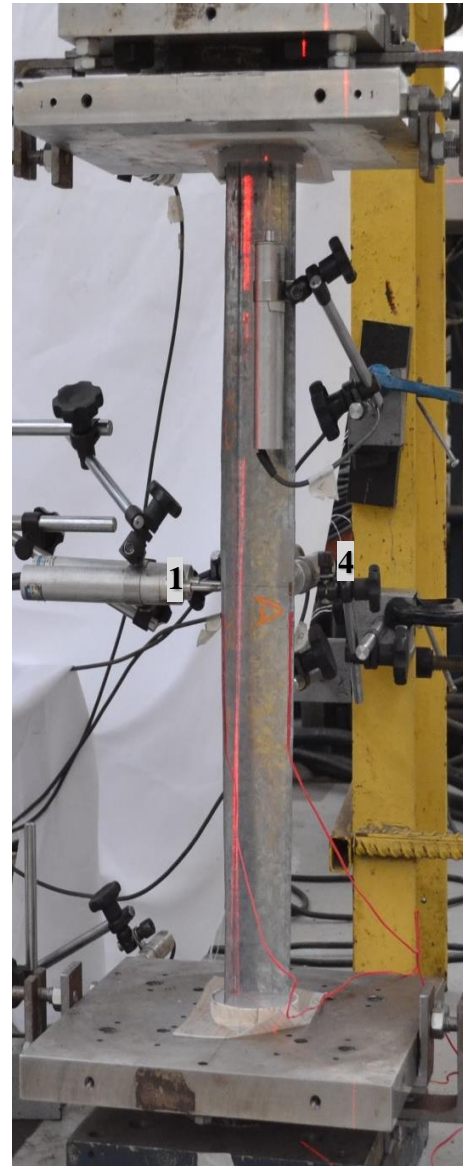


(c)

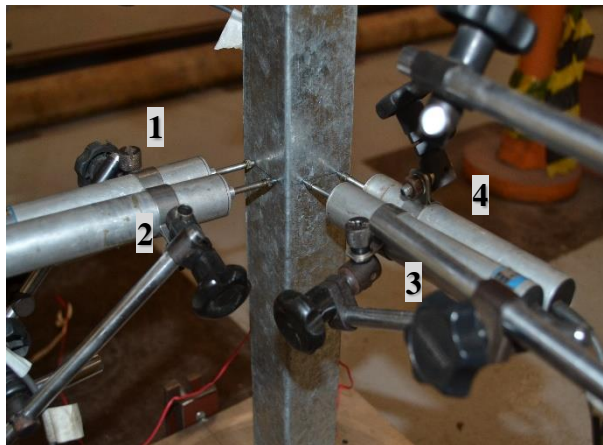
Figure 3.9: Close detail of the (a) epoxy-resin plate in the PVC cast, (b) bottom view of the epoxy-resin plate with the millimetre paper and (c) spherically-hinged support.



(a)



(c)



(b)

Figure 3.10: Arrangements to measure (a) initial geometrical imperfections and (b), (c) mid-height displacements.

## 3.7 Test Results

The experimental results obtained, namely: (i) initial geometrical imperfection configurations, (ii) equilibrium paths, (iii) failure load data and (iv) deformed configurations evidencing the presence of flexural and torsional deformations, are presented next. Such results were obtained following the procedures performed by CRUZ [20].

### 3.7.1 Initial geometrical imperfections

Initial geometrical imperfections were measured by spanning transducers DT1-4 along the specimen length. Table 3.3 provides (i) the maximum and minimum values recorded by each transducer and (ii) the computed values of the torsional rotation  $\beta$  and translations due to major and minor-axis flexure ( $d_M$  and  $d_m$ , respectively). This computation (i) is based on the fact that the cross-sections undergo rigid-body motions and (ii) takes into account that the DT1-4 remain fixed while the measured cross-sections move (this also applies to the determination of  $\beta$ ,  $d_M$  and  $d_m$  due to the applied load – see Section 3.7.2) and was made by means of the procedure described next and illustrated in Figures 3.11 (a)-(c):

- (i) Fig. 3.11(a) shows an undeformed cross-section, lying on the X-Y plane, and the locations of the four DTs: (i<sub>1</sub>) DT1-2 are placed normally to the “vertical” leg at distances  $y_1=(b-10)mm$  and  $y_2=10mm$  from the corner, and (i<sub>2</sub>) DT3-4 are placed normally to the “horizontal” leg, at distances  $x_3=10mm$  and  $x_4=(b-10)mm$  from the corner. Because the DTs are fixed, the “horizontal” and “vertical” projections of these distances obviously vary as the cross-section deforms (see Fig. 3.11(b)). The signs of the DT displacement measurements are in accordance with the coordinate system  $x$ - $y$  associated with the X-Y axes – moreover, the torsional rotation angles  $\beta$  are positive clockwise.

Table 3.3: Measured and calculated maximum and minimum specimen initial displacement and rotation values

| Column        | DT1    | DT2    | DT3    | DT4    | $d_{m0}$ | $d_{M0}$ | $\beta_0$ |
|---------------|--------|--------|--------|--------|----------|----------|-----------|
| 25t0.8L400    | 0.307  | 0.161  | 0.813  | -0.279 | -0.462   | 0.157    | -0.086    |
|               | 0.000  | 0.005  | 0.000  | 0.000  | -0.002   | 0.001    | 0.000     |
| 25t0.8L400-R  | -1.103 | -0.153 | 0.105  | -1.193 | -1.607   | -0.315   | -0.229    |
|               | -0.001 | -0.001 | 0.000  | 0.127  | 0.097    | 0.015    | 0.006     |
| 25t0.8L600    | -0.208 | 0.087  | -0.141 | -0.286 | 0.353    | -0.168   | -0.009    |
|               | 0.000  | 0.000  | 0.000  | 0.000  | 0.000    | -0.004   | 0.000     |
| 25t0.8L800    | 0.095  | 0.104  | 0.132  | 0.121  | 0.114    | 0.138    | 0.024     |
|               | 0.000  | 0.000  | 0.001  | 0.002  | 0.001    | 0.022    | 0.000     |
| 50t0.8L400    | 0.152  | -0.108 | 0.076  | -0.178 | -0.262   | -0.089   | -0.046    |
|               | 0.000  | 0.000  | -0.001 | -0.002 | -0.010   | -0.004   | 0.000     |
| 50t0.8L400-R  | -0.146 | -0.155 | 0.703  | -0.242 | -0.572   | 0.324    | -0.167    |
|               | 0.000  | 0.000  | 0.506  | 0.000  | -0.112   | 0.111    | -0.053    |
| 50t0.8L600    | -0.154 | -0.101 | -0.202 | -0.120 | 0.230    | -0.162   | 0.004     |
|               | 0.000  | 0.000  | 0.001  | 0.000  | 0.000    | -0.002   | 0.000     |
| 50t0.8L600-R  | -0.362 | -0.218 | -0.162 | -0.162 | 0.210    | -0.210   | -0.092    |
|               | -0.002 | 0.000  | 0.000  | 0.000  | 0.000    | 0.000    | 0.000     |
| 50t0.8L800    | 0.101  | -0.050 | -0.078 | -0.201 | -0.274   | -0.091   | 0.048     |
|               | 0.000  | 0.000  | 0.000  | 0.000  | 0.000    | 0.000    | 0.000     |
| 50t0.95L400   | 0.531  | 0.244  | 0.265  | 0.413  | 0.424    | 0.374    | 0.151     |
|               | 0.000  | 0.000  | 0.000  | 0.000  | -0.001   | 0.001    | 0.000     |
| 50t0.95L600   | 0.167  | 0.090  | -0.194 | -0.345 | -0.486   | 0.159    | 0.081     |
|               | 0.000  | 0.000  | 0.000  | 0.000  | -0.002   | 0.000    | 0.000     |
| 50t0.95L600-R | 0.200  | -0.208 | -0.434 | 0.834  | 1.146    | 0.239    | 0.222     |
|               | 0.000  | 0.000  | 0.000  | 0.149  | 0.171    | 0.001    | 0.002     |
| 50t0.95L800   | -0.145 | 0.276  | -0.118 | -0.122 | -0.160   | -0.125   | -0.047    |
|               | 0.000  | 0.000  | 0.000  | 0.000  | -0.001   | 0.000    | 0.000     |
| 50t0.95L1000  | -0.104 | 0.044  | 0.160  | -0.182 | -0.283   | 0.108    | -0.054    |
|               | 0.000  | 0.000  | -0.001 | 0.000  | 0.000    | 0.000    | 0.000     |
| 50t1.25L400   | 0.271  | 0.154  | -0.189 | 0.230  | 0.326    | 0.200    | 0.070     |
|               | 0.001  | 0.000  | 0.000  | 0.000  | 0.000    | 0.000    | 0.000     |
| 50t1.25L600   | 0.405  | 0.258  | 0.237  | 0.237  | -0.332   | 0.232    | 0.074     |
|               | 0.001  | 0.001  | 0.005  | 0.004  | -0.005   | 0.002    | 0.000     |
| 50t1.25L600-R | 0.589  | 0.196  | 0.116  | 0.756  | 0.732    | 0.337    | 0.134     |
|               | 0.000  | 0.002  | 0.003  | -0.005 | -0.005   | 0.021    | -0.002    |
| 50t1.25L800   | 0.275  | -0.158 | 0.829  | 2.203  | 2.592    | 0.112    | 0.060     |
|               | 0.000  | 0.000  | 0.000  | 0.000  | 0.003    | 0.000    | 0.000     |
| 50t1.25L1000  | -0.181 | 0.082  | 0.082  | 0.195  | 0.275    | 0.124    | 0.051     |
|               | 0.000  | 0.000  | 0.000  | 0.000  | 0.006    | 0.000    | 0.000     |

Note: All DTs,  $d_{m0}$  and  $d_{M0}$  measurements are in  $(mm \times 10^{-2})$ .  $\beta_0$  measurements are in  $rad \times 10^{-3}$ .

(ii) The first step consists of using the four DT measurements to calculate the cross-section torsional rotation  $\beta$  and “horizontal” ( $d_H$ ) and “vertical” ( $d_V$ ) translations. Then, a coordinate change leads to the translations along the major ( $d_m$ ) and minor ( $d_M$ ), as indicated in Fig.3.11(b).

(iii) The cross-section torsional rotation  $\beta$  is obtained from one of the expressions

$$\beta = \tan^{-1} \left( \frac{DT1 - DT2}{y_2 - y_1} \right) \text{ or } \tan^{-1} \left( \frac{DT4 - DT3}{x_4 - x_3} \right) \quad (3.1)$$

(iv) The determination of  $d_H$  and  $d_V$  is more involved, because it must account for the continuous (as deformation evolves) change in the relative position of the four DTs with respect to the cross-section, as illustrated in Fig. 9(b). Each DT displacement measurement combines two parts, one identical to a translation ( $d_H$  or  $d_V$ ) and the other equal to the product of the torsional rotation by an “horizontal” or “vertical” distance that depends on the cross-section corner location. Indeed, the DT1 and DT4 measurements can be expressed in terms of  $d_H$ ,  $d_V$ ,  $\beta$  as (see Fig. 9(b))<sup>1</sup>

$$DT1 = d_H - (y_1 - d_V) \tan \beta \quad (3.2)$$

$$DT4 = d_V + (x_4 - d_H) \tan \beta \quad (3.3)$$

(v) Solving the system formed by Eqs. (3.2) and (3.3) and taking into account Eq. (3.3), the values of  $d_H$  and  $d_V$ , defining the location of the cross-section corner, are obtained from

$$d_H = (DT1 - DT4 \tan \beta + y_1 \tan \beta + x_4 \tan^2 \beta) / (1 + \tan^2 \beta) \quad (3.4)$$

$$d_V = (DT1 \tan \beta + DT4 + y_1 \tan^2 \beta - x_4 \tan \beta) / (1 + \tan^2 \beta) \quad (3.5)$$

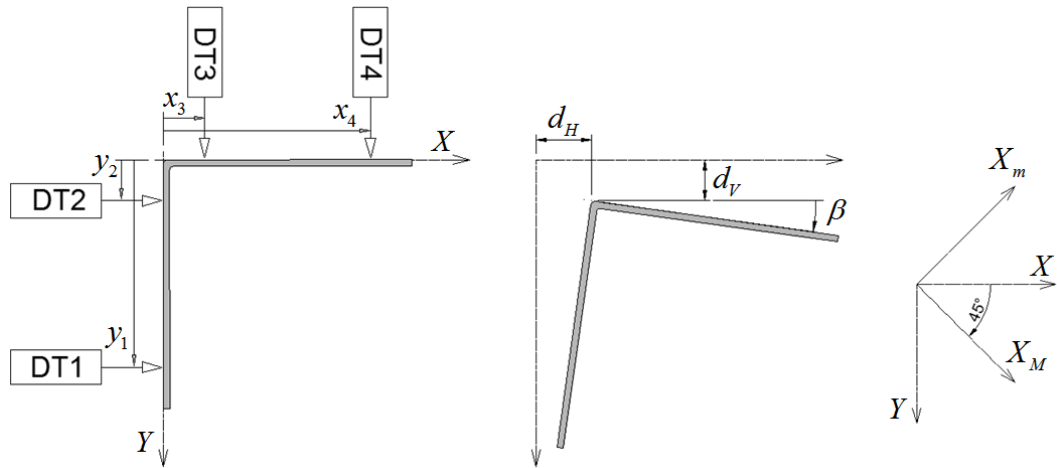


Figure 3.11: Cross-section: (a) undeformed configuration and DT locations, (b) deformed configuration and definition of  $d_H$ ,  $d_V$  and  $\beta$ , and (c) change of coordinate axes, required to determine  $d_M$  and  $d_m$  [20]

<sup>1</sup> The  $d_H$ ,  $d_V$  and  $\beta$  values are obtained from only three DT measurements – the fourth is used for verification.

(vi) The last step consists of expressing the location of the cross-section corner through its coordinates along the cross-section centroidal principal axes ( $d_M$  and  $d_m$ )<sup>2</sup>, which form  $45^\circ$  angles with the “horizontal” and “vertical” – this procedure is illustrated in Fig. 3.11(c) and leads to Eqs. 3.6 and 3.7.

$$d_M = (d_H + d_V) \sqrt{2} / 2 \quad (3.6)$$

$$d_m = (d_H - d_V) \sqrt{2} / 2 \quad (3.7)$$

Figures 3.12(a)-(b) show the initial displacement/rotation longitudinal profiles acquired from the tests of specimens *50t0.8L800-50t0.95L800-50t1.25L1000-50t0.95L1000*, obtained either (i) directly from the DT1-4 readings or (ii) using Eqs. (3.12)-(3.15) ( $\beta$ ,  $d_M$  and  $d_m$ ) – note that (i) the horizontal coordinates are normalised with respect to the column measured length  $L_0$  ( $DT5/L_0$ ) and (ii) the sign assumed for the transducer readings is also indicated (positive/negative readings for outward/inward displacements, respectively). The observation of these results prompts the following remarks:

- (i) DT1-4 measurements are considerably low (all below  $10^{-2}$  mm, a value smaller than the nominal wall thickness).
- (ii) All displacement profiles exhibit (ii<sub>1</sub>) some degree of asymmetry and (ii<sub>2</sub>) a dominant single half-wave sinusoidal shape, combined with minor participations of two and three half-wave sinusoids.
- (iii) The maximum  $d_m$  and  $d_M$  values are: about  $2.592 \text{ mm} \times 10^{-2}$  and  $0.374 \text{ mm} \times 10^{-2}$ , respectively. Moreover, the  $d_m/L_0$  and  $d_M/L_0$  ratios (iii<sub>1</sub>) vary from  $-4.02 \times 10^{-5}$  to  $0.00$ , and from  $9.35 \times 10^{-6}$  to  $0.00$ , respectively, and (iii<sub>2</sub>)  $L/1000$  is not exceeded in any case. Finally, the mid-span torsional rotation  $\beta$  ranges between  $-2.23 \times 10^{-4}$  and  $0.00 \text{ rad}$ .

---

<sup>2</sup>  $d_M$  and  $d_m$  are caused by major-axis and minor-axis bending, respectively. they take place along the cross-section centroidal principal minor ( $X_m$ ) and major ( $X_M$ ) axes, respectively.

### 3.7.2 Equilibrium paths

Figure 3.13 shows the equilibrium paths obtained from the tests involving specimens 50t0.8L800-50t0.95L800-50t1.25L800, relating the applied load  $P$ , provided by the hydraulic actuator load cell, to (i) the axial shortening  $\Delta$  (DT5 reading) and (ii) the mid-height torsional rotation  $\beta$  and translations due to minor-axis ( $d_m$ ) and major-axis ( $d_M$ ) flexure –  $\beta$ ,  $d_m$ ,  $d_M$  are caused by the applied load (*i.e.*, exclude the initial imperfections). The observation of such equilibrium paths leads to the remarks:

- (i) The equilibrium paths  $P$  vs.  $\Delta$  exhibit linear initial portions whose slopes are quite similar, thus reflecting the relatively close column axial stiffness values –  $EA/L_0=205.5-243.9-250$  kN/cm for the 50t0.8L800-50t0.95L800-50t1.25L800 columns. Moreover, note also that both the (i<sub>1</sub>) applied load level associated with the transition to a non-linear curve and (i<sub>2</sub>) length covered by such non-linear curve (prior to failure) vary considerably – they increase with the values of the column (i<sub>1</sub>) critical buckling load and (i<sub>2</sub>) parameter  $\Delta_f$  (see Table 3.1), respectively.
- (ii) The equilibrium paths  $P$  vs.  $\beta$  and  $P$  vs.  $d_m$  follow practically the same trend (accounting for the different scales, of course), which stems from the fact that they correspond to a single deformation pattern, akin to the flexural-torsional buckling mode.
- (iii) The equilibrium paths  $P$  vs.  $d_m$  only branch out of the null displacement vertical line at the load equal to approximately  $0.5$  kN, which is a moderately advanced loading stage for these cases (especially for thickness  $0.8$ mm and  $0.95$  mm). This is due to the fact that such displacements stem from a combination of (iii<sub>1</sub>) effective centroid shift effects, occurring in all columns, and (iii<sub>2</sub>) interaction with minor-axis flexural buckling, only relevant for columns with relatively close flexural-torsional and flexural buckling loads.
- (iv) The amount of deformation exhibited by the three sets of equilibrium paths  $P$  vs.  $\beta$ ,  $P$  vs.  $d_M$  and  $P$  vs.  $d_m$  prior to failure varies with  $\Delta_f$  (see Table 3.1), which is due to the influence of this parameter on the column post-critical strength and ductility prior to failure unveiled in [15]. In the case of these three columns, all  $\Delta_f$  values are quite small (the 50t1.25L800 column one is the highest) and, therefore, the differences are not very perceptible and,

moreover, can easily be “masked” by the different initial geometrical imperfections<sup>3</sup>.

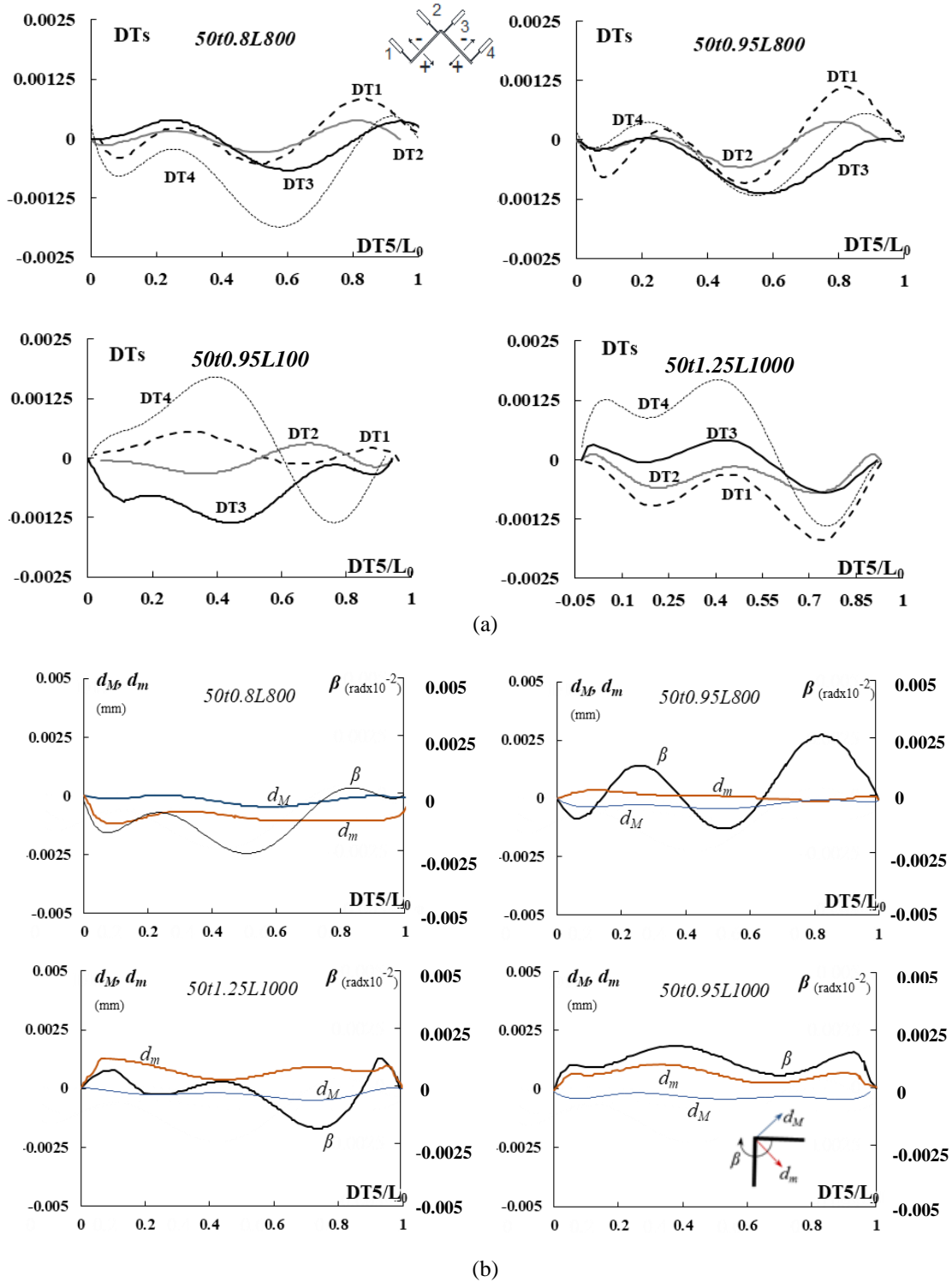


Figure 3.12: Initial displacement and rotation longitudinal profiles (horizontal coordinate normalised with respect to  $L_0$ ) concerning specimens  $50t0.8L800$ - $50t0.95L800$ - $50t1.25L1000$ - $50t0.95L1000$ : (a) DT1-4 readings and (b)  $\beta$ ,  $d_M$  and  $d_m$  values.

<sup>3</sup> An extensive parametric study was performed in [18], involving columns with identical cross-sections and initial geometrical imperfections (only the length varied along the  $P_{cr}$  vs.  $L$  “plateau”). It was shown that, as the length (and  $\Delta_y$ ) increases, the post-critical strength and ductility prior to failure increase and decrease, respectively.

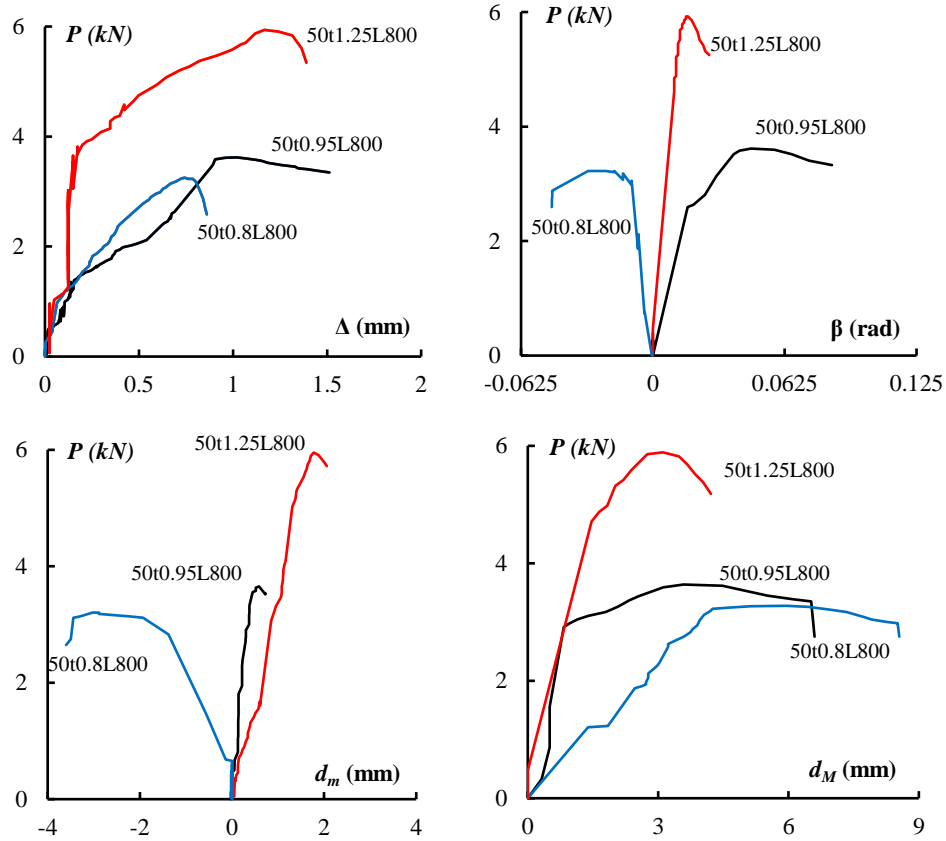


Figure 3.13: 50t0.8L800-50t0.95L800-50t01.25L800 column experimental equilibrium paths relating  $P$  to the axial shortening  $\Delta$  and the calculated mid-height torsional rotation  $\beta$  and displacements due to minor-axis ( $d_m$ ) and major-axis ( $d_M$ ) flexure.

### 3.7.3 Failure loads

Table 3.4 provides the column (i) experimental failure loads  $P_{u.Exp}$ , (ii) squash loads  $P_y$ , (iii) ratios  $P_{u.Exp}/P_y$  and (iv) failure mode natures. The values of  $P_y$  are based on (i) areas  $A$  obtained from the average values of the measured cross-section dimensions (disregarding the rounded corners) and (ii) the yield stress  $f_y=366\text{ MPa}$ , the average of the tensile coupon test results presented in Section 4.2. The specimens failed in either (i) a mode exhibiting highly predominant major-axis flexural-torsional deformations (termed “FT”) and (ii) a mode combining major-axis flexural-torsional deformations with visible minor-axis flexural ones (termed “FT+F”)<sup>4</sup>. The latter was found occur only for the

<sup>4</sup> The displacement measurements reveal that specimens failing in FT modes also exhibit minor-axis flexure, which only appears very close to failure. Nevertheless, the  $d_m$  displacements are not visible by the naked eye, unlike those exhibited by the specimens failing in FT+F modes.

column 25t0.8L800, which combines the shortest leg width with one of the highest lengths. This is just a logical consequence of the fact that the FT (critical) and F buckling loads are closer for this column, thus leading to the occurrence of stronger interaction effects between the two buckling modes. Moreover, it should also be noticed that all specimens exhibit  $P_{u,Exp}/P_y$  ratios below 0.24, which is in accordance with their high slenderness values (plasticity plays a lesser role in the column failure). Finally, it is still worth noting that the failure loads corresponding to the repeated tested specimens (25t0.8L400-R, 50t0.8L400-R and 50t0.95L600-R) differ by an average of 8%, thus evidencing good test repeatability.

Table 3.4: Experimental results: column failure loads, squash loads and observed failure modes.

| Column        | $P_{u,Exp}$<br>(kN) | $P_y$<br>(kN) | $\frac{P_{u,Exp}}{P_y}$ | Failure mode |
|---------------|---------------------|---------------|-------------------------|--------------|
| 25t0.8L400    | 3.59                | 14.87         | 0.24                    | FT           |
| 25t0.8L400-R  | 3.33                | 14.90         | 0.22                    | FT           |
| 25t0.8L600    | 3.40                | 15.10         | 0.22                    | FT           |
| 25t0.8L800    | 2.81                | 14.82         | 0.19                    | FT+F         |
| 50t0.8L400    | 3.87                | 29.63         | 0.13                    | FT           |
| 50t0.8L400-R  | 3.65                | 28.51         | 0.13                    | FT           |
| 50t0.8L600    | 3.15                | 29.96         | 0.11                    | FT           |
| 50t0.8L600-R  | 2.89                | 30.37         | 0.10                    | FT           |
| 50t0.8L800    | 3.20                | 29.21         | 0.11                    | FT           |
| 50t0.95L400   | 5.90                | 34.70         | 0.17                    | FT           |
| 50t0.95L600   | 4.63                | 35.26         | 0.13                    | FT           |
| 50t0.95L600-R | 3.88                | 35.42         | 0.11                    | FT           |
| 50t0.95L800   | 3.65                | 34.70         | 0.11                    | FT           |
| 50t0.95L1000  | 3.72                | 34.67         | 0.11                    | FT           |
| 50t1.25L400   | 9.30                | 44.88         | 0.21                    | FT           |
| 50t1.25L600   | 5.96                | 45.15         | 0.13                    | FT           |
| 50t1.25L600-R | 7.51                | 44.97         | 0.17                    | FT           |
| 50t1.25L800   | 6.53                | 44.17         | 0.15                    | FT           |
| 50t1.25L1000  | 5.94                | 44.47         | 0.13                    | FT           |

### 3.7.4 Deformed configurations and failure modes

Figs. 3.14(a)-(b) concern specimen 50t0.95L600 and provide its (i) equilibrium path  $P$  vs.  $\Delta$  and (ii) deformed configuration evolution during the test – the six deformed configuration shown in Fig. 3.14(b) correspond to the equilibrium states  $I$  to  $VI$  indicated by yellow circles on the equilibrium path depicted in Fig. 12(a). Figs. 3.15(a)-(c) and 3.16(a)-(b) show (i) the deformed configurations, at the onset of collapse ( $P \approx P_{u.Exp}$ ), of specimens 25t0.8L400, 25t0.8L600 and 25t0.8L800, (ii) a close view of the specimen 25t0.8L400 most deformed region just after collapse and (iii) a joint view of the deformed shapes of the four specimens with leg width  $b=25mm$  (25t0.8 series) after the load removal. The observation of these column deformed configurations makes it possible to conclude that:

- (i) The evolution of the specimen 50t0.95L600 deformed configuration, depicted in Fig. 3.14(b), nicely illustrates the emergence and development of predominantly torsional flexural-torsional deformations towards failure in a single half-wave FT mode, akin to the corresponding critical buckling mode<sup>5</sup>. The specimen remains almost undeformed until state  $I$  (about 30% of the failure load). However, beyond this stage flexural-torsional displacements become clearly visible and grow progressively until failure, which occurs at state  $V$ . After the peak load has been reached, the deformation becomes slightly more pronounced, as illustrated by means of state  $VI$ .
- (ii) The collapse mechanisms exhibited by all the specimens are triggered by the formation of “plastic hinges” close to the one and three quarter-height cross-sections, as can be observed in Figs. 3.14(b-V) and 3.15(a)-(c) – note that numerical evidence of this feature was recently reported in [22]<sup>6</sup>. No correlation with the measured initial geometrical imperfections (shape and amplitude) could be found – indeed, the column failure mode seemed to be independent of its initial configuration.

---

<sup>5</sup> Of course, the designation “single half-wave” takes into account the two “quarter-waves” appearing near the specimen supports, fixed with respect to torsion and major-axis flexure. Moreover, there are also minute minor-axis flexural deformations due to the effective centroid shift effects [22]

<sup>6</sup> These “plastic hinges” were found to be closer to the mid-height region in specimens 50t1.25L600 and 25t0.8L400-R – no rational explanation can be provided for this fact.

(iii) The specimens deformed configurations depicted in Fig. 3.16(b) make it possible to assess the amount of elastic deformation undergone by the compressed columns during the test, which is subsequently recovered after the load was removed – *e.g.*, it suffices to compare the deformed configurations displayed in Figs. 3.15(a)-(c) and 3.16(b).

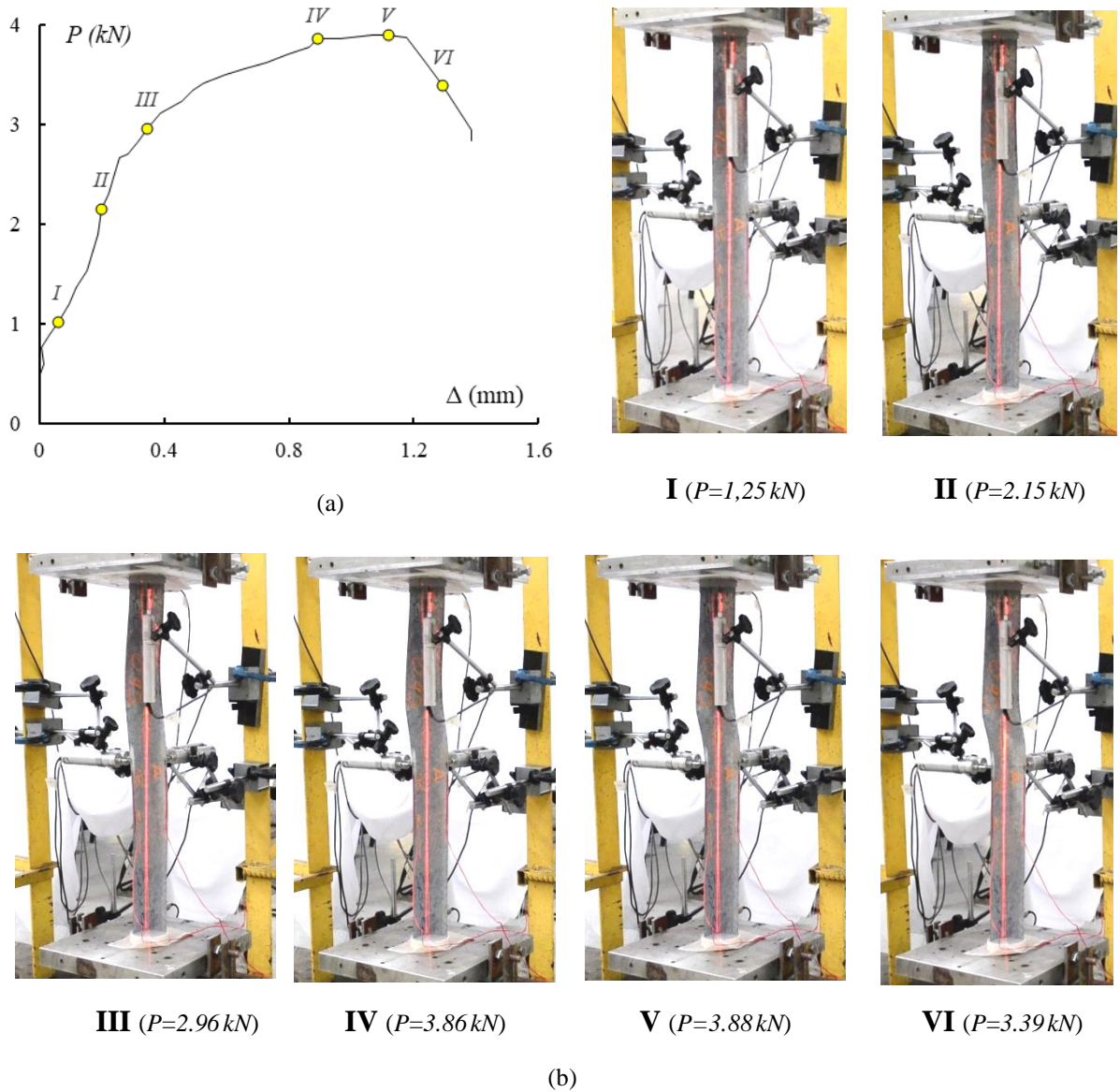


Figure 3.14: 50t0.95L600 specimen (a) equilibrium path  $P$  vs.  $\Delta$  and (b) deformed configuration evolution.

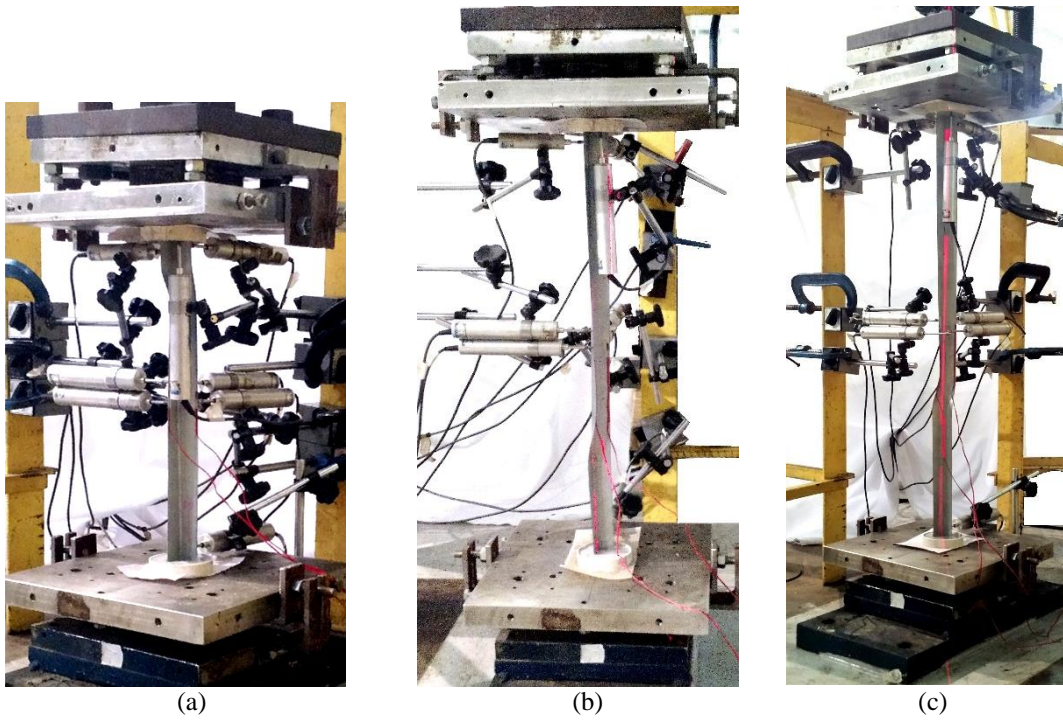


Figure 3.15: Deformed configurations at the onset of collapse of specimens (a) 25t0.8L400, (b) 25t0.8L600 and (c) 25t0.8L800.



Figure 3.16: (a) Close view of the most deformed region of specimen 25t0.8 L400 just after collapse and (b) joint view of the specimens belonging to the 25t0.80 series after the load removal.

## 4 Numerical Simulations

---

After briefly addressing the main features of the ANSYS [45] shell finite element (SFE) model adopted to perform the numerical simulation of the column tests, its validation is presented by comparing experimental results reported in Section 3.7 with the corresponding values provided by the column geometrically and materially non-linear analyses. Then, the (validated) SFE model is employed to analyse the columns identified in Table 3.2, in order to gather additional failure load data concerning slender pin-ended equal-leg angle columns.

### 4.1 ANSYS Shell Finite Element Model

The equilibrium paths and the ultimate loads of the selected columns were obtained through a non-linear finite-element model, by means of an ANSYS code.

The columns were discretised into SHELL181 elements (ANSYS nomenclature – 4-node shear deformable thin-shell elements with six degrees of freedom per node and full integration) – convergence studies [50] showed that  $5\text{ mm} \times 5\text{ mm}$  meshes provide accurate results, while involving a reasonable computational effort. The analyses were performed by means of an incremental-iterative technique combining Newton-Raphson's method with an arc-length control strategy.

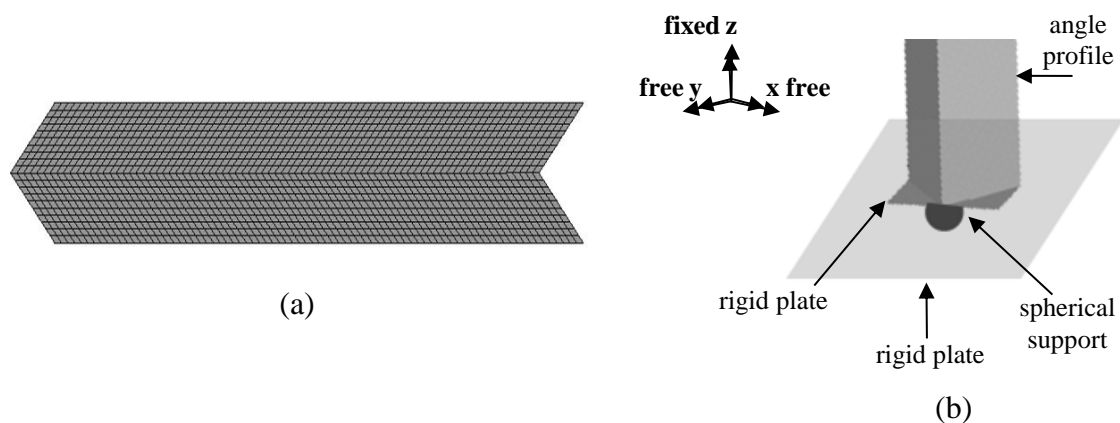


Figure 4.1: (a) Shell finite elements in a  $5\text{ mm} \times 5\text{ mm}$  mesh and (b) support conditions adopted.

All columns exhibited (i) an elastic-perfectly plastic material behaviour (Prandtl-Reuss's model: von Mises yield criterion and associated flow rule), characterised by  $E=205\text{ GPa}$ ,  $\nu=0.3$  and 17 yield stresses ( $f_y=366$  and  $f_y=150; 200; 250; 275; 300; 350; 375; 400; 450; 475; 500; 550; 575; 600; 650; 700\text{ MPa}$ , respectively for the validation and parametric studies<sup>7</sup>), (ii) spherically-hinged end supports materialised by attaching the member end sections to rigid end plates (thus ensuring full secondary warping and local displacement/rotation restraint) with prevented flexural displacements and torsional rotations (spherically-hinged supports, see Section 4.3), and (iii) initial imperfections either taken from the initial imperfection measurements (validation study) or combining a critical flexural-torsional component, with amplitude equal to 10% of the wall thickness  $t$ , and a non-critical minor-axis flexural component, with amplitude equal to  $L/1000$  (parametric study)<sup>8</sup> – value in line with the measurements reported for the specimens tested in [10] and made in the specimens tested in this work. Each buckling mode shape was determined by means of a preliminary ANSYS SFE buckling analysis, performed with exactly the same mesh employed to carry out the subsequent non-linear analysis – this procedure makes it very easy to “transform” the buckling analysis output into a non-linear analysis input. However, in the validation study, the initial geometrical imperfections considered were obtained through a procedure based on the Fourier series approximation of the measured (i) cross-section torsional rotation ( $\beta$ ), (ii) “horizontal” displacement ( $d_H$ ) and (iii) “vertical” displacement ( $d_V$ ) longitudinal profiles (see Figure 4.1). In order to illustrate the quality of the output of this procedure, Figs. 4.1(a)-(d) compare the measured 50t0.95L400 column  $d_H$  and  $d_V$  longitudinal profiles with their approximations obtained by means of linear combination of trigonometric functions – it is clear that there is an excellent correlation.

---

<sup>7</sup> Obviously, the steel grades between 400 MPa and 700MPa are rarely used in cold-formed steel structures applications, even if they are currently available. The sole purpose of their adoption was covering a wide slenderness range – the alternative would be to select additional column geometries (cross-section dimensions and lengths), leading to a much more involved modelling task.

<sup>8</sup> Although the shorter columns are virtually insensitive to the minor-axis flexural imperfections (only the flexural-torsional ones are relevant), it was decided to analyse only columns containing both flexural-torsional and minor-axis flexural initial imperfections. Moreover, note that the initial  $d_m$  values always “point” towards the cross-section corner, thus reinforcing the effective centroid shift effects (most detrimental situation).

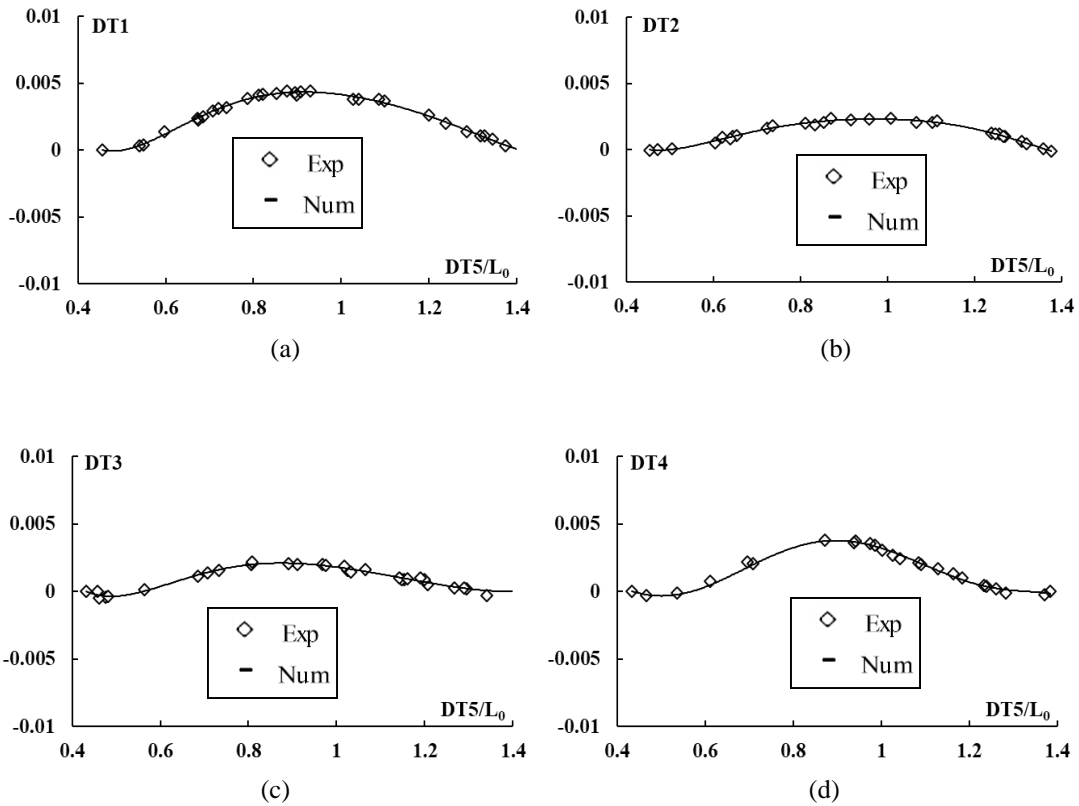


Figure 4.1: Comparison between the measured and approximated 50t0.95L400 column (a) DT1, (b) DT2, (c) DT3 and (d) DT4 displacement profiles.

The three initial approximation longitudinal functions are then used to obtain the column “initially imperfect configuration” and incorporate it in the shell finite element mesh – when necessary, a linear displacement variation along the cross-section wall mid-line is assumed between the equally spaced leg nodes. Since the tensile coupon tests showed that the steel material behaviour is clearly elastic-perfectly plastic, no strain-hardening was considered. Moreover, no residual stresses (not measured in the tested specimens) and corner strength effects were included in the analyses – note that it has been reported in the literature (*e.g.*, [51] and [52]) that the combined influence of strain hardening, residual stresses and rounded corner effects has little impact on the angle column failure loads. The axial compression is applied through concentrated forces applied on the rigid end plate points corresponding to the end section centroids (the longitudinal displacement of one mid-height cross-section point is prevented). The above axial forces are always increased in small increments, by means of the ANSYS automatic load stepping procedure.

## 4.2 Validation Study

The experimental results reported in Section 3.7 (19 specimens) are now used to show the adequacy of the adopted ANSYS SFE model. Table 4.1 provides the data concerning the 19 columns considered, namely their (i) measured geometries and maximum initial displacement and rotation amplitudes, and (ii) experimental failure loads. Moreover, this table also includes the (i) column numerical failure loads and (ii) the percentage differences with respect to the experimental ones – these percentage differences are plotted against  $\lambda_{fte}$  in Fig 4.2. On the other hand, Figs. 4.3(a)-4.5(b) show comparisons between the three specimen numerical and experimental (i) equilibrium paths ( $P$  vs.  $\Delta$ ,  $\beta$ ,  $d_m$ ,  $d_M$ ) (ii) failure modes (deformed shapes at the onset of collapse). The observation of these comparisons leads to the following comments:

- (i) The numerical post-buckling equilibrium paths are always reasonably close to the experimental ones and replicate very well their peak loads – the average of the percentage difference absolute values is equal to 6.4% and only three of them exceed 10%. Moreover, they provide confirmation of the occurrence of interaction between major-axis flexural-torsional and minor-axis flexural buckling – the column collapse modes combine significant mid-span rigid-body rotations ( $\beta > 0.1 \text{ rad}$ ) and displacements due to minor-axis bending.
- (ii) Although there is very good qualitative agreement between the numerical and experimental equilibrium paths, there are visible quantitative differences, namely those concerning the ductility prior to failure, which is considerably higher in the numerical results. Those differences concern mostly the equilibrium path shapes and stem, essentially, from the fact that (ii<sub>1</sub>) the experimental displacement control provided by the test set-up was not fine enough to enable capturing adequately the ductility prior to failure obtained in the numerical simulations, and (ii<sub>2</sub>) the displacement transducer tips “slip” during a test, due to the mid-height cross-section rigid-body motion, which means that the measured displacements do not concern exactly the same points throughout a given test.
- (iii) There is a quite satisfactory match between the ANSYS failure modes and the observed collapse mechanisms: both are fairly symmetric and provide clear evidence of flexural-torsional deformations.

- (iv) The specimen failure loads are safely and reasonably accurately estimated by incorporating into the analyses initial geometrical imperfections combining a critical flexural-torsional component, with amplitude  $0.1t$ , and a non-critical minor-axis flexural component, with amplitude  $L/1000$ . Indeed, the failure loads ( $P_{u,Num}$ ) obtained underestimated the experimental ones by a percentage amount varying between 15.6% and 0.13%.
- (v) On the basis of the above comparisons, it seems fair to conclude that the SFE model employed is able to capture adequately the geometrically and materially non-linear (post-buckling) behaviour and strength of the short-to-intermediate pin-ended equal-leg angle columns under consideration. Therefore, this model will be used to perform the parametric study presented in the next section, aimed at gathering additional column failure loads, covering a wider slenderness range.

Table 4.1: Specimens considered in the validation study: (i) geometries, maximum initial displacement and rotation amplitudes, (ii) experimental and numerical failure loads, and (iii) percentage difference between them.

| Column        | $b$<br>(mm) | $t$<br>(mm) | $\theta_b$<br>(deg) | $L_o$<br>(mm) | $d_{m0}$<br>( $mm \times 10^{-2}$ ) | $d_{M0}$<br>( $mm \times 10^{-2}$ ) | $\beta_0$<br>( $rad \times 10^{-3}$ ) | $P_{u,Exp}$<br>(kN) | $P_{u,Num}$<br>(kN) | $\frac{P_{u,Exp} - P_{u,Num}}{P_{u,Exp}}$ |
|---------------|-------------|-------------|---------------------|---------------|-------------------------------------|-------------------------------------|---------------------------------------|---------------------|---------------------|---|
| 25t0.8L400    | 25.63       | 0.8         | 88                  | 401.25        | -0.462                              | 0.157                               | -0.086                                | 3.59                | 3.29                | 8.08%                                     |
| 25t0.8L400-R  | 25.495      | 0.8         | 87                  | 400.5         | -1.607                              | -0.315                              | -0.229                                | 3.33                | 3.37                | -1.28%                                    |
| 25t0.8L600    | 26.03       | 0.805       | 89                  | 601           | 0.353                               | -0.168                              | -0.009                                | 3.40                | 3.36                | 1.18%                                     |
| 25t0.8L800    | 25.555      | 0.795       | 89                  | 800           | 0.114                               | 0.138                               | 0.024                                 | 2.81                | 2.60                | 7.47%                                     |
| 50t0.8L400    | 50.015      | 0.8         | 91                  | 401           | -0.262                              | -0.089                              | -0.046                                | 3.87                | 3.30                | 14.73%                                    |
| 50t0.8L400-R  | 49.09       | 0.8         | 90                  | 400.5         | -0.572                              | 0.324                               | -0.167                                | 3.65                | 3.60                | 1.37%                                     |
| 50t0.8L600    | 50.98       | 0.8025      | 90                  | 600           | 0.230                               | -0.162                              | 0.004                                 | 3.15                | 2.90                | 7.94%                                     |
| 50t0.8L600-R  | 52.005      | 0.8         | 87                  | 600           | 0.210                               | -0.210                              | -0.092                                | 2.89                | 2.80                | 3.11%                                     |
| 50t0.8L800    | 50.21       | 0.8         | 87                  | 800           | -0.274                              | -0.091                              | 0.048                                 | 3.20                | 3.7                 | -15.63%                                   |
| 50t0.95L400   | 49.86       | 0.96        | 88                  | 400           | 0.424                               | 0.374                               | 0.151                                 | 5.90                | 5.40                | 8.47%                                     |
| 50t0.95L600   | 50.65       | 0.96        | 84                  | 599           | -0.486                              | 0.159                               | 0.081                                 | 4.63                | 4.60                | 0.65%                                     |
| 50t0.95L600-R | 50.65       | 0.96        | 86                  | 600           | 1.146                               | 0.239                               | 0.222                                 | 3.88                | 3.60                | 7.22%                                     |
| 50t0.95L800   | 49.86       | 0.96        | 88.5                | 800.75        | -0.160                              | -0.125                              | -0.047                                | 3.65                | 3.30                | 9.59%                                     |
| 50t0.95L1000  | 49.845      | 0.96        | 89.5                | 1001          | -0.283                              | 0.108                               | -0.054                                | 3.72                | 3.50                | 5.91%                                     |
| 50t1.25L400   | 50.095      | 1.225       | 87                  | 400           | 0.326                               | 0.200                               | 0.070                                 | 9.30                | 8.80                | 5.38%                                     |
| 50t1.25L600   | 50.97       | 1.22        | 86                  | 600           | -0.332                              | 0.232                               | 0.074                                 | 5.96                | 6.70                | -12.42%                                   |
| 50t1.25L600-R | 51.125      | 1.22        | 86                  | 600           | 0.732                               | 0.337                               | 0.134                                 | 7.51                | 7.50                | 0.13%                                     |
| 50t1.25L800   | 49.85       | 1.22        | 87                  | 800.25        | 2.592                               | 0.112                               | 0.060                                 | 6.53                | 7.00                | -7.20%                                    |
| 50t1.25L1000  | 50.005      | 1.23        | 88                  | 1001.2        | 0.275                               | 0.124                               | 0.051                                 | 5.94                | 6.20                | -4.38%                                    |

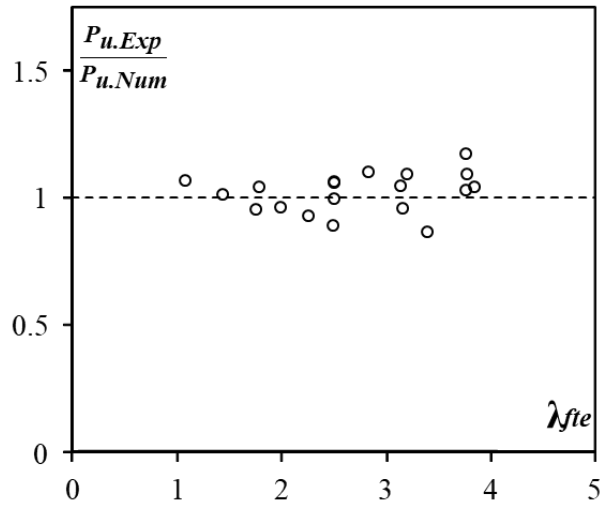


Figure 4.2: Plot of the percentage difference between the experimental and numerical failure loads against the slenderness  $\lambda_{fte}$ .

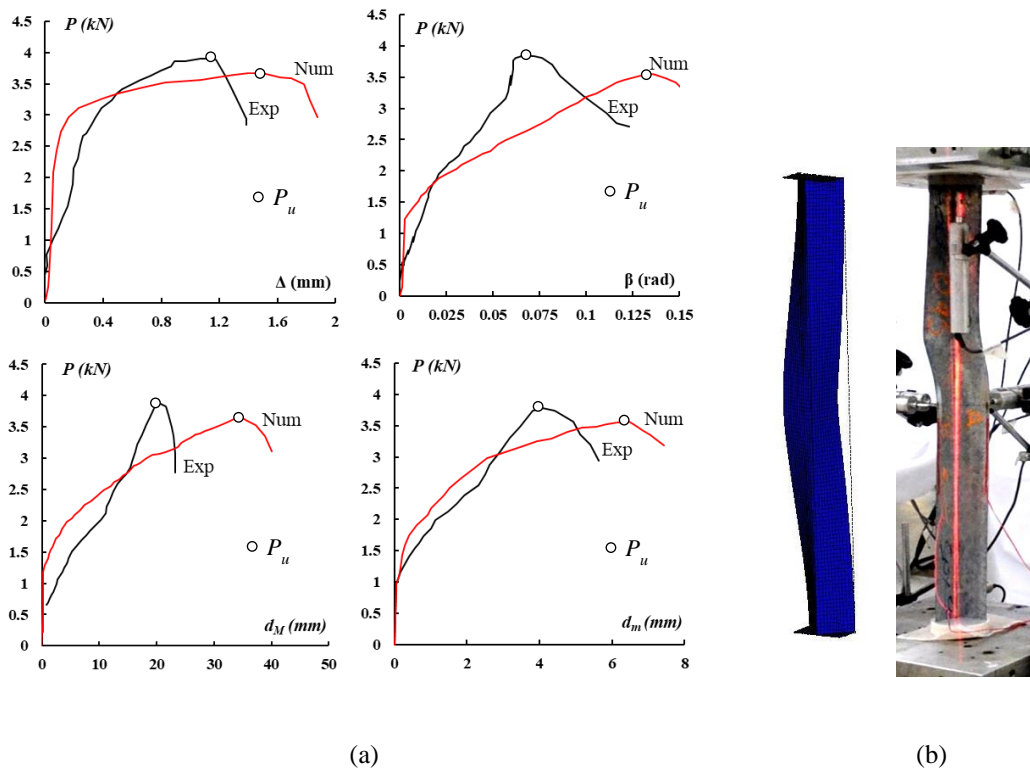


Figure 4.3: 50t0.95L600 column experimental and numerical (a) equilibrium paths  $P$  vs.  $\Delta$  and the mid-height  $\beta$  and displacements  $d_m$  and  $d_M$ , and (b) collapse mechanisms.

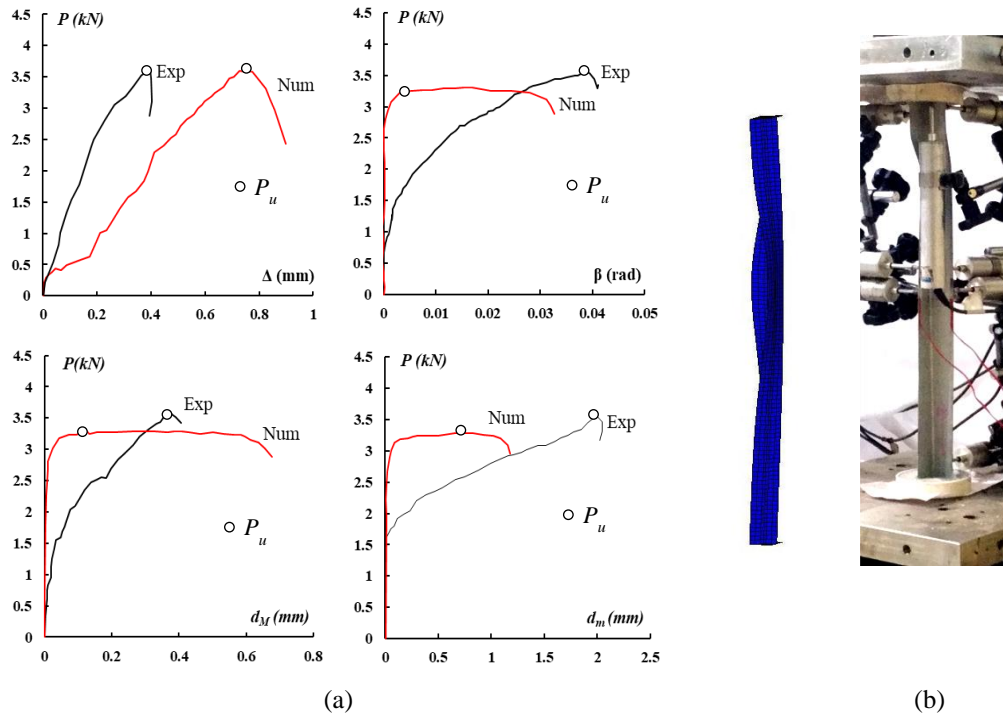


Figure 4.4: 25t0.8L400 column experimental and numerical (a) equilibrium paths  $P$  vs.  $\Delta$  and the mid-height  $\beta$  and displacements  $d_m$  and  $d_M$ , and (b) collapse mechanisms.

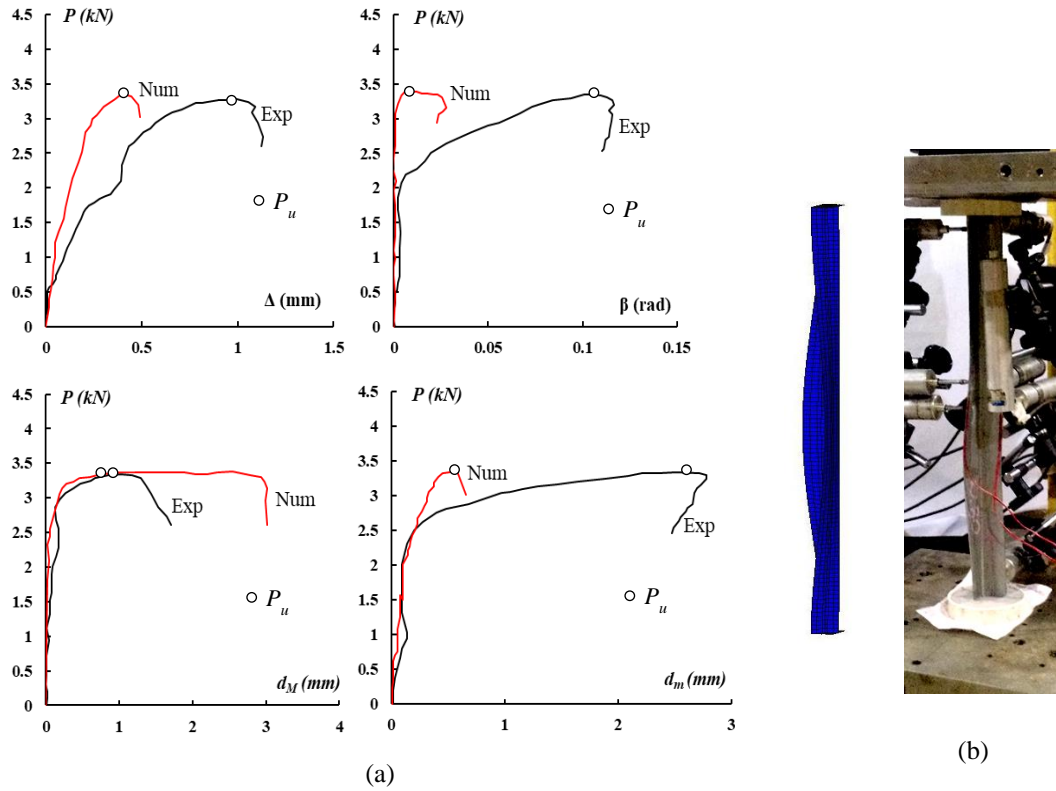


Figure 4.5: 25t0.8L400-R column experimental and numerical (a) equilibrium paths  $P$  vs.  $\Delta$  and the mid-height  $\beta$  and displacements  $d_m$  and  $d_M$ , and (b) collapse mechanisms.

### 4.3 Parametric Study – Numerical Failure Loads

The aim of this section is to present the numerical failure load data gathered from the parametric study carried out, involving a total of 256 columns that correspond to all combinations of the 16 geometries and 16 yield stresses (see table 4.2).

Table 4.2: Analysed columns' geometries and yield stresses for parametric study.

| Column designation | $b$<br>(mm) | $t$<br>(mm) | $L$<br>(mm) | $f_y$<br>(MPa) |
|--------------------|-------------|-------------|-------------|----------------|
| 25t0.8L400         | 25          | 0.8         | 400         | 150            |
| 25t0.8L600         |             |             | 600         | 200            |
| 25t0.8L800         |             |             | 800         | 250            |
| 25t0.8L1000        |             |             | 1000        | 275            |
| 50t0.8L400         | 50          | 0.8         | 400         | 300            |
| 50t0.8L600         |             |             | 600         | 350            |
| 50t0.8L800         |             |             | 800         | 375            |
| 50t0.8L1000        |             |             | 1000        | 400            |
| 50t0.95L400        | 50          | 0.95        | 400         | 450            |
| 50t0.95L600        |             |             | 600         | 475            |
| 50t0.95L800        |             |             | 800         | 500            |
| 50t0.95L1000       |             |             | 1000        | 550            |
| 50t1.25L400        | 50          | 1.25        | 400         | 575            |
| 50t1.25L600        |             |             | 600         | 600            |
| 50t1.25L800        |             |             | 800         | 650            |
| 50t1.25L1000       |             |             | 1000        | 700            |

### 4.3.1 Post-buckling Elastic Behaviour

The SFE model, validated according to the exposed on section 4.2, was used to estimate the elastic post-buckling equilibrium paths. At this point, it is worth noting that all columns present initial geometrical imperfections combining a critical flexural-torsional component, with amplitude equal to 10% of the wall thickness  $t$ , and a non-critical minor-axis flexural component, with amplitude equal to  $L/1000$ .

Figure 4.6 contains the equilibrium paths for columns 50t0.8L600 and 50t0.95L600 in the elastic post-buckling stage. It is noticeable that the thickness  $t$  has considerable influence on the equilibrium paths, although both columns follow the same trend.

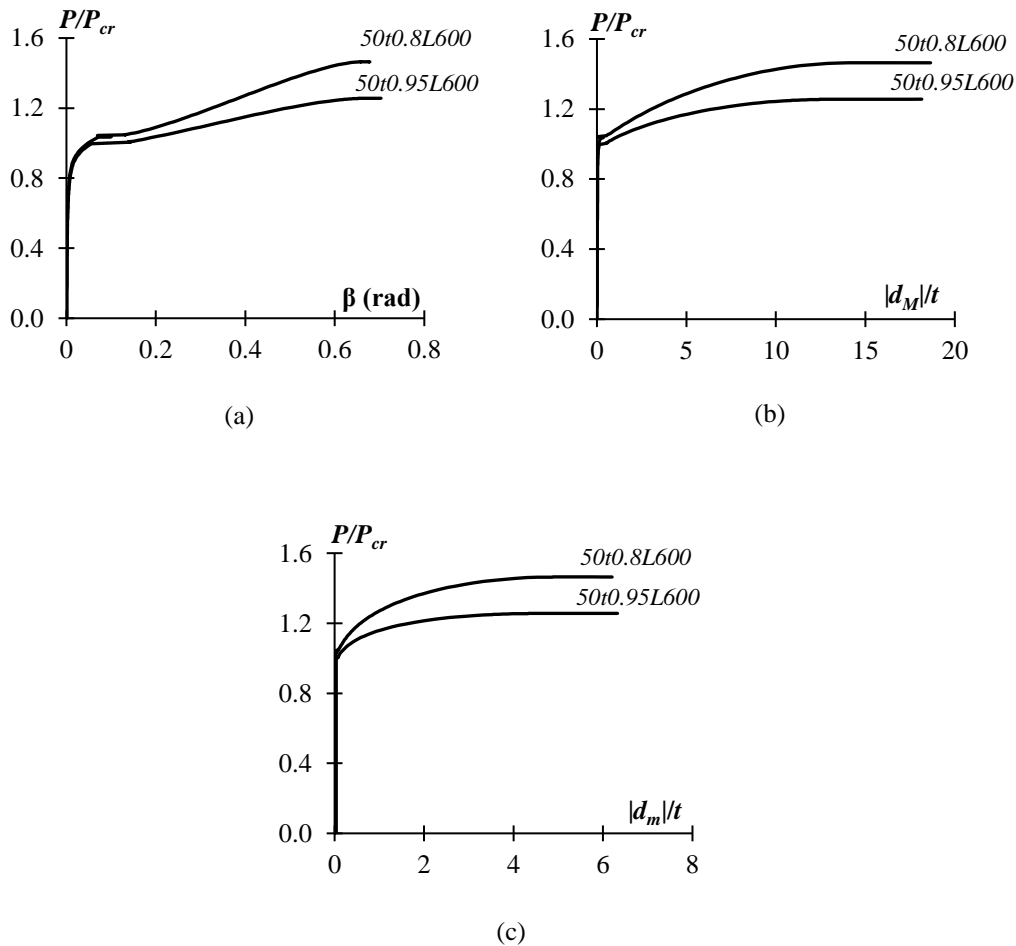


Figure 4.6: Elastic post-buckling of columns 50t0.8L600 and 50t0.95L600: (a)  $P/P_{cr}$  vs.  $\beta$  and  $P/P_{cr}$  vs. displacements (b)  $d_M$  and (c)  $d_m$ .

### 4.3.2 Post-buckling Elastic-plastic Behaviour and Ultimate Strength

This section promotes an investigation of the elastic-plastic post-buckling behaviour and the ultimate strength of the columns numerically assessed.

The numerical results found correspond to 256 columns with: (i) 16 different geometries (see table 4.2) and (ii) 16 different yield stresses (see table 4.2). A complete report comprising all numerical data concerning this analysis can be found in Annex B, which assesses the columns' numerical critical stresses, ultimate strengths and DSM estimates. Figure 4.7 exhibits columns 50t0.8L600 and 50t0.95L600 equilibrium paths for the elastic and elastic-plastic post-buckling stage, containing curves for 4 out of 16 yield stresses employed in this analysis, namely  $f_y=150-250-350-700$  MPa. This was done in order to only show the stresses which presented the greatest difference between them. For illustration purposes, Figure 4.7 also contains the collapse configuration for both columns.

The observation of those results, the equilibrium paths in figure 4.7 and the data reported in Annex B lead to the following remarks:

- (i) According to the expectations by observing the elastic post-buckling behaviour (see section 4.3.1), the elastic-plastic post-buckling behaviour of columns 50t0.8L600 and 50t0.95L600 are only slightly different, although both columns follow the same trend. Column 50t0.95L600 exhibits a higher ultimate load due to its higher thickness, which means a lower  $P/P_{cr}$  ratio, as it is possible to observe on Figure 4.7.
- (ii) It is observed that the columns analysed cover a quite wide slenderness range ( $1.27 \leq \lambda_{fte} \leq 4.34$ ).
- (iii) Finally, within each column section, the ratio  $f_u/f_{fte}$  varies with the length, which reflects the relevance of instability effects. Nevertheless, the ratio  $f_u/f_{fte}$  depends not only on the length, but also on the leg width and the thickness of the columns analysed.

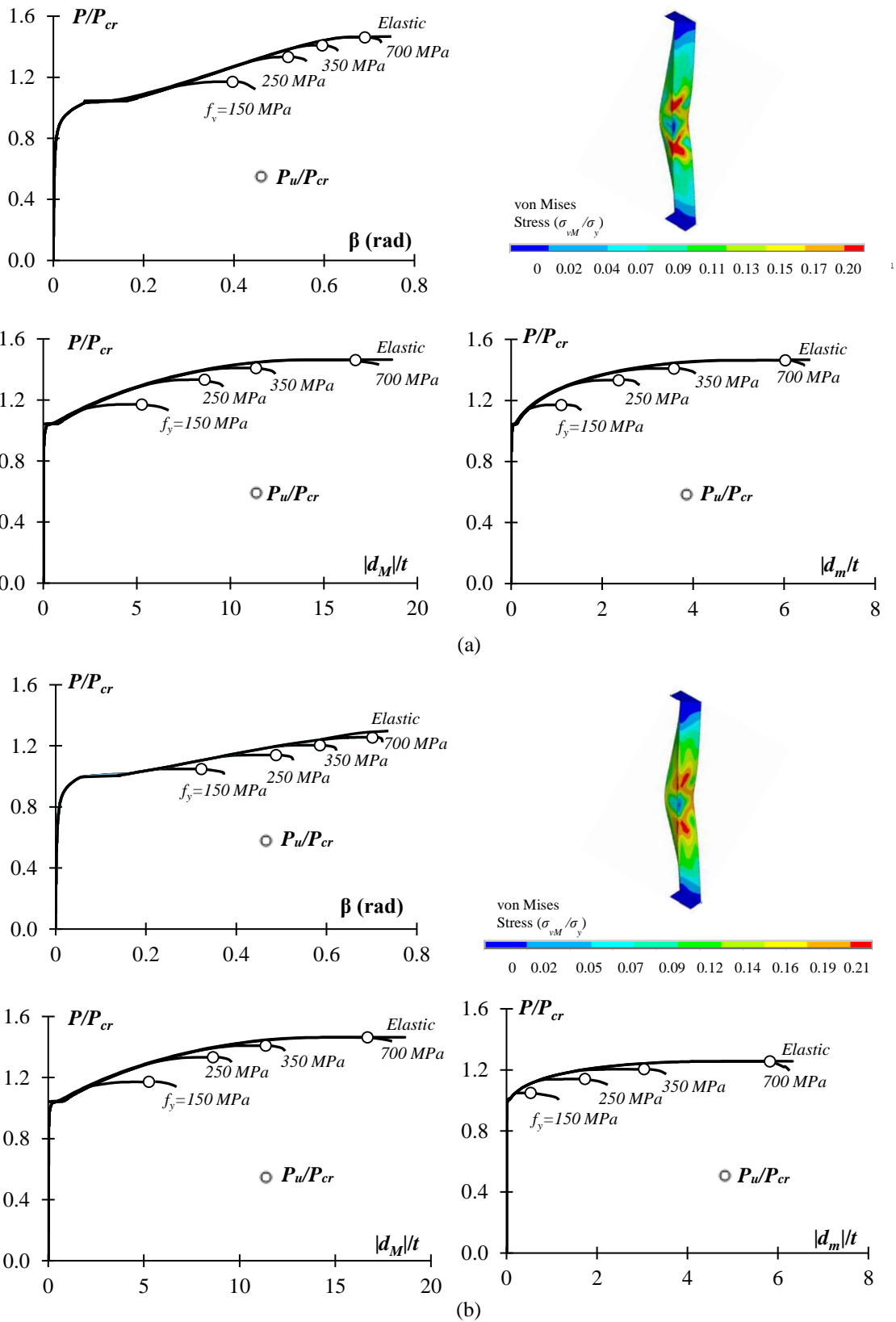


Figure 4.7: (a) 50t0.8L600 and (b) 50t0.95L600 columns' equilibrium paths: elastic, elastic-plastic post buckling and von Mises stress distribution for  $f_y=700$  MPa.

## 5 Assessment of the Proposed DSM Approach

---

Attention is now turned to assessing the performance of the DSM-based design approach proposed in [18], which was presented in Section 2. The ultimate strength predictions ( $f_{nfte}$ ) provided by this approach for the columns experimentally tested and numerically analysed in this work are given in the tables included in Annex A, as well as the corresponding failure-to-predicted ultimate strength ratios  $f_u/f_{nfte}$  – while Table A.1 concerns the experimentally tested columns, Tables B.1 to B.16 deal with the numerically analysed ones. Figs. 20(a)-(b) plot against  $\lambda_{fte}$ , the experimental and numerical  $f_u/f_{nfte}$  values (i) obtained in this work (grey circles) and (ii) previously available, as reported in [18] (white circles). Moreover, the indicators (averages, standard deviations and maximum/minimum values) concerning the failure loads (i) obtained in this work, (ii) reported in [18] and (iii) available (the whole set) are provided in Table 8 – in each case, separate indicators are given for the experimental, numerical and combined failure loads. The observation of the results presented in these figures and table prompts the following remarks:

- (i) The columns tested in the experimental campaign reported in this work exhibit high slenderness ( $\lambda_{fte}$ ) values, thus providing the intended complement to the previously available test results. As for the numerical results obtained in this work, they “mingle” quite well with the existing ones.
- (ii) The experimental and numerical failure loads obtained in this work are (ii<sub>1</sub>) underestimated, some by a large margin, and (ii<sub>2</sub>) fairly well predicted by the proposed DSM-based design approach, respectively. The underestimation of the experimental failure loads stems from the fact that most columns exhibited beneficial initial geometrical imperfections (*i.e.*, minor-axis flexure initial displacement “pointing” towards the cross-section leg tips), as attested by the positive  $d_{m0}$  values presented by the majority of the sections, as shown in Table 4.1. The  $f_u/f_{nfte}$  averages and standard deviations are (ii<sub>1</sub>) 1.36/0.15 (experimental), (ii<sub>2</sub>) 1.09/0.09 (numerical) and (ii<sub>3</sub>) 1.11/0.10 (experimental + numerical). Moreover, the maximum and minimum  $f_u/f_{nfte}$  values read (ii<sub>1</sub>) 1.70/0.98 (experimental), (ii<sub>2</sub>) 1.30/0.91 (numerical) and (ii<sub>3</sub>) 1.70/0.91 (experimental + numerical).

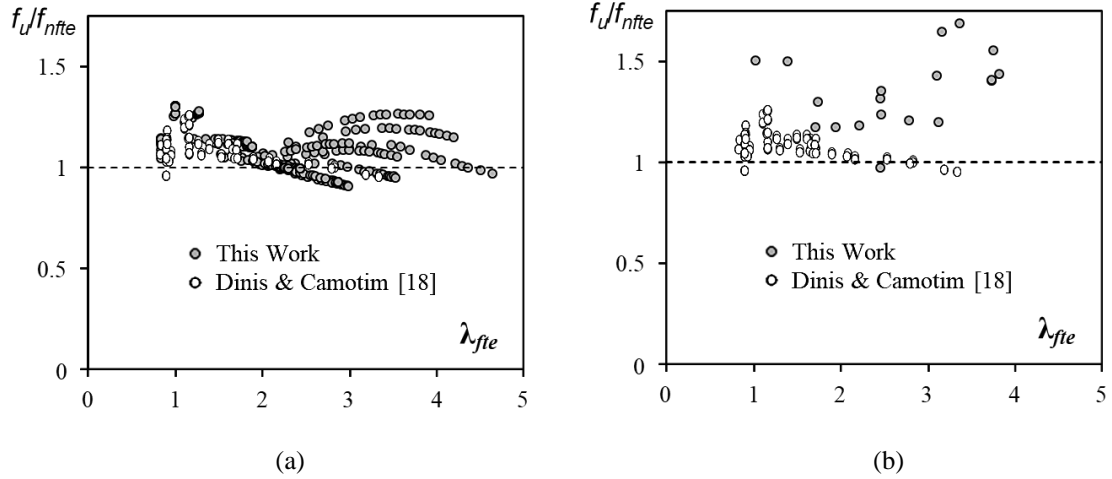


Figure 5.1: (a) Numerical and (b) experimental  $f_u/f_{nfte}$  vs.  $\lambda_{fte}$  plots concerning the values (i) obtained in this work and (ii) reported in [18].

Table 5.1: Averages, standard deviations and maximum/minimum values of  $f_u/f_{nfte}$  experimental, numerical and combined failure loads obtained in this work, reported in [18] and both (whole set).

| $\frac{f_u}{f_{nfte}}$ | This Work |      |           | Dinis and Camotim [18] |      |           | Whole Set |      |           |
|------------------------|-----------|------|-----------|------------------------|------|-----------|-----------|------|-----------|
|                        | Exp.      | Num. | Exp + Num | Exp.                   | Num. | Exp + Num | Exp       | Num. | Exp + Num |
| Mean                   | 1.36      | 1.09 | 1.11      | -                      | 1.06 | 1.06      | 1.16      | 1.08 | 1.09      |
| Sd. Dev.               | 0.15      | 0.09 | 0.10      | -                      | 0.08 | 0.08      | 0.15      | 0.08 | 0.09      |
| Max                    | 1.70      | 1.30 | 1.70      | -                      | 1.26 | 1.26      | 1.70      | 1.30 | 1.70      |
| Min                    | 0.98      | 0.91 | 0.91      | -                      | 0.91 | 0.91      | 0.98      | 0.91 | 0.91      |

(iii) The above performance indicators are similar to those obtained for the failure loads reported in [18] – indeed, those dealing with the numerical  $f_u/f_{nfte}$  ratios are virtually identical. Concerning the experimental failure loads, note that all those obtained in this work are underestimated, while large fractions of the values reported by other researchers are overestimated (severely in a few cases) or excessively underestimated.

(iv) Given the content of the previous item, it is not surprising that the inclusion of the experimental and numerical failure loads obtained in this work practically does not change (numerical) the  $f_u/f_{nfte}$  indicators determined in [18]. Indeed, the average and standard deviation changes are minute: (iv<sub>1</sub>) +0.02/0.0 (numerical) and (iv<sub>2</sub>) +0.03/+0.01 (experimental + numerical). This implies that the failure loads obtained in this work are perfectly in line with their predecessors.

## 5.1 Load and Resistance Factor Design (LRFD)

This section addresses the evaluation of the LRFD (Load and Resistance Factor Design) resistance factor  $\phi$  associated with the proposed DSM-based design approach. According to the North American cold-formed steel specification [33],  $\phi$  is calculated by the formula given in section F.1.1 of chapter F,

$$\phi = C_{\phi}(M_m F_m P_m) e^{-\beta_0 \sqrt{V_M^2 + V_F^2 + C_P V_P^2 + V_Q^2}} \quad \text{with} \quad C_P = \left(1 + \frac{1}{n}\right) \frac{m}{m-2} \quad (5.1)$$

where (i)  $C_{\phi}$  is a calibration coefficient ( $C_{\phi}=1.52$  for LRFD), (ii)  $M_m=1.10$  and  $F_m=1.00$  are the mean values of the material and fabrication factor, respectively, (iii)  $\beta_0$  is the target reliability index ( $\beta_0=2.5$  for structural members in LRFD), (iv)  $V_M=0.10$ ,  $V_F=0.05$  and  $V_Q=0.21$  are the coefficients of variation of the material factor, fabrication factor and load effect, respectively<sup>9</sup>, and (v)  $C_P$  is a correction factor that depends on the numbers of tests ( $n$ ) and degrees of freedom ( $m=n-1$ ). In order to evaluate  $\phi$  for the proposed DSM procedure, it is necessary to calculate  $P_m$  and  $V_P$ , the average and standard deviation of the  $f_u/f_{nfe}$  ratios – the  $f_u$  values are either experimental, numerical or experimental and numerical.

Table 5.2 shows the  $n$ ,  $C_P$ ,  $P_m$ ,  $V_P$  and  $\phi$  values obtained for the column failure load predictions provided by the DSM design approach for the experimental, numerical and whole failure data (i) obtained in this work and (ii) reported in [18].

Table 5.2: LRFD  $\phi$  values according to [33] concerning the experimental, numerical and combined failure loads obtained in this work, reported in [18] and both (whole set) by the proposed DSM design approach.

|        | This Work |      |           | Dinis and Camotim [18] |      |           | Whole Set |      |           |
|--------|-----------|------|-----------|------------------------|------|-----------|-----------|------|-----------|
|        | Exp.      | Num. | Exp + Num | Exp.                   | Num. | Exp + Num | Exp       | Num. | Exp + Num |
| $n$    | 19        | 256  | 275       | -                      | 144  | 144       | 19        | 400  | 419       |
| $C_P$  | 1.18      | 1.01 | 1.01      | -                      | 1.02 | 1.02      | 1.18      | 1.01 | 1.01      |
| $P_m$  | 1.36      | 1.09 | 1.11      | -                      | 1.06 | 1.06      | 1.36      | 1.08 | 1.09      |
| $V_P$  | 0.15      | 0.09 | 0.10      | -                      | 0.08 | 0.08      | 0.15      | 0.08 | 0.09      |
| $\phi$ | 1.11      | 0.96 | 0.96      | -                      | 0.95 | 0.95      | 1.11      | 0.96 | 0.96      |

<sup>9</sup> Values prescribed, for concentrically loaded compression members, in [33]– Chapter F, Section F1.1, Table F1 and text.

It is observed that:

- (i) The inclusion of the experimental and numerical failure loads obtained in this work leads to  $\phi$  values that, with respect to those reported in [18], are marginally higher (numerical and experimental + numerical – 0.96 to 0.95).
- (ii) The results obtained in this work reinforce the conclusion drawn in [18]: there is evidence that  $\phi=0.85$  can be recommended for cold-formed steel angle columns designed with the proposed DSM-based approach, which is currently not the case [53].

## 6 Concluding Remarks

---

This work mainly reported the results of an experimental investigation on the behaviour and collapse of cold-formed steel short-to-intermediate spherically-hinged equal-leg angle columns with high slenderness values, which was carried out to fill a gap detected in [18], in the context of the development and performance assessment of a DSM-based design procedure for such members. After briefly reviewing this DSM procedure, this work addressed the selection of the geometries of (i) the column specimens to be fabricated and tested at LABEST (UFRJ) and also (ii) additional columns to be analysed numerically by means of ANSYS SFE simulations. Then, detailed descriptions of the experimental, displacement measurements (prior to and during the test) and test procedure were provided, followed by the presentation and discussion of the results obtained, including the (i) initial geometrical imperfection measurements, (ii) equilibrium paths relating the applied load to column displacements, (iii) deformed configurations (including the collapse modes) and (iv) failure loads.

Next, those experimental results were used to validate a previously developed SFE model, which was subsequently employed to obtain additional numerical failure load data concerning the spherically-hinged angle columns under scrutiny. Then, it was shown that the experimental and numerical failure loads obtained in this work could be efficiently (safely and reasonably accurately) predicted by the DSM design approach proposed in [18], thus providing further evidence of its merits. Finally, the whole column failure load data available (comprising the values determined in this work and those taken from [18]), totalling 19 experimental and 400 (144 + 256) numerical values, were used to assess the performance of the proposed DSM design approach. It was found that the indicators of the failure-to-predicted ultimate strength ratio ( $f_u/f_{nftc}$ ) are very close to those reported in [18], thus ensuring the same quality and reliability levels. In particular, it was confirmed (even reinforced) that the LRFD resistance factor  $\phi=0.85$ , currently prescribed in [33] for the design of compression members, can also be safely adopted for the failure load prediction of pin-ended angle by the proposed DSM design approach (angle columns are current explicitly excluded from the application of this resistance factor).

Finally, it was shown the DSM design procedure was found to be accurate, presenting good quality and reliability of the failure load predictions.

## 6.1 Suggestions for Future Work

Observing the results obtained in this study, it is possible to infer that the approach suggested in [18] provides good failure load predictions. However, the analyses on CFS angle columns for the spherically-hinged support condition are still scarce – in fact, the only work published in this area is the one by DINIS & CAMOTIM [18]. Therefore, besides the acquisition of additional numerical data, this research line could benefit from future efforts, *e.g.*:

- (i) Performing additional experimental tests, varying: (i) the leg width ( $b_f$ ), (ii) the length ( $L$ ), (iii) the thickness ( $t$ ) and (iv) employing new support conditions.
- (ii) Refining the initial imperfection measurements by the use of other methods, which would provide a higher precision.

## 7 References

---

- [1] AMERICAN IRON AND STEEL INSTITUTE, 1940. *Reports of research at Cornell University on light gage cold-formed steel structural members – Index and Synopses*. Washington: AISI.
- [2] CHILVER, A. H. “The Stability and Strength of Thin-Walled Steel Struts”, *The Engineer*, pp. 180-183, 1953.
- [3] DUBINA, D., UNGUREANU, V. “Effect of imperfections on numerical simulation of instability behaviour of cold-formed steel members”, *Thin-Walled Structures*, vol. 40, pp. 239-262, March 2002.
- [4] SCHAFFER, B. W., 1997. *Cold-Formed Steel Behavior and Design: Analytical and Numerical Modeling of Elements and Members with Longitudinal Stiffeners*. PhD. Dissertation, Cornell University, Ithaca.
- [5] CHODRAUI G. M. B., SHIFFERAW. Y., MALITE M., SCHAFFER B. W. “Cold-formed steel angles under axial compression”, In: *Proceedings of 18th International Specialty Conference on Cold-Formed Steel Structures*. R. LaBoube, W.W. Yu (eds.), pp. 285-300, Orlando, October 2006.
- [6] YU, W. W., 2000. *Cold-formed steel design*. New York, John Wiley & Sons.
- [7] RASMUSSEN, K. J. R., 2003. *Design of Angle Columns with Locally Unstable Legs*. In: Department of Civil Engineering, Research Report No. R830, University of Sydney. Australia.
- [8] PRABHU, T. S., 1982 *Ultimate Strength of cold-formed equal-leg single angles*. M.Sc. Dissertation, University of Windsor, Windsor, Ontario, Canada.
- [9] WILHOITE G. M., ZANDONINI R., ZAVELANI A. “Behaviour and strength of angles in compression: an experimental investigation”, In: *Proceedings of ASCE Annual Convention and Structures Congress*. San Francisco, October 1984.
- [10] POPOVIC D., HANCOCK G. J., RASMUSSEN K. J. “Axial compression tests of cold-formed angles”, *Journal of Structural Engineering (ASCE)*, 125(5), pp. 515-523, May 1999.
- [11] YOUNG, B. “Tests and design of fixed-ended cold-formed steel plain angle columns”, *Journal of Structural Engineering (ASCE)*, 130(12), pp. 1931-1940, December 2004.
- [12] MAIA W. F., Neto J. M., MALITE M. “Stability of cold-formed steel simple and lipped angles under compression”, In: *Proceedings of 19th International Specialty Conference on Recent Research and Developments in Cold-Formed Steel Design and Construction.*, R. LaBoube, W.-W. Yu (eds.), pp. 111-125, St. Louis, October 2008.
- [13] MESACASA Jr., E. C., 2012. *Structural Behaviour and Design of Cold-Formed Steel Angle Columns*, M.Sc. Dissertation, School of Engineering at São Carlos, University of São Paulo, Brazil. (Portuguese)
- [14] LANDESMANN A., CAMOTIM D., Dinis P. B., CRUZ R. “Short-to-Intermediate Slender Pin-Ended Cold-Formed Steel Equal-Leg Angle Columns: Experimental

- Investigation, Numerical Simulations and DSM Design”, *Engineering Structures*, v. 132, pp. 471-493, February 2017.
- [15] ABNT - *Brazilian Association of Technical Standards*. NBR 14762: Design of cold-formed profile steel structures, Rio de Janeiro, 2010. (Portuguese)
- [16] SILVESTRE, N., DINIS, P. B., CAMOTIM, D. “Developments on the design of cold-formed steel angles” *Journal of Structural Engineering*, v. 139, n. 5, pp. 680-694, May 2013.
- [17] DINIS P. B., CAMOTIM D. “A novel DSM-based approach for the rational design of fixed-ended and pin-ended short-to-intermediate thin-walled angle columns”, *Thin-Walled Structures*, v. 87, pp. 158-182, December 2014.
- [18] DINIS P. B., CAMOTIM D. “Spherically-Hinged Short-to-Intermediate Angle Columns: Stability, Non-Linear Behavior and DSM Design”, In: *Proceedings of the Annual Stability Conference Structural Stability Research Council*. v. 132, pp. 471-493, March 2017.
- [19] RASMUSSEN K. J. R. (2005). “Design of angle columns with locally unstable legs”, *Journal of Structural Engineering (ASCE)*, 131(10), pp. 1553-1560, October 2005.
- [20] CRUZ R., 2015. *Experimental Analysis and Design of Slender Pin-Ended Cold-Formed Steel Equal-Leg Angle Columns*, M.Sc. Dissertation, COPPE, Federal University of Rio de Janeiro. (Portuguese)
- [21] TIMOSHENKO, S.P., GERE, J. M., 1961. *Theory of elastic stability*. New York, McGraw-Hill.
- [22] DINIS P. B., CAMOTIM D., Silvestre N. “On the mechanics of angle column instability”, *Thin-Walled Structures*, v. 52, pp. 80-89, March 2012.
- [23] BEBIANO R., SILVESTRE N., CAMOTIM D. “GBTUL – A code for the buckling analysis of cold-formed steel members”, In: *Proceedings of 19th International Specialty Conference on Recent Research and Developments in Cold-Formed Steel Design and Construction*, R. LaBoube, W.-W. Yu (eds.), pp.61-79, St Louis, October 2008.
- [24] SCHAFER, B. W., PEKÖZ, T. “Direct Strength Prediction of Cold-Formed Steel Members using Numerical Elastic Buckling Solutions”. In: *Fourteenth International Specialty Conference on Cold-Formed Steel Structures*. St Louis, October 1998.
- [25] HANCOCK, G. J.; MURRAY, T. M.; ELLIFRITT, D. S., 2001. *Cold-formed steel structures to the AISI Specification*. New York, Marcel Dekker.
- [26] SCHAFER, B. W. “Finite Strip Analysis of Thin-walled Members”. In: *CU-FSM: Cornell University – Finite Strip Method*. pp. 193-210, September 2001.
- [27] SCHAFER, B. W. (2001). “Thin-walled column design considering local, distortional and Euler Buckling”. In: *Proceedings: Structural Stability Research Council – Annual Technical Session and Meeting*. pp. 193-210, September 2001.
- [28] SCHAFER, B. W. “Progress on the direct strength method”. In: *16th international Specialty Conference on Recent Research and Developments in Cold-Formed Steel Design and Construction*, pp. 647-662, Orlando, Florida, October 2002.

- [29] SCHAFER, B. W. (2006). “Design Guide for Direct Strength Method (DSM)”. *American Iron and Steel Institute – Committee on Specifications for the Design of Cold-Formed Steel Structural Members*, January, 2006.
- [30] MESACASA Jr., E. C., DINIS P. B., CAMOTIM D., MALITE M. “Flexural buckling of simply supported columns with ‘rigid end links’ – the key to interpret pin-ended angle column test results?”, In: *USB Key Drive Proceedings of Structural Stability Research Council Annual Stability Conference*, paper 4, Grapevine, April 2012.
- [31] VON KARMAN, T.; SECHLER, E. E.; DONNELL, L. H. “The strength of thin plates in compression”. In: *Transactions, American Society of Mechanical Engineers*, v.54, p.53-57, June 1932.
- [32] WINTER, G. “Strength of thin steel compression flanges”. In: *Transactions, ASCE*, v.112, p.527-554, 1947.
- [33] AISI - *American Iron and Steel Institute. AISI-S100-12: North American Specification (NAS) for the Design of Cold-Formed Steel Structural Members*, Washington DC, 2012.
- [34] AS/NZS - STANDARDS AUSTRALIA/STANDARDS NEW ZEALAND. *AS/NZS 4600:1996, Cold-formed steel structures*, Sydney, 1996.
- [35] AISI - *American Iron and Steel Institute. AISI-S100-96. North American Specification (NAS) for the Design of Cold-Formed Steel Structural Members*, Washington DC, 1996.
- [36] KWON, Y. B.; HANCOCK, G. J. “Strength tests of cold-formed channel sections undergoing local and distortional buckling”. *Journal of Structural Engineering, ASCE*, 117(2), pp. 1786-1803, 1992.
- [37] POPOVIC D., HANCOCK G. J., RASMUSSEN K. J. R. “Compression tests on cold-formed angles loaded parallel with a leg”, *Journal of Structural Engineering (ASCE)*, 127(6), pp. 600-607, 2001.
- [38] RHODES J., Harvey J. M. “Interaction behaviour of plain channel columns under concentric or eccentric loading.” In: *Proceedings, 2<sup>nd</sup> International Colloquium on the Stability of Steel Structures, ECCS*, pp. 439–444, Liege, 1977.
- [39] AISI - *American Iron and Steel Institute. AISI-S100-01: North American Specification (NAS) for the Design of Cold-Formed Steel Structural Members*, Washington DC, 2001.
- [40] BAMBACH M. R., RASMUSSEN K. J. R. “Elastic and plastic effective width equations for unstiffened elements.” *Journal of Structural Engineering*, 130(10), pp. 1611–1619, 2002.
- [41] BAMBACH M. R., RASMUSSEN K. J. R. “Tests on unstiffened elements under bending and compression.” *Journal of Structural Engineering*, 130(10), pp. 1602–1610, 2002.
- [42] STOWELL, E. Z. “Compressive strength of flanges.” *Technical Note No. 1556, National Advisory Committee for Aeronautics (NACA)*, 1949.
- [43] DASSAULT SYSTÈMES SIMULIA CORP. (DS Simulia). 2008. *ABAQUS version 6.7-5 user’s manual*, Dassault Systèmes, Providence, RI.

- [44] RASMUSSEN K. J. R. “Design of slender angle section beam-columns by the direct strength method”, *Journal of Structural Engineering (ASCE)*, 132(2), pp. 204-211, 2006.
- [45] AISI - *American Iron and Steel Institute. AISI-S100-07: North American Specification (NAS) for the Design of Cold-Formed Steel Structural Members*, Washington DC, 2007.
- [46] ANSYS. Version 12: SAS – Swanson Analysis Systems Inc., 2009.
- [47] DINIS P. B., CAMOTIM D., SILVESTRE N. “On the local and global buckling behaviour of angle, T-section and cruciform thin-walled columns and beams”, *Thin-Walled Structures*, 48(10-11), pp. 786-797, 2010.
- [48] ABNT - *Brazilian Association of Technical Standards. NBR ISO 6892-1. Metallic Materials – Tensile Testing – Part 1: Method of Test at Room Temperature*, Rio de Janeiro, 2015. (Portuguese)
- [49] ASTM - *American Society for Testing and Materials. Test Methods for Tension Testing of Metallic Materials, ASTM E8/E8M-15a*, West Conshohocken, 2015.
- [50] LANDESMANN, A., CAMOTIM, D. “On the Direct Strength Method (DSM) design of cold-formed steel columns against distortional failure”, *Thin-Walled Structures*, vol. 67, pp. 168-187, 2013.
- [51] ELLOBODY E., YOUNG B. “Behavior of cold-formed steel plain angle columns”, *Journal of Structural Engineering (ASCE)*, 131(3), pp. 469-478, 2005.
- [52] SHI G., LIU Z., BAN H. Y., Zhang Y., SHI Y. J., WANG Y. Q. “Tests and finite element analysis on the local buckling of 420 MPa steel equal angle columns under axial compression”, *Steel and Composite Structures*, 12(1), pp. 31-51, 2011.
- [53] GANESAN K., MOEN C.D. “LRFD resistance factor for cold-formed steel compression members”, *Journal of Constructional Steel Research*, v. 72, pp. 261-266, May 2012.
- [54] ABNT - *Brazilian Association of Technical Standards. Steel-Coated Coils and Plates with Zinc or Zinc-Iron Alloy by Hot-Dip Continuous Process Immersion – Part 1: Requirements*, ABNT NBR 7008-1, Rio de Janeiro, 2012. (Portuguese)
- [55] KITIPORNCHAI S., CHAN S. L. “Nonlinear finite-element analysis of angle and tee beam-columns”, *Journal of Structural Engineering (ASCE)*, 113(4), pp. 721-739, 1987.
- [56] KITIPORNCHAI S., ALBERMANI F. G. A., CHAN S. L. “Elastoplastic finite-element models for angle steel frames”, *Journal of Structural Engineering (ASCE)*, 116(10), pp. 2567-2581, 1990.
- [57] ZHUGE Y., MILLS J. E., MA X. “Modelling of steel lattice tower angle legs reinforced for increased load capacity”, *Engineering Structures*, 43(10), pp. 160-168, 2012.
- [58] SHIFFERAW Y., SCHAFER B. W. “Cold-formed steel lipped and plain angle columns with fixed ends”, *Thin-Walled Structures*, v. 80, pp. 142-152, July 2014.
- [59] ZHAO J., WU B., LI W., OU J. “Local buckling behavior of steel angle core members in buckling-restrained braces: Cyclic tests, theoretical analysis, and design recommendations”, *Engineering Structures*, 66(1), pp. 129-145, 2014.

- [60] MOŽE P., CAJOT L. G., SINUR F., REJEC K., BEG D. “Residual stress distribution of large steel equal leg angles”, *Engineering Structures*, 71(15), pp. 35-47, 2014.
- [61] MESACASA Jr. EC, DINIS PB, CAMOTIM D, MALITE M (2014). “Mode-interaction in thin-walled equal-leg angle columns”, *Thin-Walled Structures*, 81(August), 138-149.
- [62] ASTM - *American Society for Testing and Materials*. Standard Specification for Steel Sheet, Zinc-Coated (Galvanized) or Zinc-Iron Alloy-Coated (Galvannealed) by the Hot-Dip Process, ASTM A653, West Conshohocken, 2011.

## ANNEX A: Spherically-hinged Column Experimental Failure Load Data

**Table A.1:** Spherically-hinged column critical stresses, ultimate strengths and DSM estimates ( $f_y=366\text{MPa}$ )

| <i>Column</i> | <i>L</i> | $f_{bf}$ | $f_{erft}$ | $f_{ere}$ | $\Delta_f$ | <i>a</i> | <i>b</i> | <i>c</i> | <i>d</i> | $\beta$ | $f_{nfte}$ | $f_u$ | $\lambda_{fte}$ | $\frac{f_u}{f_{nfte}}$ |
|---------------|----------|----------|------------|-----------|------------|----------|----------|----------|----------|---------|------------|-------|-----------------|------------------------|
| 25t0.8L400    | 401      | 1382.56  | 79.1       | 345.6     | 2.22       | 0.46     | 0.15     | 0.36     | 0.87     | 0.52    | 67.60      | 88.27 | 1.72            | 1.31                   |
| 25t0.8L400-R  | 401      | 1368.32  | 81.7       | 342.1     | 2.33       | 0.46     | 0.15     | 0.36     | 0.87     | 0.53    | 69.24      | 81.78 | 1.69            | 1.18                   |
| 25t0.8L600    | 601      | 635.65   | 73.4       | 158.9     | 4.67       | 0.57     | 0.16     | 0.30     | 0.92     | 0.63    | 54.39      | 82.28 | 1.38            | 1.51                   |
| 25t0.8L800    | 800      | 343.29   | 73.1       | 85.8      | 9.21       | 0.82     | 0.18     | 0.12     | 1.00     | 0.76    | 45.73      | 69.39 | 1.01            | 1.52                   |
| 50t0.8L400    | 401      | 5271.42  | 23.9       | 1317.9    | 0.17       | 0.40     | 0.15     | 0.53     | 0.68     | 0.31    | 33.81      | 47.74 | 3.70            | 1.41                   |
| 50t0.8L400-R  | 401      | 5090.93  | 23.7       | 1272.7    | 0.18       | 0.40     | 0.15     | 0.52     | 0.69     | 0.30    | 33.00      | 46.85 | 3.70            | 1.42                   |
| 50t0.8L600    | 600      | 2472.30  | 20.7       | 618.1     | 0.32       | 0.40     | 0.15     | 0.43     | 0.81     | 0.26    | 24.59      | 38.48 | 3.71            | 1.56                   |
| 50t0.8L600-R  | 600      | 2545.19  | 20.1       | 636.3     | 0.30       | 0.40     | 0.15     | 0.43     | 0.81     | 0.25    | 24.04      | 34.83 | 3.78            | 1.45                   |
| 50t0.8L800    | 800      | 1331.56  | 20.8       | 332.9     | 0.59       | 0.40     | 0.14     | 0.42     | 0.82     | 0.28    | 23.54      | 40.10 | 3.33            | 1.70                   |
| 50t0.95L400   | 400      | 5265.02  | 33.2       | 1316.3    | 0.24       | 0.40     | 0.15     | 0.44     | 0.81     | 0.30    | 37.48      | 62.23 | 3.13            | 1.66                   |
| 50t0.95L600   | 599      | 2422.82  | 30.1       | 605.7     | 0.47       | 0.40     | 0.14     | 0.43     | 0.82     | 0.31    | 33.40      | 48.07 | 3.07            | 1.44                   |
| 50t0.95L600-R | 600      | 2436.73  | 29.8       | 609.2     | 0.46       | 0.40     | 0.15     | 0.43     | 0.82     | 0.31    | 33.17      | 40.04 | 3.09            | 1.21                   |
| 50t0.95L800   | 801      | 1313.79  | 30.1       | 328.4     | 0.87       | 0.40     | 0.14     | 0.41     | 0.83     | 0.33    | 31.67      | 38.50 | 2.76            | 1.22                   |
| 50t0.95L1000  | 1001     | 839.04   | 29.6       | 209.8     | 1.35       | 0.42     | 0.14     | 0.39     | 0.84     | 0.37    | 28.85      | 39.28 | 2.44            | 1.36                   |
| 50t1.25L400   | 400      | 5307.35  | 54.9       | 1326.8    | 0.39       | 0.40     | 0.15     | 0.43     | 0.82     | 0.39    | 57.26      | 75.85 | 2.44            | 1.32                   |
| 50t1.25L600   | 600      | 2444.88  | 48.2       | 611.2     | 0.75       | 0.40     | 0.14     | 0.41     | 0.83     | 0.38    | 49.42      | 48.27 | 2.43            | 0.98                   |
| 50t1.25L600-R | 600      | 2445.36  | 47.8       | 611.3     | 0.74       | 0.40     | 0.14     | 0.41     | 0.83     | 0.38    | 49.09      | 61.12 | 2.44            | 1.25                   |
| 50t1.25L800   | 800      | 1326.54  | 47.9       | 331.6     | 1.39       | 0.42     | 0.14     | 0.39     | 0.84     | 0.41    | 45.49      | 54.07 | 2.19            | 1.19                   |
| 50t1.25L1000  | 1001     | 845.28   | 47.9       | 211.3     | 2.20       | 0.46     | 0.15     | 0.36     | 0.87     | 0.46    | 41.40      | 48.89 | 1.92            | 1.18                   |

Note 1: dimensions in *mm*, stresses in *MPa*

Note 2: the above  $\Delta_f$  values and DSM estimates are based on the average measured cross-section dimensions (see Table 3)

## ANNEX B: Spherically-hinged Column Numerical Failure Load Data

**Table B.1:** Spherically-hinged column critical stresses, ultimate strengths and DSM estimates ( $f_y=150MPa$ )

| <i>Column</i> | <i>L</i> | $f_{bf}$ | $f_{cft}$ | $f_{cre}$ | $\Delta_f$ | <i>a</i> | <i>b</i> | <i>c</i> | <i>d</i> | $\beta$ | $f_{nftc}$ | $f_u$ | $\lambda_{ftc}$ | $\frac{f_u}{f_{yftc}}$ |
|---------------|----------|----------|-----------|-----------|------------|----------|----------|----------|----------|---------|------------|-------|-----------------|------------------------|
| 25t0.8L400    | 400      | 1349.4   | 83.4      | 337.3     | 2.41       | 0.47     | 0.15     | 0.36     | 0.87     | 0.77    | 69.91      | 79.67 | 1.22            | 1.14                   |
| 25t0.8L600    | 600      | 599.7    | 79.4      | 149.9     | 5.41       | 0.61     | 0.16     | 0.27     | 0.94     | 0.80    | 59.20      | 72.36 | 1.11            | 1.22                   |
| 25t0.8L800    | 800      | 337.3    | 75.3      | 84.3      | 9.73       | 0.85     | 0.18     | 0.12     | 1.00     | 0.79    | 47.85      | 59.97 | 0.97            | 1.25                   |
| 25t0.8L1000   | 1000     | 215.9    | 70.4      | 54.0      | 15.35      | 0.87     | 0.18     | 0.12     | 1.00     | 0.96    | 45.64      | 47.69 | 0.82            | 1.05                   |
| 50t0.8L400    | 400      | 5397.4   | 23.4      | 1349.4    | 0.16       | 0.40     | 0.15     | 0.54     | 0.66     | 0.44    | 28.30      | 28.80 | 2.47            | 1.02                   |
| 50t0.8L600    | 600      | 2398.9   | 21.8      | 599.7     | 0.34       | 0.40     | 0.15     | 0.43     | 0.81     | 0.38    | 22.94      | 25.28 | 2.49            | 1.10                   |
| 50t0.8L800    | 800      | 1349.4   | 21.2      | 337.3     | 0.60       | 0.40     | 0.14     | 0.42     | 0.82     | 0.38    | 21.91      | 22.31 | 2.42            | 1.02                   |
| 50t0.8L1000   | 1000     | 863.6    | 20.9      | 215.9     | 0.92       | 0.40     | 0.14     | 0.41     | 0.83     | 0.40    | 20.98      | 20.87 | 2.32            | 0.99                   |
| 50t0.95L400   | 400      | 5397.4   | 33.0      | 1349.4    | 0.23       | 0.40     | 0.15     | 0.44     | 0.81     | 0.45    | 33.21      | 35.55 | 2.08            | 1.07                   |
| 50t0.95L600   | 600      | 2398.9   | 30.7      | 599.7     | 0.48       | 0.40     | 0.14     | 0.43     | 0.82     | 0.45    | 30.71      | 31.95 | 2.10            | 1.04                   |
| 50t0.95L800   | 800      | 1349.4   | 29.9      | 337.3     | 0.84       | 0.40     | 0.14     | 0.41     | 0.83     | 0.45    | 29.20      | 29.64 | 2.04            | 1.01                   |
| 50t0.95L1000  | 1000     | 863.6    | 29.4      | 215.9     | 1.30       | 0.42     | 0.14     | 0.39     | 0.84     | 0.47    | 27.49      | 28.80 | 1.95            | 1.05                   |
| 50t1.25L400   | 400      | 5397.4   | 57.0      | 1349.4    | 0.40       | 0.40     | 0.15     | 0.43     | 0.82     | 0.60    | 53.86      | 56.65 | 1.58            | 1.05                   |
| 50t1.25L600   | 600      | 2398.9   | 53.0      | 599.7     | 0.84       | 0.40     | 0.14     | 0.41     | 0.83     | 0.59    | 49.36      | 51.79 | 1.60            | 1.05                   |
| 50t1.25L800   | 800      | 1349.4   | 51.4      | 337.3     | 1.46       | 0.43     | 0.14     | 0.38     | 0.85     | 0.59    | 45.88      | 48.88 | 1.56            | 1.07                   |
| 50t1.25L1000  | 1000     | 863.6    | 50.4      | 215.9     | 2.27       | 0.46     | 0.15     | 0.36     | 0.87     | 0.61    | 42.58      | 47.62 | 1.49            | 1.12                   |

Note: dimensions in *mm*, stresses in *MPa*

**Table B.2:** Spherically-hinged column critical stresses, ultimate strengths and DSM estimates ( $f_y=200MPa$ )

| <i>Column</i> | <i>L</i> | $f_{bf}$ | $f_{cft}$ | $f_{cre}$ | $\Delta_f$ | <i>a</i> | <i>b</i> | <i>c</i> | <i>d</i> | $\beta$ | $f_{nftc}$ | $f_u$ | $\lambda_{ftc}$ | $\frac{f_u}{f_{yftc}}$ |
|---------------|----------|----------|-----------|-----------|------------|----------|----------|----------|----------|---------|------------|-------|-----------------|------------------------|
| 25t0.8L400    | 400      | 1349.4   | 83.4      | 337.3     | 2.41       | 0.47     | 0.15     | 0.36     | 0.87     | 0.67    | 69.80      | 79.68 | 1.37            | 1.14                   |
| 25t0.8L600    | 600      | 599.7    | 79.4      | 149.9     | 5.41       | 0.61     | 0.16     | 0.27     | 0.94     | 0.73    | 58.09      | 72.36 | 1.20            | 1.25                   |
| 25t0.8L800    | 800      | 337.3    | 75.3      | 84.3      | 9.73       | 0.85     | 0.18     | 0.12     | 1.00     | 0.78    | 47.46      | 59.97 | 0.99            | 1.26                   |
| 25t0.8L1000   | 1000     | 215.9    | 70.4      | 54.0      | 15.35      | 0.87     | 0.18     | 0.12     | 1.00     | 0.96    | 45.64      | 49.58 | 0.82            | 1.09                   |
| 50t0.8L400    | 400      | 5397.4   | 23.4      | 1349.4    | 0.16       | 0.40     | 0.15     | 0.54     | 0.66     | 0.39    | 30.00      | 32.00 | 2.83            | 1.07                   |
| 50t0.8L600    | 600      | 2398.9   | 21.8      | 599.7     | 0.34       | 0.40     | 0.15     | 0.43     | 0.81     | 0.33    | 23.78      | 27.32 | 2.82            | 1.15                   |
| 50t0.8L800    | 800      | 1349.4   | 21.2      | 337.3     | 0.60       | 0.40     | 0.14     | 0.42     | 0.82     | 0.34    | 22.60      | 23.08 | 2.71            | 1.02                   |
| 50t0.8L1000   | 1000     | 863.6    | 20.9      | 215.9     | 0.92       | 0.40     | 0.14     | 0.41     | 0.83     | 0.36    | 21.49      | 20.87 | 2.55            | 0.97                   |
| 50t0.95L400   | 400      | 5397.4   | 33.0      | 1349.4    | 0.23       | 0.40     | 0.15     | 0.44     | 0.81     | 0.40    | 34.41      | 38.70 | 2.39            | 1.12                   |
| 50t0.95L600   | 600      | 2398.9   | 30.7      | 599.7     | 0.48       | 0.40     | 0.14     | 0.43     | 0.82     | 0.39    | 31.72      | 33.34 | 2.38            | 1.05                   |
| 50t0.95L800   | 800      | 1349.4   | 29.9      | 337.3     | 0.84       | 0.40     | 0.14     | 0.41     | 0.83     | 0.40    | 29.99      | 29.65 | 2.29            | 0.99                   |
| 50t0.95L1000  | 1000     | 863.6    | 29.4      | 215.9     | 1.30       | 0.42     | 0.14     | 0.39     | 0.84     | 0.42    | 28.00      | 28.80 | 2.15            | 1.03                   |
| 50t1.25L400   | 400      | 5397.4   | 57.0      | 1349.4    | 0.40       | 0.40     | 0.15     | 0.43     | 0.82     | 0.52    | 55.29      | 58.06 | 1.82            | 1.05                   |
| 50t1.25L600   | 600      | 2398.9   | 53.0      | 599.7     | 0.84       | 0.40     | 0.14     | 0.41     | 0.83     | 0.51    | 50.52      | 52.16 | 1.81            | 1.03                   |
| 50t1.25L800   | 800      | 1349.4   | 51.4      | 337.3     | 1.46       | 0.43     | 0.14     | 0.38     | 0.85     | 0.52    | 46.56      | 48.89 | 1.74            | 1.05                   |
| 50t1.25L1000  | 1000     | 863.6    | 50.4      | 215.9     | 2.27       | 0.46     | 0.15     | 0.36     | 0.87     | 0.55    | 42.79      | 47.62 | 1.64            | 1.11                   |

Note: dimensions in *mm*, stresses in *MPa*

**Table B.3:** Spherically-hinged column critical stresses, ultimate strengths and DSM estimates ( $f_y=250\text{ MPa}$ )

| <i>Column</i> | <i>L</i> | $f_{bf}$ | $f_{erft}$ | $f_{cre}$ | $\Delta_f$ | <i>a</i> | <i>b</i> | <i>c</i> | <i>d</i> | $\beta$ | $f_{nfte}$ | $f_u$ | $\lambda_{fte}$ | $\frac{f_u}{f_{yfe}}$ |
|---------------|----------|----------|------------|-----------|------------|----------|----------|----------|----------|---------|------------|-------|-----------------|-----------------------|
| 25t0.8L400    | 400      | 1349.4   | 83.4       | 337.3     | 2.41       | 0.47     | 0.15     | 0.36     | 0.87     | 0.61    | 69.88      | 79.68 | 1.48            | 1.14                  |
| 25t0.8L600    | 600      | 599.7    | 79.4       | 149.9     | 5.41       | 0.61     | 0.16     | 0.27     | 0.94     | 0.69    | 57.49      | 72.36 | 1.25            | 1.26                  |
| 25t0.8L800    | 800      | 337.3    | 75.3       | 84.3      | 9.73       | 0.85     | 0.18     | 0.12     | 1.00     | 0.78    | 47.46      | 59.97 | 0.99            | 1.26                  |
| 25t0.8L1000   | 1000     | 215.9    | 70.4       | 54.0      | 15.35      | 0.87     | 0.18     | 0.12     | 1.00     | 0.96    | 45.64      | 50.64 | 0.82            | 1.11                  |
| 50t0.8L400    | 400      | 5397.4   | 23.4       | 1349.4    | 0.16       | 0.40     | 0.15     | 0.54     | 0.66     | 0.36    | 31.42      | 34.44 | 3.14            | 1.10                  |
| 50t0.8L600    | 600      | 2398.9   | 21.8       | 599.7     | 0.34       | 0.40     | 0.15     | 0.43     | 0.81     | 0.31    | 24.46      | 28.76 | 3.10            | 1.18                  |
| 50t0.8L800    | 800      | 1349.4   | 21.2       | 337.3     | 0.60       | 0.40     | 0.14     | 0.42     | 0.82     | 0.32    | 23.13      | 23.54 | 2.94            | 1.02                  |
| 50t0.8L1000   | 1000     | 863.6    | 20.9       | 215.9     | 0.92       | 0.40     | 0.14     | 0.41     | 0.83     | 0.34    | 21.85      | 20.87 | 2.71            | 0.96                  |
| 50t0.95L400   | 400      | 5397.4   | 33.0       | 1349.4    | 0.23       | 0.40     | 0.15     | 0.44     | 0.81     | 0.36    | 35.42      | 41.52 | 2.65            | 1.17                  |
| 50t0.95L600   | 600      | 2398.9   | 30.7       | 599.7     | 0.48       | 0.40     | 0.14     | 0.43     | 0.82     | 0.36    | 32.55      | 34.70 | 2.61            | 1.07                  |
| 50t0.95L800   | 800      | 1349.4   | 29.9       | 337.3     | 0.84       | 0.40     | 0.14     | 0.41     | 0.83     | 0.37    | 30.61      | 29.65 | 2.48            | 0.97                  |
| 50t0.95L1000  | 1000     | 863.6    | 29.4       | 215.9     | 1.30       | 0.42     | 0.14     | 0.39     | 0.84     | 0.40    | 28.37      | 28.80 | 2.29            | 1.02                  |
| 50t1.25L400   | 400      | 5397.4   | 57.0       | 1349.4    | 0.40       | 0.40     | 0.15     | 0.43     | 0.82     | 0.47    | 56.60      | 59.58 | 2.01            | 1.05                  |
| 50t1.25L600   | 600      | 2398.9   | 53.0       | 599.7     | 0.84       | 0.40     | 0.14     | 0.41     | 0.83     | 0.47    | 51.54      | 52.57 | 1.99            | 1.02                  |
| 50t1.25L800   | 800      | 1349.4   | 51.4       | 337.3     | 1.46       | 0.43     | 0.14     | 0.38     | 0.85     | 0.48    | 47.15      | 48.90 | 1.89            | 1.04                  |
| 50t1.25L1000  | 1000     | 863.6    | 50.4       | 215.9     | 2.27       | 0.46     | 0.15     | 0.36     | 0.87     | 0.51    | 42.97      | 47.62 | 1.75            | 1.11                  |

Note: dimensions in *mm*, stresses in *MPa***Table B.4:** Spherically-hinged column critical stresses, ultimate strengths and DSM estimates ( $f_y=275\text{ MPa}$ )

| <i>Column</i> | <i>L</i> | $f_{bf}$ | $f_{erft}$ | $f_{cre}$ | $\Delta_f$ | <i>a</i> | <i>b</i> | <i>c</i> | <i>d</i> | $\beta$ | $f_{nfte}$ | $f_u$ | $\lambda_{fte}$ | $\frac{f_u}{f_{yfe}}$ |
|---------------|----------|----------|------------|-----------|------------|----------|----------|----------|----------|---------|------------|-------|-----------------|-----------------------|
| 25t0.8L400    | 400      | 1349.4   | 83.4       | 337.3     | 2.41       | 0.47     | 0.15     | 0.36     | 0.87     | 0.59    | 69.95      | 79.68 | 1.53            | 1.14                  |
| 25t0.8L600    | 600      | 599.7    | 79.4       | 149.9     | 5.41       | 0.61     | 0.16     | 0.27     | 0.94     | 0.68    | 57.31      | 72.36 | 1.27            | 1.26                  |
| 25t0.8L800    | 800      | 337.3    | 75.3       | 84.3      | 9.73       | 0.85     | 0.18     | 0.12     | 1.00     | 0.78    | 47.46      | 59.97 | 0.99            | 1.26                  |
| 25t0.8L1000   | 1000     | 215.9    | 70.4       | 54.0      | 15.35      | 0.87     | 0.18     | 0.12     | 1.00     | 0.96    | 45.64      | 51.00 | 0.82            | 1.12                  |
| 50t0.8L400    | 400      | 5397.4   | 23.4       | 1349.4    | 0.16       | 0.40     | 0.15     | 0.54     | 0.66     | 0.35    | 32.05      | 35.39 | 3.28            | 1.10                  |
| 50t0.8L600    | 600      | 2398.9   | 21.8       | 599.7     | 0.34       | 0.40     | 0.15     | 0.43     | 0.81     | 0.29    | 24.76      | 29.32 | 3.22            | 1.18                  |
| 50t0.8L800    | 800      | 1349.4   | 21.2       | 337.3     | 0.60       | 0.40     | 0.14     | 0.42     | 0.82     | 0.31    | 23.35      | 23.62 | 3.03            | 1.01                  |
| 50t0.8L1000   | 1000     | 863.6    | 20.9       | 215.9     | 0.92       | 0.40     | 0.14     | 0.41     | 0.83     | 0.33    | 21.99      | 20.87 | 2.78            | 0.95                  |
| 50t0.95L400   | 400      | 5397.4   | 33.0       | 1349.4    | 0.23       | 0.40     | 0.15     | 0.44     | 0.81     | 0.34    | 35.88      | 42.76 | 2.77            | 1.19                  |
| 50t0.95L600   | 600      | 2398.9   | 30.7       | 599.7     | 0.48       | 0.40     | 0.14     | 0.43     | 0.82     | 0.34    | 32.91      | 35.33 | 2.72            | 1.07                  |
| 50t0.95L800   | 800      | 1349.4   | 29.9       | 337.3     | 0.84       | 0.40     | 0.14     | 0.41     | 0.83     | 0.36    | 30.87      | 29.66 | 2.56            | 0.96                  |
| 50t0.95L1000  | 1000     | 863.6    | 29.4       | 215.9     | 1.30       | 0.42     | 0.14     | 0.39     | 0.84     | 0.39    | 28.51      | 28.80 | 2.34            | 1.01                  |
| 50t1.25L400   | 400      | 5397.4   | 57.0       | 1349.4    | 0.40       | 0.40     | 0.15     | 0.43     | 0.82     | 0.45    | 57.20      | 60.39 | 2.10            | 1.06                  |
| 50t1.25L600   | 600      | 2398.9   | 53.0       | 599.7     | 0.84       | 0.40     | 0.14     | 0.41     | 0.83     | 0.45    | 51.99      | 52.61 | 2.07            | 1.01                  |
| 50t1.25L800   | 800      | 1349.4   | 51.4       | 337.3     | 1.46       | 0.43     | 0.14     | 0.38     | 0.85     | 0.47    | 47.40      | 48.90 | 1.95            | 1.03                  |
| 50t1.25L1000  | 1000     | 863.6    | 50.4       | 215.9     | 2.27       | 0.46     | 0.15     | 0.36     | 0.87     | 0.50    | 43.05      | 47.62 | 1.79            | 1.11                  |

Note: dimensions in *mm*, stresses in *MPa*

**Table B.5:** Spherically-hinged column critical stresses, ultimate strengths and DSM estimates ( $f_y=300MPa$ )

| <i>Column</i> | <i>L</i> | $f_{bf}$ | $f_{crft}$ | $f_{cre}$ | $\Delta_f$ | <i>a</i> | <i>b</i> | <i>c</i> | <i>d</i> | $\beta$ | $f_{nfte}$ | $f_u$ | $\lambda_{fte}$ | $\frac{f_u}{f_{nfte}}$ |
|---------------|----------|----------|------------|-----------|------------|----------|----------|----------|----------|---------|------------|-------|-----------------|------------------------|
| 25t0.8L400    | 400      | 1349.4   | 83.4       | 337.3     | 2.41       | 0.47     | 0.15     | 0.36     | 0.87     | 0.54    | 70.16      | 79.68 | 1.65            | 1.14                   |
| 25t0.8L600    | 600      | 599.7    | 79.4       | 149.9     | 5.41       | 0.61     | 0.16     | 0.27     | 0.94     | 0.67    | 57.10      | 72.36 | 1.29            | 1.27                   |
| 25t0.8L800    | 800      | 337.3    | 75.3       | 84.3      | 9.73       | 0.85     | 0.18     | 0.12     | 1.00     | 0.78    | 47.46      | 61.78 | 0.99            | 1.30                   |
| 25t0.8L1000   | 1000     | 215.9    | 70.4       | 54.0      | 15.35      | 0.87     | 0.18     | 0.12     | 1.00     | 0.96    | 45.64      | 51.67 | 0.82            | 1.13                   |
| 50t0.8L400    | 400      | 5397.4   | 23.4       | 1349.4    | 0.16       | 0.40     | 0.15     | 0.54     | 0.66     | 0.32    | 33.71      | 37.47 | 3.66            | 1.11                   |
| 50t0.8L600    | 600      | 2398.9   | 21.8       | 599.7     | 0.34       | 0.40     | 0.15     | 0.43     | 0.81     | 0.27    | 25.51      | 30.42 | 3.54            | 1.19                   |
| 50t0.8L800    | 800      | 1349.4   | 21.2       | 337.3     | 0.60       | 0.40     | 0.14     | 0.42     | 0.82     | 0.29    | 23.87      | 23.60 | 3.27            | 0.99                   |
| 50t0.8L1000   | 1000     | 863.6    | 20.9       | 215.9     | 0.92       | 0.40     | 0.14     | 0.41     | 0.83     | 0.32    | 22.28      | 20.87 | 2.91            | 0.94                   |
| 50t0.95L400   | 400      | 5397.4   | 33.0       | 1349.4    | 0.23       | 0.40     | 0.15     | 0.44     | 0.81     | 0.31    | 37.08      | 45.69 | 3.09            | 1.23                   |
| 50t0.95L600   | 600      | 2398.9   | 30.7       | 599.7     | 0.48       | 0.40     | 0.14     | 0.43     | 0.82     | 0.31    | 33.83      | 36.66 | 2.99            | 1.08                   |
| 50t0.95L800   | 800      | 1349.4   | 29.9       | 337.3     | 0.84       | 0.40     | 0.14     | 0.41     | 0.83     | 0.34    | 31.49      | 29.66 | 2.75            | 0.94                   |
| 50t0.95L1000  | 1000     | 863.6    | 29.4       | 215.9     | 1.30       | 0.42     | 0.14     | 0.39     | 0.84     | 0.37    | 28.81      | 28.80 | 2.46            | 1.00                   |
| 50t1.25L400   | 400      | 5397.4   | 57.0       | 1349.4    | 0.40       | 0.40     | 0.15     | 0.43     | 0.82     | 0.40    | 58.82      | 63.27 | 2.35            | 1.08                   |
| 50t1.25L600   | 600      | 2398.9   | 53.0       | 599.7     | 0.84       | 0.40     | 0.14     | 0.41     | 0.83     | 0.41    | 53.17      | 53.04 | 2.27            | 1.00                   |
| 50t1.25L800   | 800      | 1349.4   | 51.4       | 337.3     | 1.46       | 0.43     | 0.14     | 0.38     | 0.85     | 0.43    | 48.02      | 48.91 | 2.10            | 1.02                   |
| 50t1.25L1000  | 1000     | 863.6    | 50.4       | 215.9     | 2.27       | 0.46     | 0.15     | 0.36     | 0.87     | 0.47    | 43.22      | 47.62 | 1.88            | 1.10                   |

Note: dimensions in *mm*, stresses in *MPa***Table B.6:** Spherically-hinged column critical stresses, ultimate strengths and DSM estimates ( $f_y=350MPa$ )

| <i>Column</i> | <i>L</i> | $f_{bf}$ | $f_{crft}$ | $f_{cre}$ | $\Delta_f$ | <i>a</i> | <i>b</i> | <i>c</i> | <i>d</i> | $\beta$ | $f_{nfte}$ | $f_u$ | $\lambda_{fte}$ | $\frac{f_u}{f_{nfte}}$ |
|---------------|----------|----------|------------|-----------|------------|----------|----------|----------|----------|---------|------------|-------|-----------------|------------------------|
| 25t0.8L400    | 400      | 1349.4   | 83.4       | 337.3     | 2.41       | 0.47     | 0.15     | 0.36     | 0.87     | 0.54    | 70.16      | 79.68 | 1.65            | 1.14                   |
| 25t0.8L600    | 600      | 599.7    | 79.4       | 149.9     | 5.41       | 0.61     | 0.16     | 0.27     | 0.94     | 0.67    | 57.10      | 72.36 | 1.29            | 1.27                   |
| 25t0.8L800    | 800      | 337.3    | 75.3       | 84.3      | 9.73       | 0.85     | 0.18     | 0.12     | 1.00     | 0.78    | 47.46      | 61.78 | 0.99            | 1.30                   |
| 25t0.8L1000   | 1000     | 215.9    | 70.4       | 54.0      | 15.35      | 0.87     | 0.18     | 0.12     | 1.00     | 0.96    | 45.64      | 51.67 | 0.82            | 1.13                   |
| 50t0.8L400    | 400      | 5397.4   | 23.4       | 1349.4    | 0.16       | 0.40     | 0.15     | 0.54     | 0.66     | 0.32    | 33.71      | 37.47 | 3.66            | 1.11                   |
| 50t0.8L600    | 600      | 2398.9   | 21.8       | 599.7     | 0.34       | 0.40     | 0.15     | 0.43     | 0.81     | 0.27    | 25.51      | 30.42 | 3.54            | 1.19                   |
| 50t0.8L800    | 800      | 1349.4   | 21.2       | 337.3     | 0.60       | 0.40     | 0.14     | 0.42     | 0.82     | 0.29    | 23.87      | 23.60 | 3.27            | 0.99                   |
| 50t0.8L1000   | 1000     | 863.6    | 20.9       | 215.9     | 0.92       | 0.40     | 0.14     | 0.41     | 0.83     | 0.32    | 22.28      | 20.87 | 2.91            | 0.94                   |
| 50t0.95L400   | 400      | 5397.4   | 33.0       | 1349.4    | 0.23       | 0.40     | 0.15     | 0.44     | 0.81     | 0.31    | 37.08      | 45.69 | 3.09            | 1.23                   |
| 50t0.95L600   | 600      | 2398.9   | 30.7       | 599.7     | 0.48       | 0.40     | 0.14     | 0.43     | 0.82     | 0.31    | 33.83      | 36.66 | 2.99            | 1.08                   |
| 50t0.95L800   | 800      | 1349.4   | 29.9       | 337.3     | 0.84       | 0.40     | 0.14     | 0.41     | 0.83     | 0.34    | 31.49      | 29.66 | 2.75            | 0.94                   |
| 50t0.95L1000  | 1000     | 863.6    | 29.4       | 215.9     | 1.30       | 0.42     | 0.14     | 0.39     | 0.84     | 0.37    | 28.81      | 28.80 | 2.46            | 1.00                   |
| 50t1.25L400   | 400      | 5397.4   | 57.0       | 1349.4    | 0.40       | 0.40     | 0.15     | 0.43     | 0.82     | 0.40    | 58.82      | 63.27 | 2.35            | 1.08                   |
| 50t1.25L600   | 600      | 2398.9   | 53.0       | 599.7     | 0.84       | 0.40     | 0.14     | 0.41     | 0.83     | 0.41    | 53.17      | 53.04 | 2.27            | 1.00                   |
| 50t1.25L800   | 800      | 1349.4   | 51.4       | 337.3     | 1.46       | 0.43     | 0.14     | 0.38     | 0.85     | 0.43    | 48.02      | 48.91 | 2.10            | 1.02                   |
| 50t1.25L1000  | 1000     | 863.6    | 50.4       | 215.9     | 2.27       | 0.46     | 0.15     | 0.36     | 0.87     | 0.47    | 43.22      | 47.62 | 1.88            | 1.10                   |

Note: dimensions in *mm*, stresses in *MPa*

**Table B.7:** Spherically-hinged column critical stresses, ultimate strengths and DSM estimates ( $f_y=375MPa$ )

| <i>Column</i> | <i>L</i> | $f_{bf}$ | $f_{crft}$ | $f_{cre}$ | $\Delta_f$ | <i>a</i> | <i>b</i> | <i>c</i> | <i>d</i> | $\beta$ | $f_{nfte}$ | $f_u$ | $\lambda_{fte}$ | $\frac{f_u}{f_{yfe}}$ |
|---------------|----------|----------|------------|-----------|------------|----------|----------|----------|----------|---------|------------|-------|-----------------|-----------------------|
| 25t0.8L400    | 400      | 1349.4   | 83.4       | 337.3     | 2.41       | 0.47     | 0.15     | 0.36     | 0.87     | 0.53    | 70.23      | 79.68 | 1.68            | 1.13                  |
| 25t0.8L600    | 600      | 599.7    | 79.4       | 149.9     | 5.41       | 0.61     | 0.16     | 0.27     | 0.94     | 0.67    | 57.10      | 72.36 | 1.29            | 1.27                  |
| 25t0.8L800    | 800      | 337.3    | 75.3       | 84.3      | 9.73       | 0.85     | 0.18     | 0.12     | 1.00     | 0.78    | 47.46      | 61.78 | 0.99            | 1.30                  |
| 25t0.8L1000   | 1000     | 215.9    | 70.4       | 54.0      | 15.35      | 0.87     | 0.18     | 0.12     | 1.00     | 0.96    | 45.64      | 51.77 | 0.82            | 1.13                  |
| 50t0.8L400    | 400      | 5397.4   | 23.4       | 1349.4    | 0.16       | 0.40     | 0.15     | 0.54     | 0.66     | 0.31    | 34.20      | 37.65 | 3.78            | 1.10                  |
| 50t0.8L600    | 600      | 2398.9   | 21.8       | 599.7     | 0.34       | 0.40     | 0.15     | 0.43     | 0.81     | 0.26    | 25.72      | 30.66 | 3.64            | 1.19                  |
| 50t0.8L800    | 800      | 1349.4   | 21.2       | 337.3     | 0.60       | 0.40     | 0.14     | 0.42     | 0.82     | 0.28    | 24.01      | 23.47 | 3.33            | 0.98                  |
| 50t0.8L1000   | 1000     | 863.6    | 20.9       | 215.9     | 0.92       | 0.40     | 0.14     | 0.41     | 0.83     | 0.31    | 22.34      | 20.87 | 2.94            | 0.93                  |
| 50t0.95L400   | 400      | 5397.4   | 33.0       | 1349.4    | 0.23       | 0.40     | 0.15     | 0.44     | 0.81     | 0.30    | 37.43      | 46.45 | 3.18            | 1.24                  |
| 50t0.95L600   | 600      | 2398.9   | 30.7       | 599.7     | 0.48       | 0.40     | 0.14     | 0.43     | 0.82     | 0.31    | 34.09      | 36.95 | 3.06            | 1.08                  |
| 50t0.95L800   | 800      | 1349.4   | 29.9       | 337.3     | 0.84       | 0.40     | 0.14     | 0.41     | 0.83     | 0.33    | 31.66      | 29.66 | 2.81            | 0.94                  |
| 50t0.95L1000  | 1000     | 863.6    | 29.4       | 215.9     | 1.30       | 0.42     | 0.14     | 0.39     | 0.84     | 0.37    | 28.87      | 28.80 | 2.48            | 1.00                  |
| 50t1.25L400   | 400      | 5397.4   | 57.0       | 1349.4    | 0.40       | 0.40     | 0.15     | 0.43     | 0.82     | 0.39    | 59.31      | 64.22 | 2.42            | 1.08                  |
| 50t1.25L600   | 600      | 2398.9   | 53.0       | 599.7     | 0.84       | 0.40     | 0.14     | 0.41     | 0.83     | 0.40    | 53.51      | 53.14 | 2.33            | 0.99                  |
| 50t1.25L800   | 800      | 1349.4   | 51.4       | 337.3     | 1.46       | 0.43     | 0.14     | 0.38     | 0.85     | 0.42    | 48.19      | 48.91 | 2.14            | 1.01                  |
| 50t1.25L1000  | 1000     | 863.6    | 50.4       | 215.9     | 2.27       | 0.46     | 0.15     | 0.36     | 0.87     | 0.47    | 43.26      | 47.62 | 1.90            | 1.10                  |

Note: dimensions in *mm*, stresses in *MPa***Table B.8:** Spherically-hinged column critical stresses, ultimate strengths and DSM estimates ( $f_y=400MPa$ )

| <i>Column</i> | <i>L</i> | $f_{bf}$ | $f_{crft}$ | $f_{cre}$ | $\Delta_f$ | <i>a</i> | <i>b</i> | <i>c</i> | <i>d</i> | $\beta$ | $f_{nfte}$ | $f_u$ | $\lambda_{fte}$ | $\frac{f_u}{f_{yfe}}$ |
|---------------|----------|----------|------------|-----------|------------|----------|----------|----------|----------|---------|------------|-------|-----------------|-----------------------|
| 25t0.8L400    | 400      | 1349.4   | 83.4       | 337.3     | 2.41       | 0.47     | 0.15     | 0.36     | 0.87     | 0.52    | 70.30      | 79.68 | 1.71            | 1.13                  |
| 25t0.8L600    | 600      | 599.7    | 79.4       | 149.9     | 5.41       | 0.61     | 0.16     | 0.27     | 0.94     | 0.67    | 57.10      | 72.42 | 1.29            | 1.27                  |
| 25t0.8L800    | 800      | 337.3    | 75.3       | 84.3      | 9.73       | 0.85     | 0.18     | 0.12     | 1.00     | 0.78    | 47.46      | 61.78 | 0.99            | 1.30                  |
| 25t0.8L1000   | 1000     | 215.9    | 70.4       | 54.0      | 15.35      | 0.87     | 0.18     | 0.12     | 1.00     | 0.96    | 45.64      | 51.88 | 0.82            | 1.14                  |
| 50t0.8L400    | 400      | 5397.4   | 23.4       | 1349.4    | 0.16       | 0.40     | 0.15     | 0.54     | 0.66     | 0.31    | 34.66      | 37.65 | 3.89            | 1.09                  |
| 50t0.8L600    | 600      | 2398.9   | 21.8       | 599.7     | 0.34       | 0.40     | 0.15     | 0.43     | 0.81     | 0.26    | 25.91      | 30.87 | 3.72            | 1.19                  |
| 50t0.8L800    | 800      | 1349.4   | 21.2       | 337.3     | 0.60       | 0.40     | 0.14     | 0.42     | 0.82     | 0.28    | 24.13      | 23.65 | 3.39            | 0.98                  |
| 50t0.8L1000   | 1000     | 863.6    | 20.9       | 215.9     | 0.92       | 0.40     | 0.14     | 0.41     | 0.83     | 0.31    | 22.39      | 20.87 | 2.97            | 0.93                  |
| 50t0.95L400   | 400      | 5397.4   | 33.0       | 1349.4    | 0.23       | 0.40     | 0.15     | 0.44     | 0.81     | 0.29    | 37.76      | 47.11 | 3.27            | 1.25                  |
| 50t0.95L600   | 600      | 2398.9   | 30.7       | 599.7     | 0.48       | 0.40     | 0.14     | 0.43     | 0.82     | 0.30    | 34.34      | 37.22 | 3.14            | 1.08                  |
| 50t0.95L800   | 800      | 1349.4   | 29.9       | 337.3     | 0.84       | 0.40     | 0.14     | 0.41     | 0.83     | 0.32    | 31.80      | 29.66 | 2.85            | 0.93                  |
| 50t0.95L1000  | 1000     | 863.6    | 29.4       | 215.9     | 1.30       | 0.42     | 0.14     | 0.39     | 0.84     | 0.36    | 28.92      | 28.80 | 2.50            | 1.00                  |
| 50t1.25L400   | 400      | 5397.4   | 57.0       | 1349.4    | 0.40       | 0.40     | 0.15     | 0.43     | 0.82     | 0.38    | 59.77      | 65.10 | 2.49            | 1.09                  |
| 50t1.25L600   | 600      | 2398.9   | 53.0       | 599.7     | 0.84       | 0.40     | 0.14     | 0.41     | 0.83     | 0.39    | 53.83      | 53.12 | 2.39            | 0.99                  |
| 50t1.25L800   | 800      | 1349.4   | 51.4       | 337.3     | 1.46       | 0.43     | 0.14     | 0.38     | 0.85     | 0.42    | 48.34      | 48.91 | 2.18            | 1.01                  |
| 50t1.25L1000  | 1000     | 863.6    | 50.4       | 215.9     | 2.27       | 0.46     | 0.15     | 0.36     | 0.87     | 0.46    | 43.29      | 47.62 | 1.91            | 1.10                  |

Note: dimensions in *mm*, stresses in *MPa*

**Table B.9:** Spherically-hinged column critical stresses, ultimate strengths and DSM estimates ( $f_y=450MPa$ )

| <i>Column</i> | <i>L</i> | $f_{bf}$ | $f_{crft}$ | $f_{cre}$ | $\Delta_f$ | <i>a</i> | <i>b</i> | <i>c</i> | <i>d</i> | $\beta$ | $f_{nfte}$ | $f_u$ | $\lambda_{fte}$ | $\frac{f_u}{f_{nfte}}$ |
|---------------|----------|----------|------------|-----------|------------|----------|----------|----------|----------|---------|------------|-------|-----------------|------------------------|
| 25t0.8L400    | 400      | 1349.4   | 83.4       | 337.3     | 2.41       | 0.47     | 0.15     | 0.36     | 0.87     | 0.51    | 70.42      | 79.68 | 1.76            | 1.13                   |
| 25t0.8L600    | 600      | 599.7    | 79.4       | 149.9     | 5.41       | 0.61     | 0.16     | 0.27     | 0.94     | 0.67    | 57.10      | 72.47 | 1.29            | 1.27                   |
| 25t0.8L800    | 800      | 337.3    | 75.3       | 84.3      | 9.73       | 0.85     | 0.18     | 0.12     | 1.00     | 0.78    | 47.46      | 61.78 | 0.99            | 1.30                   |
| 25t0.8L1000   | 1000     | 215.9    | 70.4       | 54.0      | 15.35      | 0.87     | 0.18     | 0.12     | 1.00     | 0.96    | 45.64      | 52.02 | 0.82            | 1.14                   |
| 50t0.8L400    | 400      | 5397.4   | 23.4       | 1349.4    | 0.16       | 0.40     | 0.15     | 0.54     | 0.66     | 0.29    | 35.52      | 37.65 | 4.09            | 1.06                   |
| 50t0.8L600    | 600      | 2398.9   | 21.8       | 599.7     | 0.34       | 0.40     | 0.15     | 0.43     | 0.81     | 0.25    | 26.27      | 31.18 | 3.88            | 1.19                   |
| 50t0.8L800    | 800      | 1349.4   | 21.2       | 337.3     | 0.60       | 0.40     | 0.14     | 0.42     | 0.82     | 0.27    | 24.34      | 23.58 | 3.48            | 0.97                   |
| 50t0.8L1000   | 1000     | 863.6    | 20.9       | 215.9     | 0.92       | 0.40     | 0.14     | 0.41     | 0.83     | 0.31    | 22.46      | 20.87 | 3.00            | 0.93                   |
| 50t0.95L400   | 400      | 5397.4   | 33.0       | 1349.4    | 0.23       | 0.40     | 0.15     | 0.44     | 0.81     | 0.28    | 38.38      | 48.23 | 3.44            | 1.26                   |
| 50t0.95L600   | 600      | 2398.9   | 30.7       | 599.7     | 0.48       | 0.40     | 0.14     | 0.43     | 0.82     | 0.29    | 34.77      | 37.61 | 3.27            | 1.08                   |
| 50t0.95L800   | 800      | 1349.4   | 29.9       | 337.3     | 0.84       | 0.40     | 0.14     | 0.41     | 0.83     | 0.32    | 32.05      | 29.66 | 2.94            | 0.93                   |
| 50t0.95L1000  | 1000     | 863.6    | 29.4       | 215.9     | 1.30       | 0.42     | 0.14     | 0.39     | 0.84     | 0.36    | 28.99      | 28.80 | 2.53            | 0.99                   |
| 50t1.25L400   | 400      | 5397.4   | 57.0       | 1349.4    | 0.40       | 0.40     | 0.15     | 0.43     | 0.82     | 0.36    | 60.63      | 66.70 | 2.62            | 1.10                   |
| 50t1.25L600   | 600      | 2398.9   | 53.0       | 599.7     | 0.84       | 0.40     | 0.14     | 0.41     | 0.83     | 0.37    | 54.41      | 53.26 | 2.49            | 0.98                   |
| 50t1.25L800   | 800      | 1349.4   | 51.4       | 337.3     | 1.46       | 0.43     | 0.14     | 0.38     | 0.85     | 0.40    | 48.60      | 48.91 | 2.24            | 1.01                   |
| 50t1.25L1000  | 1000     | 863.6    | 50.4       | 215.9     | 2.27       | 0.46     | 0.15     | 0.36     | 0.87     | 0.46    | 43.33      | 47.62 | 1.93            | 1.10                   |

Note: dimensions in *mm*, stresses in *MPa***Table B.10:** Spherically-hinged column critical stresses, ultimate strengths and DSM estimates ( $f_y=475MPa$ )

| <i>Column</i> | <i>L</i> | $f_{bf}$ | $f_{crft}$ | $f_{cre}$ | $\Delta_f$ | <i>a</i> | <i>b</i> | <i>c</i> | <i>d</i> | $\beta$ | $f_{nfte}$ | $f_u$ | $\lambda_{fte}$ | $\frac{f_u}{f_{nfte}}$ |
|---------------|----------|----------|------------|-----------|------------|----------|----------|----------|----------|---------|------------|-------|-----------------|------------------------|
| 25t0.8L400    | 400      | 1349.4   | 83.4       | 337.3     | 2.41       | 0.47     | 0.15     | 0.36     | 0.87     | 0.50    | 70.47      | 79.68 | 1.78            | 1.13                   |
| 25t0.8L600    | 600      | 599.7    | 79.4       | 149.9     | 5.41       | 0.61     | 0.16     | 0.27     | 0.94     | 0.67    | 57.10      | 72.48 | 1.29            | 1.27                   |
| 25t0.8L800    | 800      | 337.3    | 75.3       | 84.3      | 9.73       | 0.85     | 0.18     | 0.12     | 1.00     | 0.78    | 47.46      | 61.78 | 0.99            | 1.30                   |
| 25t0.8L1000   | 1000     | 215.9    | 70.4       | 54.0      | 15.35      | 0.87     | 0.18     | 0.12     | 1.00     | 0.96    | 45.64      | 52.01 | 0.82            | 1.14                   |
| 50t0.8L400    | 400      | 5397.4   | 23.4       | 1349.4    | 0.16       | 0.40     | 0.15     | 0.54     | 0.66     | 0.29    | 35.92      | 37.65 | 4.19            | 1.05                   |
| 50t0.8L600    | 600      | 2398.9   | 21.8       | 599.7     | 0.34       | 0.40     | 0.15     | 0.43     | 0.81     | 0.24    | 26.42      | 31.28 | 3.95            | 1.18                   |
| 50t0.8L800    | 800      | 1349.4   | 21.2       | 337.3     | 0.60       | 0.40     | 0.14     | 0.42     | 0.82     | 0.27    | 24.43      | 23.63 | 3.52            | 0.97                   |
| 50t0.8L1000   | 1000     | 863.6    | 20.9       | 215.9     | 0.92       | 0.40     | 0.14     | 0.41     | 0.83     | 0.31    | 22.48      | 20.87 | 3.01            | 0.93                   |
| 50t0.95L400   | 400      | 5397.4   | 33.0       | 1349.4    | 0.23       | 0.40     | 0.15     | 0.44     | 0.81     | 0.27    | 38.66      | 48.70 | 3.53            | 1.26                   |
| 50t0.95L600   | 600      | 2398.9   | 30.7       | 599.7     | 0.48       | 0.40     | 0.14     | 0.43     | 0.82     | 0.28    | 34.97      | 37.75 | 3.33            | 1.08                   |
| 50t0.95L800   | 800      | 1349.4   | 29.9       | 337.3     | 0.84       | 0.40     | 0.14     | 0.41     | 0.83     | 0.31    | 32.16      | 29.66 | 2.97            | 0.92                   |
| 50t0.95L1000  | 1000     | 863.6    | 29.4       | 215.9     | 1.30       | 0.42     | 0.14     | 0.39     | 0.84     | 0.36    | 29.01      | 28.80 | 2.54            | 0.99                   |
| 50t1.25L400   | 400      | 5397.4   | 57.0       | 1349.4    | 0.40       | 0.40     | 0.15     | 0.43     | 0.82     | 0.35    | 61.03      | 67.40 | 2.68            | 1.10                   |
| 50t1.25L600   | 600      | 2398.9   | 53.0       | 599.7     | 0.84       | 0.40     | 0.14     | 0.41     | 0.83     | 0.36    | 54.67      | 53.28 | 2.54            | 0.97                   |
| 50t1.25L800   | 800      | 1349.4   | 51.4       | 337.3     | 1.46       | 0.43     | 0.14     | 0.38     | 0.85     | 0.40    | 48.71      | 48.91 | 2.26            | 1.00                   |
| 50t1.25L1000  | 1000     | 863.6    | 50.4       | 215.9     | 2.27       | 0.46     | 0.15     | 0.36     | 0.87     | 0.46    | 43.34      | 47.62 | 1.94            | 1.10                   |

Note: dimensions in *mm*, stresses in *MPa*

**Table B.11:** Spherically-hinged column critical stresses, ultimate strengths and DSM estimates ( $f_y=500MPa$ )

| <i>Column</i> | <i>L</i> | $f_{bf}$ | $f_{cft}$ | $f_{cre}$ | $\Delta_f$ | <i>a</i> | <i>b</i> | <i>c</i> | <i>d</i> | $\beta$ | $f_{nftc}$ | $f_u$ | $\lambda_{fte}$ | $\frac{f_u}{f_{nftc}}$ |
|---------------|----------|----------|-----------|-----------|------------|----------|----------|----------|----------|---------|------------|-------|-----------------|------------------------|
| 25t0.8L400    | 400      | 1349.4   | 83.4      | 337.3     | 2.41       | 0.47     | 0.15     | 0.36     | 0.87     | 0.50    | 70.52      | 79.68 | 1.80            | 1.13                   |
| 25t0.8L600    | 600      | 599.7    | 79.4      | 149.9     | 5.41       | 0.61     | 0.16     | 0.27     | 0.94     | 0.67    | 57.10      | 72.48 | 1.29            | 1.27                   |
| 25t0.8L800    | 800      | 337.3    | 75.3      | 84.3      | 9.73       | 0.85     | 0.18     | 0.12     | 1.00     | 0.78    | 47.46      | 61.78 | 0.99            | 1.30                   |
| 25t0.8L1000   | 1000     | 215.9    | 70.4      | 54.0      | 15.35      | 0.87     | 0.18     | 0.12     | 1.00     | 0.96    | 45.64      | 52.01 | 0.82            | 1.14                   |
| 50t0.8L400    | 400      | 5397.4   | 23.4      | 1349.4    | 0.16       | 0.40     | 0.15     | 0.54     | 0.66     | 0.28    | 36.30      | 37.65 | 4.28            | 1.04                   |
| 50t0.8L600    | 600      | 2398.9   | 21.8      | 599.7     | 0.34       | 0.40     | 0.15     | 0.43     | 0.81     | 0.24    | 26.57      | 31.36 | 4.02            | 1.18                   |
| 50t0.8L800    | 800      | 1349.4   | 21.2      | 337.3     | 0.60       | 0.40     | 0.14     | 0.42     | 0.82     | 0.27    | 24.51      | 23.66 | 3.56            | 0.97                   |
| 50t0.8L1000   | 1000     | 863.6    | 20.9      | 215.9     | 0.92       | 0.40     | 0.14     | 0.41     | 0.83     | 0.31    | 22.48      | 20.87 | 3.01            | 0.93                   |
| 50t0.95L400   | 400      | 5397.4   | 33.0      | 1349.4    | 0.23       | 0.40     | 0.15     | 0.44     | 0.81     | 0.27    | 38.94      | 49.11 | 3.60            | 1.26                   |
| 50t0.95L600   | 600      | 2398.9   | 30.7      | 599.7     | 0.48       | 0.40     | 0.14     | 0.43     | 0.82     | 0.28    | 35.15      | 37.88 | 3.39            | 1.08                   |
| 50t0.95L800   | 800      | 1349.4   | 29.9      | 337.3     | 0.84       | 0.40     | 0.14     | 0.41     | 0.83     | 0.31    | 32.25      | 29.66 | 3.00            | 0.92                   |
| 50t0.95L1000  | 1000     | 863.6    | 29.4      | 215.9     | 1.30       | 0.42     | 0.14     | 0.39     | 0.84     | 0.36    | 29.01      | 28.80 | 2.54            | 0.99                   |
| 50t1.25L400   | 400      | 5397.4   | 57.0      | 1349.4    | 0.40       | 0.40     | 0.15     | 0.43     | 0.82     | 0.34    | 61.42      | 68.05 | 2.74            | 1.11                   |
| 50t1.25L600   | 600      | 2398.9   | 53.0      | 599.7     | 0.84       | 0.40     | 0.14     | 0.41     | 0.83     | 0.36    | 54.91      | 53.30 | 2.58            | 0.97                   |
| 50t1.25L800   | 800      | 1349.4   | 51.4      | 337.3     | 1.46       | 0.43     | 0.14     | 0.38     | 0.85     | 0.39    | 48.80      | 48.91 | 2.29            | 1.00                   |
| 50t1.25L1000  | 1000     | 863.6    | 50.4      | 215.9     | 2.27       | 0.46     | 0.15     | 0.36     | 0.87     | 0.46    | 43.35      | 47.62 | 1.94            | 1.10                   |

Note: dimensions in *mm*, stresses in *MPa***Table B.12:** Spherically-hinged column critical stresses, ultimate strengths and DSM estimates ( $f_y=550MPa$ )

| <i>Column</i> | <i>L</i> | $f_{bf}$ | $f_{cft}$ | $f_{cre}$ | $\Delta_f$ | <i>a</i> | <i>b</i> | <i>c</i> | <i>d</i> | $\beta$ | $f_{nftc}$ | $f_u$ | $\lambda_{fte}$ | $\frac{f_u}{f_{nftc}}$ |
|---------------|----------|----------|-----------|-----------|------------|----------|----------|----------|----------|---------|------------|-------|-----------------|------------------------|
| 25t0.8L400    | 400      | 1349.4   | 83.4      | 337.3     | 2.41       | 0.47     | 0.15     | 0.36     | 0.87     | 0.49    | 70.60      | 79.68 | 1.83            | 1.13                   |
| 25t0.8L600    | 600      | 599.7    | 79.4      | 149.9     | 5.41       | 0.61     | 0.16     | 0.27     | 0.94     | 0.67    | 57.10      | 72.49 | 1.29            | 1.27                   |
| 25t0.8L800    | 800      | 337.3    | 75.3      | 84.3      | 9.73       | 0.85     | 0.18     | 0.12     | 1.00     | 0.78    | 47.46      | 61.78 | 0.99            | 1.30                   |
| 25t0.8L1000   | 1000     | 215.9    | 70.4      | 54.0      | 15.35      | 0.87     | 0.18     | 0.12     | 1.00     | 0.96    | 45.64      | 52.02 | 0.82            | 1.14                   |
| 50t0.8L400    | 400      | 5397.4   | 23.4      | 1349.4    | 0.16       | 0.40     | 0.15     | 0.54     | 0.66     | 0.28    | 37.00      | 37.65 | 4.45            | 1.02                   |
| 50t0.8L600    | 600      | 2398.9   | 21.8      | 599.7     | 0.34       | 0.40     | 0.15     | 0.43     | 0.81     | 0.23    | 26.84      | 31.47 | 4.14            | 1.17                   |
| 50t0.8L800    | 800      | 1349.4   | 21.2      | 337.3     | 0.60       | 0.40     | 0.14     | 0.42     | 0.82     | 0.26    | 24.63      | 23.60 | 3.62            | 0.96                   |
| 50t0.8L1000   | 1000     | 863.6    | 20.9      | 215.9     | 0.92       | 0.40     | 0.14     | 0.41     | 0.83     | 0.31    | 22.48      | 20.87 | 3.01            | 0.93                   |
| 50t0.95L400   | 400      | 5397.4   | 33.0      | 1349.4    | 0.23       | 0.40     | 0.15     | 0.44     | 0.81     | 0.26    | 39.45      | 49.81 | 3.75            | 1.26                   |
| 50t0.95L600   | 600      | 2398.9   | 30.7      | 599.7     | 0.48       | 0.40     | 0.14     | 0.43     | 0.82     | 0.27    | 35.49      | 38.05 | 3.49            | 1.07                   |
| 50t0.95L800   | 800      | 1349.4   | 29.9      | 337.3     | 0.84       | 0.40     | 0.14     | 0.41     | 0.83     | 0.30    | 32.40      | 29.66 | 3.05            | 0.92                   |
| 50t0.95L1000  | 1000     | 863.6    | 29.4      | 215.9     | 1.30       | 0.42     | 0.14     | 0.39     | 0.84     | 0.36    | 29.01      | 28.80 | 2.54            | 0.99                   |
| 50t1.25L400   | 400      | 5397.4   | 57.0      | 1349.4    | 0.40       | 0.40     | 0.15     | 0.43     | 0.82     | 0.33    | 62.14      | 69.19 | 2.85            | 1.11                   |
| 50t1.25L600   | 600      | 2398.9   | 53.0      | 599.7     | 0.84       | 0.40     | 0.14     | 0.41     | 0.83     | 0.35    | 55.36      | 53.31 | 2.66            | 0.96                   |
| 50t1.25L800   | 800      | 1349.4   | 51.4      | 337.3     | 1.46       | 0.43     | 0.14     | 0.38     | 0.85     | 0.39    | 48.96      | 48.91 | 2.33            | 1.00                   |
| 50t1.25L1000  | 1000     | 863.6    | 50.4      | 215.9     | 2.27       | 0.46     | 0.15     | 0.36     | 0.87     | 0.46    | 43.35      | 47.62 | 1.94            | 1.10                   |

Note: dimensions in *mm*, stresses in *MPa*

**Table B.13:** Spherically-hinged column critical stresses, ultimate strengths and DSM estimates ( $f_y=575\text{MPa}$ )

| <i>Column</i> | <i>L</i> | $f_{bf}$ | $f_{cft}$ | $f_{cre}$ | $\Delta_f$ | <i>a</i> | <i>b</i> | <i>c</i> | <i>d</i> | $\beta$ | $f_{nftc}$ | $f_u$ | $\lambda_{fte}$ | $\frac{f_u}{f_{fte}}$ |
|---------------|----------|----------|-----------|-----------|------------|----------|----------|----------|----------|---------|------------|-------|-----------------|-----------------------|
| 25t0.8L400    | 400      | 1349.4   | 83.4      | 337.3     | 2.41       | 0.47     | 0.15     | 0.36     | 0.87     | 0.48    | 70.63      | 79.68 | 1.84            | 1.13                  |
| 25t0.8L600    | 600      | 599.7    | 79.4      | 149.9     | 5.41       | 0.61     | 0.16     | 0.27     | 0.94     | 0.67    | 57.10      | 72.48 | 1.29            | 1.27                  |
| 25t0.8L800    | 800      | 337.3    | 75.3      | 84.3      | 9.73       | 0.85     | 0.18     | 0.12     | 1.00     | 0.78    | 47.46      | 61.78 | 0.99            | 1.30                  |
| 25t0.8L1000   | 1000     | 215.9    | 70.4      | 54.0      | 15.35      | 0.87     | 0.18     | 0.12     | 1.00     | 0.96    | 45.64      | 52.02 | 0.82            | 1.14                  |
| 50t0.8L400    | 400      | 5397.4   | 23.4      | 1349.4    | 0.16       | 0.40     | 0.15     | 0.54     | 0.66     | 0.27    | 37.34      | 37.65 | 4.53            | 1.01                  |
| 50t0.8L600    | 600      | 2398.9   | 21.8      | 599.7     | 0.34       | 0.40     | 0.15     | 0.43     | 0.81     | 0.23    | 26.96      | 31.49 | 4.20            | 1.17                  |
| 50t0.8L800    | 800      | 1349.4   | 21.2      | 337.3     | 0.60       | 0.40     | 0.14     | 0.42     | 0.82     | 0.26    | 24.68      | 23.66 | 3.64            | 0.96                  |
| 50t0.8L1000   | 1000     | 863.6    | 20.9      | 215.9     | 0.92       | 0.40     | 0.14     | 0.41     | 0.83     | 0.31    | 22.48      | 20.87 | 3.01            | 0.93                  |
| 50t0.95L400   | 400      | 5397.4   | 33.0      | 1349.4    | 0.23       | 0.40     | 0.15     | 0.44     | 0.81     | 0.25    | 39.68      | 50.10 | 3.82            | 1.26                  |
| 50t0.95L600   | 600      | 2398.9   | 30.7      | 599.7     | 0.48       | 0.40     | 0.14     | 0.43     | 0.82     | 0.27    | 35.64      | 38.11 | 3.54            | 1.07                  |
| 50t0.95L800   | 800      | 1349.4   | 29.9      | 337.3     | 0.84       | 0.40     | 0.14     | 0.41     | 0.83     | 0.30    | 32.47      | 29.66 | 3.07            | 0.91                  |
| 50t0.95L1000  | 1000     | 863.6    | 29.4      | 215.9     | 1.30       | 0.42     | 0.14     | 0.39     | 0.84     | 0.36    | 29.01      | 28.80 | 2.54            | 0.99                  |
| 50t1.25L400   | 400      | 5397.4   | 57.0      | 1349.4    | 0.40       | 0.40     | 0.15     | 0.43     | 0.82     | 0.32    | 62.47      | 69.69 | 2.91            | 1.12                  |
| 50t1.25L600   | 600      | 2398.9   | 53.0      | 599.7     | 0.84       | 0.40     | 0.14     | 0.41     | 0.83     | 0.34    | 55.56      | 53.31 | 2.69            | 0.96                  |
| 50t1.25L800   | 800      | 1349.4   | 51.4      | 337.3     | 1.46       | 0.43     | 0.14     | 0.38     | 0.85     | 0.39    | 49.03      | 48.91 | 2.34            | 1.00                  |
| 50t1.25L1000  | 1000     | 863.6    | 50.4      | 215.9     | 2.27       | 0.46     | 0.15     | 0.36     | 0.87     | 0.46    | 43.35      | 47.73 | 1.94            | 1.10                  |

Note: dimensions in *mm*, stresses in *MPa***Table B.14:** Spherically-hinged column critical stresses, ultimate strengths and DSM estimates ( $f_y=600\text{MPa}$ )

| <i>Column</i> | <i>L</i> | $f_{bf}$ | $f_{cft}$ | $f_{cre}$ | $\Delta_f$ | <i>a</i> | <i>b</i> | <i>c</i> | <i>d</i> | $\beta$ | $f_{nftc}$ | $f_u$ | $\lambda_{fte}$ | $\frac{f_u}{f_{fte}}$ |
|---------------|----------|----------|-----------|-----------|------------|----------|----------|----------|----------|---------|------------|-------|-----------------|-----------------------|
| 25t0.8L400    | 400      | 1349.4   | 83.4      | 337.3     | 2.41       | 0.47     | 0.15     | 0.36     | 0.87     | 0.48    | 70.66      | 79.68 | 1.85            | 1.13                  |
| 25t0.8L600    | 600      | 599.7    | 79.4      | 149.9     | 5.41       | 0.61     | 0.16     | 0.27     | 0.94     | 0.67    | 57.10      | 72.48 | 1.29            | 1.27                  |
| 25t0.8L800    | 800      | 337.3    | 75.3      | 84.3      | 9.73       | 0.85     | 0.18     | 0.12     | 1.00     | 0.78    | 47.46      | 61.78 | 0.99            | 1.30                  |
| 25t0.8L1000   | 1000     | 215.9    | 70.4      | 54.0      | 15.35      | 0.87     | 0.18     | 0.12     | 1.00     | 0.96    | 45.64      | 52.17 | 0.82            | 1.14                  |
| 50t0.8L400    | 400      | 5397.4   | 23.4      | 1349.4    | 0.16       | 0.40     | 0.15     | 0.54     | 0.66     | 0.27    | 37.65      | 37.65 | 4.61            | 1.00                  |
| 50t0.8L600    | 600      | 2398.9   | 21.8      | 599.7     | 0.34       | 0.40     | 0.15     | 0.43     | 0.81     | 0.23    | 27.07      | 31.52 | 4.25            | 1.16                  |
| 50t0.8L800    | 800      | 1349.4   | 21.2      | 337.3     | 0.60       | 0.40     | 0.14     | 0.42     | 0.82     | 0.26    | 24.73      | 23.60 | 3.66            | 0.95                  |
| 50t0.8L1000   | 1000     | 863.6    | 20.9      | 215.9     | 0.92       | 0.40     | 0.14     | 0.41     | 0.83     | 0.31    | 22.48      | 20.87 | 3.01            | 0.93                  |
| 50t0.95L400   | 400      | 5397.4   | 33.0      | 1349.4    | 0.23       | 0.40     | 0.15     | 0.44     | 0.81     | 0.25    | 39.91      | 50.36 | 3.89            | 1.26                  |
| 50t0.95L600   | 600      | 2398.9   | 30.7      | 599.7     | 0.48       | 0.40     | 0.14     | 0.43     | 0.82     | 0.27    | 35.78      | 38.15 | 3.58            | 1.07                  |
| 50t0.95L800   | 800      | 1349.4   | 29.9      | 337.3     | 0.84       | 0.40     | 0.14     | 0.41     | 0.83     | 0.30    | 32.52      | 29.66 | 3.09            | 0.91                  |
| 50t0.95L1000  | 1000     | 863.6    | 29.4      | 215.9     | 1.30       | 0.42     | 0.14     | 0.39     | 0.84     | 0.36    | 29.01      | 28.80 | 2.54            | 0.99                  |
| 50t1.25L400   | 400      | 5397.4   | 57.0      | 1349.4    | 0.40       | 0.40     | 0.15     | 0.43     | 0.82     | 0.32    | 62.80      | 70.14 | 2.96            | 1.12                  |
| 50t1.25L600   | 600      | 2398.9   | 53.0      | 599.7     | 0.84       | 0.40     | 0.14     | 0.41     | 0.83     | 0.34    | 55.75      | 53.31 | 2.73            | 0.96                  |
| 50t1.25L800   | 800      | 1349.4   | 51.4      | 337.3     | 1.46       | 0.43     | 0.14     | 0.38     | 0.85     | 0.38    | 49.09      | 48.91 | 2.35            | 1.00                  |
| 50t1.25L1000  | 1000     | 863.6    | 50.4      | 215.9     | 2.27       | 0.46     | 0.15     | 0.36     | 0.87     | 0.46    | 43.35      | 47.73 | 1.94            | 1.10                  |

Note: dimensions in *mm*, stresses in *MPa*

**Table B.15:** Spherically-hinged column critical stresses, ultimate strengths and DSM estimates ( $f_y=650MPa$ )

| <i>Column</i> | <i>L</i> | $f_{bf}$ | $f_{cft}$ | $f_{cre}$ | $\Delta_f$ | <i>a</i> | <i>b</i> | <i>c</i> | <i>d</i> | $\beta$ | $f_{nfe}$ | $f_u$ | $\lambda_{fte}$ | $\frac{f_u}{f_{yfe}}$ |
|---------------|----------|----------|-----------|-----------|------------|----------|----------|----------|----------|---------|-----------|-------|-----------------|-----------------------|
| 25t0.8L400    | 400      | 1349.4   | 83.4      | 337.3     | 2.41       | 0.47     | 0.15     | 0.36     | 0.87     | 0.48    | 70.70     | 79.68 | 1.87            | 1.13                  |
| 25t0.8L600    | 600      | 599.7    | 79.4      | 149.9     | 5.41       | 0.61     | 0.16     | 0.27     | 0.94     | 0.67    | 57.10     | 72.48 | 1.29            | 1.27                  |
| 25t0.8L800    | 800      | 337.3    | 75.3      | 84.3      | 9.73       | 0.85     | 0.18     | 0.12     | 1.00     | 0.78    | 47.46     | 61.78 | 0.99            | 1.30                  |
| 25t0.8L1000   | 1000     | 215.9    | 70.4      | 54.0      | 15.35      | 0.87     | 0.18     | 0.12     | 1.00     | 0.96    | 45.64     | 52.02 | 0.82            | 1.14                  |
| 50t0.8L400    | 400      | 5397.4   | 23.4      | 1349.4    | 0.16       | 0.40     | 0.15     | 0.54     | 0.66     | 0.26    | 38.25     | 37.65 | 4.76            | 0.98                  |
| 50t0.8L600    | 600      | 2398.9   | 21.8      | 599.7     | 0.34       | 0.40     | 0.15     | 0.43     | 0.81     | 0.22    | 27.28     | 31.55 | 4.35            | 1.16                  |
| 50t0.8L800    | 800      | 1349.4   | 21.2      | 337.3     | 0.60       | 0.40     | 0.14     | 0.42     | 0.82     | 0.26    | 24.80     | 23.69 | 3.70            | 0.96                  |
| 50t0.8L1000   | 1000     | 863.6    | 20.9      | 215.9     | 0.92       | 0.40     | 0.14     | 0.41     | 0.83     | 0.31    | 22.48     | 20.87 | 3.01            | 0.93                  |
| 50t0.95L400   | 400      | 5397.4   | 33.0      | 1349.4    | 0.23       | 0.40     | 0.15     | 0.44     | 0.81     | 0.24    | 40.34     | 50.78 | 4.01            | 1.26                  |
| 50t0.95L600   | 600      | 2398.9   | 30.7      | 599.7     | 0.48       | 0.40     | 0.14     | 0.43     | 0.82     | 0.26    | 36.04     | 38.21 | 3.67            | 1.06                  |
| 50t0.95L800   | 800      | 1349.4   | 29.9      | 337.3     | 0.84       | 0.40     | 0.14     | 0.41     | 0.83     | 0.30    | 32.60     | 29.66 | 3.12            | 0.91                  |
| 50t0.95L1000  | 1000     | 863.6    | 29.4      | 215.9     | 1.30       | 0.42     | 0.14     | 0.39     | 0.84     | 0.36    | 29.01     | 28.80 | 2.54            | 0.99                  |
| 50t1.25L400   | 400      | 5397.4   | 57.0      | 1349.4    | 0.40       | 0.40     | 0.15     | 0.43     | 0.82     | 0.31    | 63.41     | 70.92 | 3.05            | 1.12                  |
| 50t1.25L600   | 600      | 2398.9   | 53.0      | 599.7     | 0.84       | 0.40     | 0.14     | 0.41     | 0.83     | 0.33    | 56.10     | 53.32 | 2.79            | 0.95                  |
| 50t1.25L800   | 800      | 1349.4   | 51.4      | 337.3     | 1.46       | 0.43     | 0.14     | 0.38     | 0.85     | 0.38    | 49.18     | 48.91 | 2.38            | 0.99                  |
| 50t1.25L1000  | 1000     | 863.6    | 50.4      | 215.9     | 2.27       | 0.46     | 0.15     | 0.36     | 0.87     | 0.46    | 43.35     | 47.73 | 1.94            | 1.10                  |

Note: dimensions in *mm*, stresses in *MPa***Table B.16:** Spherically-hinged column critical stresses, ultimate strengths and DSM estimates ( $f_y=700MPa$ )

| <i>Column</i> | <i>L</i> | $f_{bf}$ | $f_{cft}$ | $f_{cre}$ | $\Delta_f$ | <i>a</i> | <i>b</i> | <i>c</i> | <i>d</i> | $\beta$ | $f_{nfe}$ | $f_u$ | $\lambda_{fte}$ | $\frac{f_u}{f_{yfe}}$ |
|---------------|----------|----------|-----------|-----------|------------|----------|----------|----------|----------|---------|-----------|-------|-----------------|-----------------------|
| 25t0.8L400    | 400      | 1349.4   | 83.4      | 337.3     | 2.41       | 0.47     | 0.15     | 0.36     | 0.87     | 0.47    | 70.73     | 79.68 | 1.88            | 1.13                  |
| 25t0.8L600    | 600      | 599.7    | 79.4      | 149.9     | 5.41       | 0.61     | 0.16     | 0.27     | 0.94     | 0.67    | 57.10     | 72.84 | 1.29            | 1.28                  |
| 25t0.8L800    | 800      | 337.3    | 75.3      | 84.3      | 9.73       | 0.85     | 0.18     | 0.12     | 1.00     | 0.78    | 47.46     | 61.67 | 0.99            | 1.30                  |
| 25t0.8L1000   | 1000     | 215.9    | 70.4      | 54.0      | 15.35      | 0.87     | 0.18     | 0.12     | 1.00     | 0.96    | 45.64     | 52.02 | 0.82            | 1.14                  |
| 50t0.8L400    | 400      | 5397.4   | 23.4      | 1349.4    | 0.16       | 0.40     | 0.15     | 0.54     | 0.66     | 0.26    | 38.81     | 37.65 | 4.91            | 0.97                  |
| 50t0.8L600    | 600      | 2398.9   | 21.8      | 599.7     | 0.34       | 0.40     | 0.15     | 0.43     | 0.81     | 0.22    | 27.46     | 31.57 | 4.44            | 1.15                  |
| 50t0.8L800    | 800      | 1349.4   | 21.2      | 337.3     | 0.60       | 0.40     | 0.14     | 0.42     | 0.82     | 0.26    | 24.85     | 23.60 | 3.72            | 0.95                  |
| 50t0.8L1000   | 1000     | 863.6    | 20.9      | 215.9     | 0.92       | 0.40     | 0.14     | 0.41     | 0.83     | 0.31    | 22.48     | 20.87 | 3.01            | 0.93                  |
| 50t0.95L400   | 400      | 5397.4   | 33.0      | 1349.4    | 0.23       | 0.40     | 0.15     | 0.44     | 0.81     | 0.24    | 40.74     | 51.09 | 4.13            | 1.25                  |
| 50t0.95L600   | 600      | 2398.9   | 30.7      | 599.7     | 0.48       | 0.40     | 0.14     | 0.43     | 0.82     | 0.26    | 36.26     | 38.24 | 3.74            | 1.05                  |
| 50t0.95L800   | 800      | 1349.4   | 29.9      | 337.3     | 0.84       | 0.40     | 0.14     | 0.41     | 0.83     | 0.30    | 32.66     | 29.66 | 3.14            | 0.91                  |
| 50t0.95L1000  | 1000     | 863.6    | 29.4      | 215.9     | 1.30       | 0.42     | 0.14     | 0.39     | 0.84     | 0.36    | 29.01     | 28.80 | 2.54            | 0.99                  |
| 50t1.25L400   | 400      | 5397.4   | 57.0      | 1349.4    | 0.40       | 0.40     | 0.15     | 0.43     | 0.82     | 0.30    | 63.98     | 71.57 | 3.14            | 1.12                  |
| 50t1.25L600   | 600      | 2398.9   | 53.0      | 599.7     | 0.84       | 0.40     | 0.14     | 0.41     | 0.83     | 0.33    | 56.40     | 53.32 | 2.85            | 0.95                  |
| 50t1.25L800   | 800      | 1349.4   | 51.4      | 337.3     | 1.46       | 0.43     | 0.14     | 0.38     | 0.85     | 0.38    | 49.24     | 48.91 | 2.39            | 0.99                  |
| 50t1.25L1000  | 1000     | 863.6    | 50.4      | 215.9     | 2.27       | 0.46     | 0.15     | 0.36     | 0.87     | 0.46    | 43.35     | 47.73 | 1.94            | 1.10                  |

Note: dimensions in *mm*, stresses in *MPa*